Journal of Power Sources 556 (2023) 232256

Contents lists available at ScienceDirect

Journal of Power Sources

journal homepage: www.elsevier.com/locate/jpowsour

Review article

Next generation 2D materials for anodes in battery applications

Madhu Raj Kumar [a], Sangeeta Singh [a,*], Heba Mohamed Fahmy [d,**], Neeraj K. Jaiswal [e], Seckin Akin [f], Ahmed Esmail Shalan [b,c], Senentxu Lanceros-Mendez [b,g,****], Manuel Salado [b,***]

[a] Microelectronics & VLSI Lab, National Institute of Technology, Patna, 800005, India
[b] BCMaterials, Basque Center for Materials, Applications and Nanostructures, Martina Casiano, UPV/EHU Science Park, Barrio Sarriena s/n, Leioa, 48940, Spain
[c] Central Metallurgical Research and Development Institute (CMRDI), P.O. Box 87, Helwan, Cairo, 11421, Egypt
[d] Biophysics Department, Faculty of Science, Cairo University, 12613, Egypt
[e] 2-D Materials Research Laboratory, Discipline of Physics, Indian Institute of Information Technology, Design & Manufacturing, Jabalpur, 482005, India
[f] Department of Metallurgical and Materials Engineering, Faculty of Engineering, Necmettin Erbakan University, Konya, 42060, Turkey
[g] IKERBASQUE, Basque Foundation for Science, 48013, Bilbao, Spain

HIGHLIGHTS

- Comprehensive review of 2D materials for anodes applications.
- Synthesis and properties of graphene, TCM and MXenes based materials.
- Future outlook of 2D based materials for energy storage.

GRAPHICAL ABSTRACT

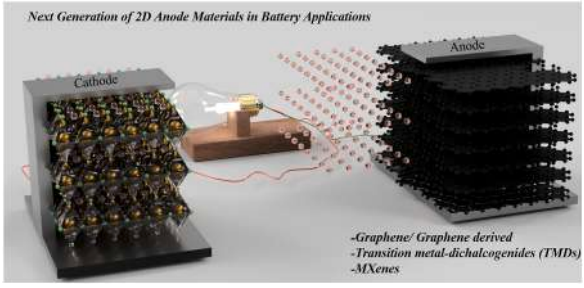

ARTICLE INFO

Keywords:
2D materials
Battery
Graphene
Applications

ABSTRACT

Two-dimensional (2D) materials, for instance, graphene/graphene derivatives, transition metal-dichalcogenides (TMDs), and MXenes (e.g. transition metal carbides (TMCs) as well as nitrides (TMNs)) are under increasing research attention due to their unique physical, mechanical, magnetic, electrical, optical, and chemical properties. They are explored for a variety of applications, including energy generation and storage systems. Notwithstanding the developing interest in these materials, with respect to the later area, there is an absence of comprehensive overview and analysis on the synthesis and application of 2D materials aimed at lithium (Li) ion batteries. In this review, we have gathered and discussed the main issues faced by the different methods involved in the synthesis of 2D inorganic materials and their composites, along with their main properties in addition to applications for lithium, sodium (Na), and potassium (K) ion batteries. In addition, the problems raised during the charging and discharging of batteries for those materials are also discussed and possible proposed solutions

* Corresponding author.
** Corresponding author.
*** Corresponding author
**** Corresponding author. BCMaterials, Basque Center for Materials, Applications and Nanostructures, Martina Casiano, UPV/EHU Science Park, Barrio Sarriena s/n, Leioa, 48940, Spain.
E-mail addresses: sangeeta.singh@nitp.ac.in (S. Singh), hfahmy@sci.cu.edu.eg (H.M. Fahmy), senentxu.lanceros@bcmaterials.net (S. Lanceros-Mendez), manuel.salado@bcmaterials.net (M. Salado).

https://doi.org/10.1016/j.jpowsour.2022.232256
Received 23 June 2022; Received in revised form 2 October 2022; Accepted 12 October 2022
Available online 26 November 2022

are also included here. Overall, this review provides a road-map on current demands and future research directions on 2D materials to address the critical limitations of Li, Na and K ion batteries, for the afterward generation of high-performance energy storage systems.

1. Introduction

Environment and energy (generation and storage) have become issues of increasing concern and activity in the entire world. The exploitation and utilization of renewable energy sources (solar, wind, andthermal) attract growing research attention. However, due to the variability of those sources, energy storage becomes an important cornerstone in the efficient utilization of energy [1]. In relation to the efforts in the area of energy generation and storage and to the relevance in the upcoming "Green deal" [2], John B Goodenough, M Stanley Whittingham, and Akira Yoshino were awarded by the Nobel Prize for their work in the field of Li ion battery. Various energy storage systems, such as batteries, capacitors, and supercapacitors, are available based on the eventual usage [3]. However, the output power of these devices is highly dependent on the electrode materials' efficiency, stability, and cost. For example, new metals like Ir and Pt are good electrode materials in energy storage technologies, but their high cost and restricted availability make them uneconomical [4–10]. Hence, a number of novel non-metals, such as Co, Ni and Fe [11–14] have been suggested as possible candidates for battery applications but their poor performance compared to the used noble metals entailed to find other research lines.

Numerous researchers have focused their attention on two-dimensional (2D) materials since the discovery of graphene's remarkable physical and chemical properties during the early days of experimentation. Research in laboratories has made possible to create many different types of nanomaterials, such as hexagonal Boron Nitrides (h-BNs) [15,16], transition metal dichalcogenides (TMDs) [17–19], silicene [20], germanene [21], and phosphorene [22–24]. In terms of energy storage devices, 2D materials' high electronic mobility and energy density are made possible by their enormous surface area to volume ratio and interior surfaces [25].

In particular, MXene 2D material were developed, composed by a family of transition metal carbides and transition metal nitrides [26]. Generally, MXenes can be prepared by selective etching of "A" layers from MAX phase. With the general formula $M_{n+1}AX_nT_x$ where (n = 1–3), "M" represents early transitional metal (such as Ti, V, Mo, Sc, Nb, etc.), "A" is an element of group IIIA or IVA (such as Al, Ga, Si or Ge), "X" represents carbon and/or nitrogen and "T" represents a surface functional group attached on the surface during selective etching process, such as O, OH and/or F. Recently, MXenes with surface termination of Cl [27,28] are reported to be deployed for 2D battery applications. As previously mentioned, up to now, most of the MXenes have been prepared by selective etching of the Al layer from MAX phases, which can be prepared by using the solid solutions of "M", "A" and "X", such as Ti (Nb_2AlC) [29], $Ti_3(Al_{0.5}Si_{0.5})C_2$ [30] and $Ti_2Al(C_{0.5}N_{0.5})$ [31]. To date, over 70 MAX phases have been reported, and the number continues to grow. Bonds containing "A" are more chemically active than strong M–X bonds [32,33].

This review presents and discusses the preparation, features, and trends of graphene, graphene derivatives, transition metal dichalcogenides (TMD), and MXene focusing on the application of these materials as anodes for metal-ion batteries as well as electrodes for supercapacitor. Fig. 1 illustrates the classification of 2D inorganic materials for metal-ion battery applications.

With the advancement of 2D materials, wider ranges of applications are now possible. They are, however, well suited to energy harvesting and storage due to their high ion transport efficiency and huge surface area with many readily accessible active sites. Fig. 2 shows the different synthesis methods and properties of 2D materials and in Fig. 3, battery applications are using 2D materials that are the newest in research.

This review is organized as follows: Section 2 covers graphene and its derived materials. Section 3 is devoted to transition metal dichalcogenides. Section 4 focusses in MXenes. In all those sections, synthesis, main properties and applications in the area of batteries are covered. Section 5 covers some others materials used as anode for metal ion batteries. Section 6 covers limitation of 2D materials. Section 7 the basic requirements of 2D promising anode materials in battery application and section 8 concludes this review by summarizing the current trends of 2D materials for battery systems.

2. Graphene and related materials

Graphene is a single atom thick sp^2 hybridized carbon layer prescribed in a honeycomb crystal lattice [34]. Although it is a 2D material,

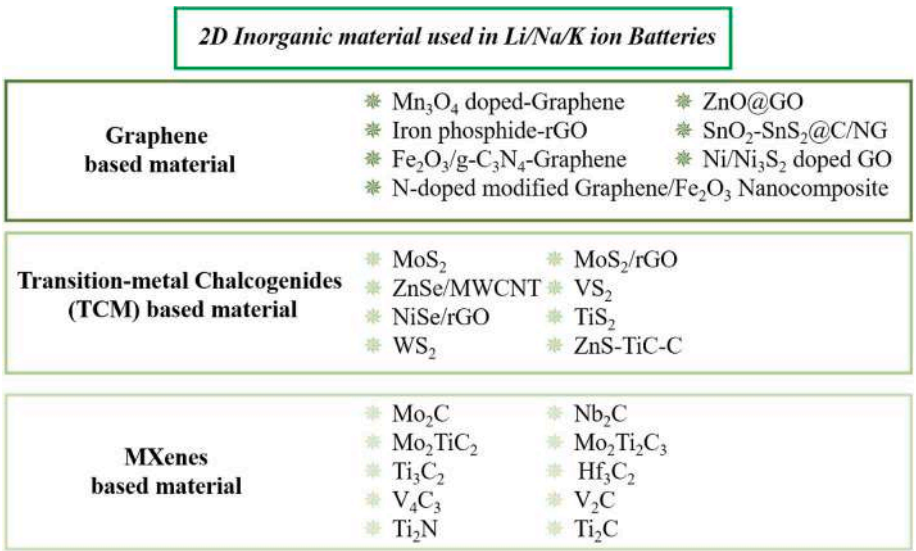

Fig. 1. Classification of 2D inorganic anode materials in battery applications.

which means all atoms of graphene are on the same surface, it can form all the basic structures of the other carbon materials like graphite, carbon nanotube in addition to fullerenes. Novosolov et al. obtained graphene in an easy way and attracted worldwide attention due to its innovative structure and properties. Specifically, with a specific surface area of 2600 m^2g^{-1}, graphene is a great candidate for lithium storage as anode electrode [35,36]. It has very high electron mobility, 1500 $cm^2V^{-1}s^{-1}$, outstanding thermal conductivity 300 $Wm^{-1}k^{-1}$, great chemical stability, as well as exceptional mechanical properties.

2.1. Synthesis approaches for graphene & its derived materials

Different approaches have been adopted for graphene synthesis that can be divided into: (i) Top-down and (ii) Bottom-up approaches (see Fig. 4 a).

(i) Top-down approach

To synthesize high-quality graphene with no defects, scientists turned to the scotch tape method or the peel-off method, which involves the micromechanical fracturing of graphite [35]. Graphite is in the form of a stack of graphene layer by van der Waals forces. Thus to get a stable one atom thick graphene, compensation of van der Waals force of attraction is needed. During this approach, graphite is broken into layers. As a consequence, many defects appear as surface defects during sheet separation, leading also to a low yield [37]. On the other hand, exfoliation of graphite oxide or derivatives is suitable for large production, cost effective, and scalable yields [38].

ii) Bottom-up approach

In this approach, carbon molecules from different carbon sources are implemented as a building block, allowing to produce large surface area sheets, in addition to graphene nanoribbons (GNRs) and graphene dots (so-called nanoflakes) as it offers the possibility of large-scale production [39]. Chemical vapor deposition (CVD) was used as a common approach to fabricate defect-free graphene sheets. However, compared with micro-mechanical cleavage approach, it was realized that this method cannot produce large yields, as it takes a larger time, and it is not cost-effective, limiting the effective and full exploitation of these

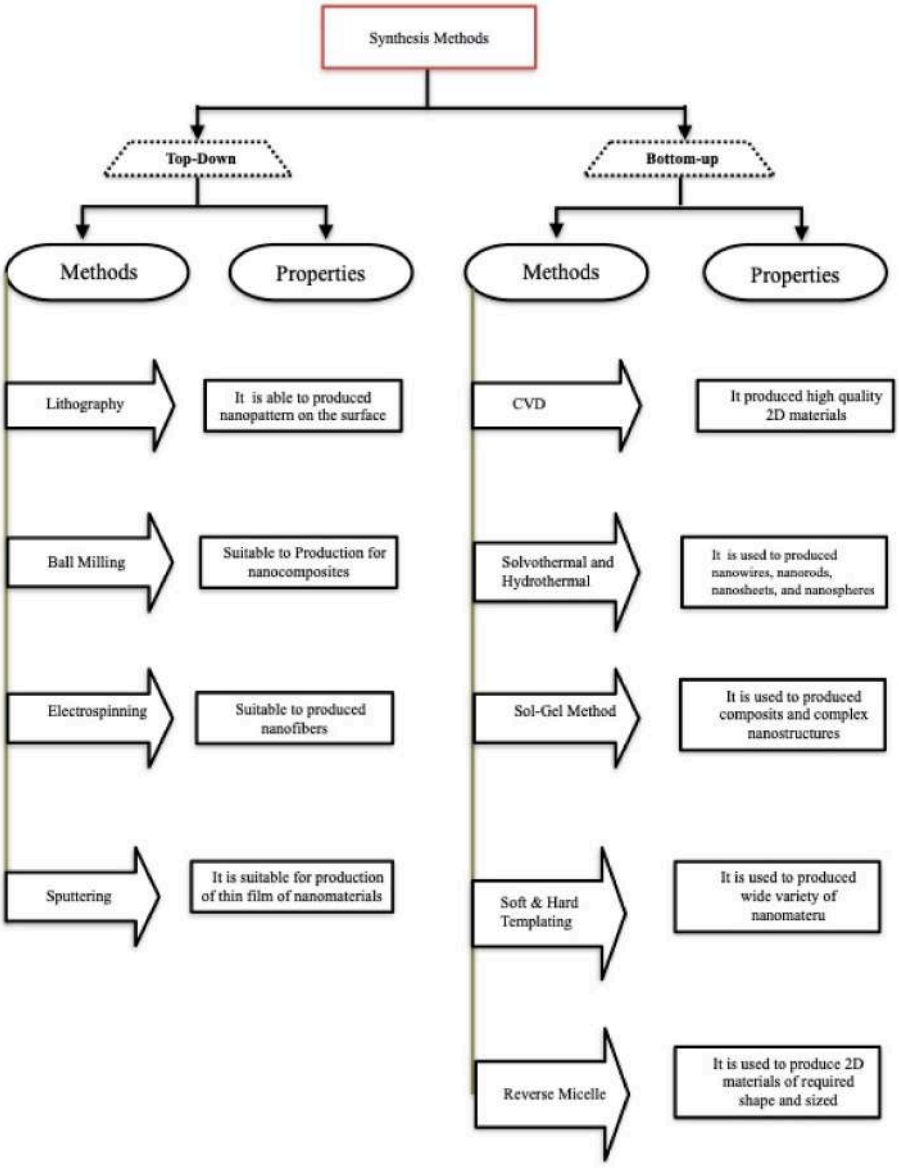

Fig. 2. Different synthesis method and its properties.

materials [40–42]. Nevertheless, techniques are being developed to produce high quality crystals up to100 μm in size, which can be easily separated with graphite intercalated compounds (termed as GIC) [43]. Focusing on the bottom-up approaches designed to obtain 2D material, relevant approaches are (i) Progress from metal-carbon melts (ii) Epitaxial development on silicon carbide (SiC) (iii) Dry-ice (iv) Deposition.

(i) *Growth from metal-carbon melts:* This is a simple approach for the production of single/few layers of graphene, where precursor of graphene is placed in contact with a transition metal and then heated up to the melting temperature of metal. When carbon starts to dissolve in the metal, the temperature is reduced to control the excessive carbon precipitation. Although nickel is the most suited transition metal for this process [44], ruthenium and iridium are also used. But the quality of produced graphene is less than the quality of graphene produced by nickel and copper [45, 46]. The most suitable method for the growth of graphene on nickel films is CVD. In this method, nickel film is heated up to 900 to 1000 °C with an inert gas (flow of Ar), where methane gas is introduced in the system along with inert gas (Ar) as a precursor for the extraction of carbon. After absorption of the carbon on the nickel film the system is cooled down, allowing the diffusion of carbon on nickel film to form graphene sheet [47–50].

(ii) *Epitaxial growth on silicon carbide (SiC):* This technique is able to produce graphene films of more than 50 μm. The graphene layer is obtained on a SiC substrate by using heat treatment of silicon carbide at 1100 °C [51]. The graphene obtained from this method has more mobility and carrier density compared to chemical exfoliation methods [52].

(iii) *Dry ice method:* Chakrabarti et al. was the first group that introduced the dry ice method. In this method, 3 g Mg ribbon is burned out in a dry ice bowl, which is covered with another dry ice (solid CO_2) slab. Besides, Mg must burn completely and the residue is agitated overnight in the presence of 100 mL of 1 M HCl. Since both Mg and MgO are water soluble, the mixture is filtered out to extract graphene sheets, resulting in a graphene yield of 92% (680 mg) [53].

(iv) *Deposition:* Due to easy scalability and feasibility, researcher have reported many deposition-based techniques for the graphene synthesis [54–57]. Although large size and good quality of graphene films are obtained [41,47,58], most of the CVD techniques are scalable but financially not suitable. On the other hand, spin coating method is characterized for being an easy and fast deposition technique. In addition, this technique enables the use of nanotubes to reinforce graphene. In particular, Yan et al. used a solution containing trichloromethane and dodecyl-functionalized single wall carbon nanotubes (DF-SWCNT). It contains a 200 mL solution of DF-SWCNT $CHCl_3$ at a concentration 3.2 mg/ml. The solution was then spun coated on a treated Cu foil of size 1 cm^2 at 500 rpm for 10 s. The Cu foil was loaded into a CVD furnace and annealed for 15 min at the temperature of 1080 °C, under the flow of H_2 (flow rate of 50 standard cubic centimeter per minute (sccm)) and Ar (500 sccm) at the pressure of 7 Torr. After annealing, the Cu foils were quickly removed from the hot chamber by using a magnetic rod and then cool down to room temperature [59]. Another interesting approach consists of the use of a supersonic spray providing a simple and low-cost option to deposit graphene films on different substrates. This method allows to reduce the defects density and provides a very low I_D/I_G ratio (0.02). In this system, the spray is assisted by the supersonic acceleration of droplets through a converging and diverging De Laval nozzle [60]. Wang et al. deposited GO sheets on silica/quartz substrates and then reduced them into graphene by thermal treatment under uniform flow of Ar/H_2, producing ultrathin and homogeneous graphene films. This

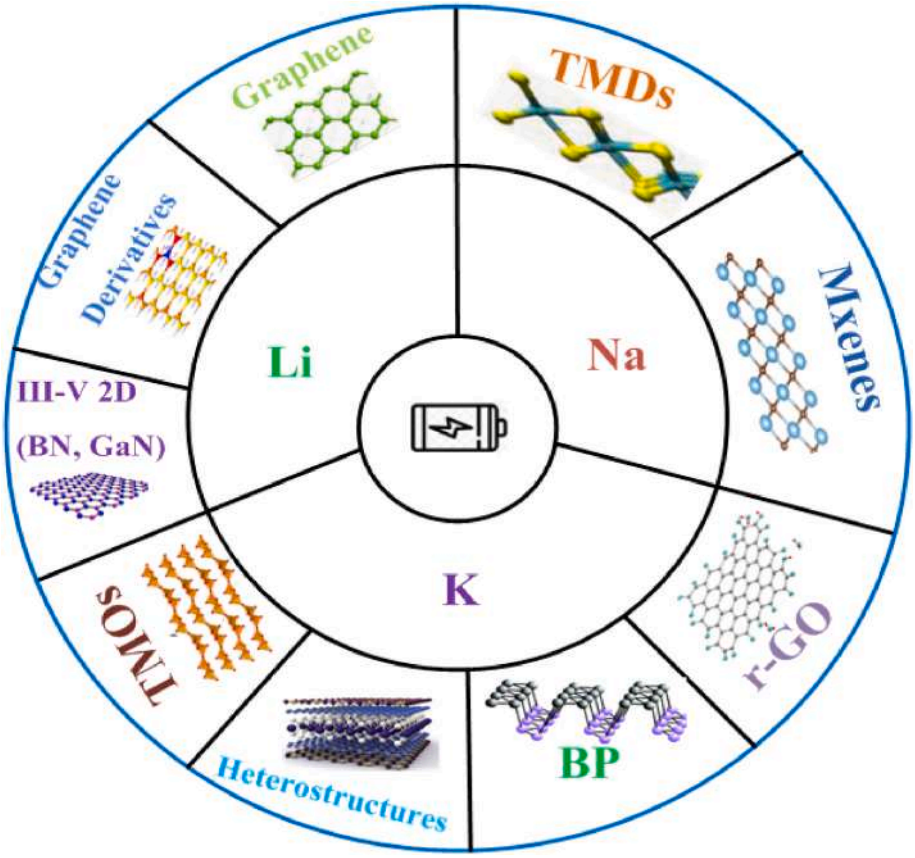

Fig. 3. Overview of 2D material for battery applications.

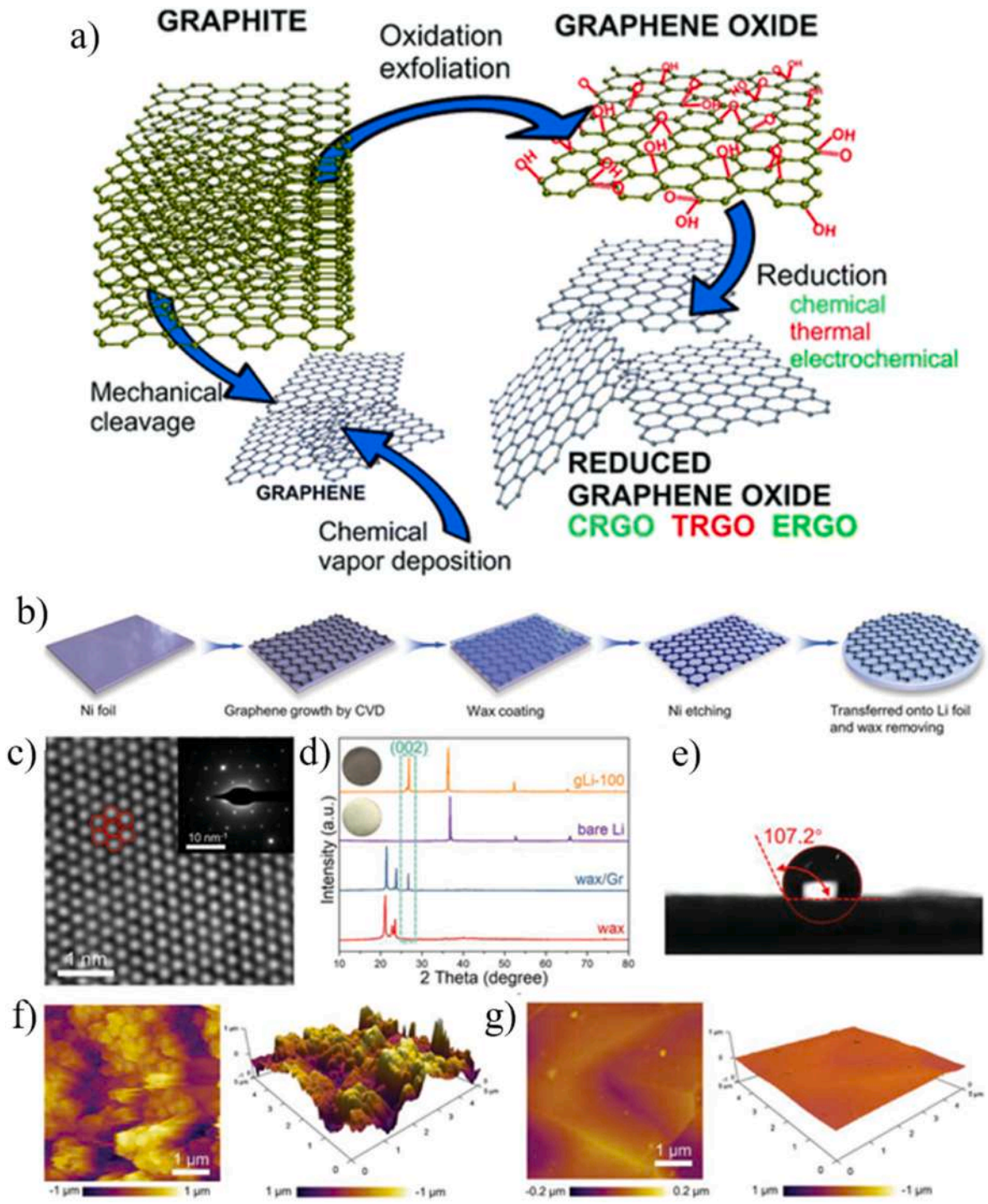

Fig. 4. (a)Diagram sketch of conceivable approaches for the fabrication of graphene, GO and rGO from graphite by means of mechanical cleavage, exfoliation, CVD in addition to reduction systems, together with chemical, thermal and electrochemical approaches. [Reprinted with permission from ref. [289]]. Fabrication and characterization of the gLi anodes.(b) The schematic diagram showing the coating of Li surface with a CVD graphene film via the wax-assisted protocol. (c) FFT-filtered aberration corrected TEM image taken on the CVD graphene film. Insert is the corresponding selected-area electron diffraction (SAED) pattern. (d) XRD pattern of the gLi-100 anode displaying the co-existence of Li and graphene signatures. Inserts are the optical pictures of the corresponding bare-Li and gLi-100 anodes. (e) Measurement of water contract angle on the gLi-100 electrode. AFM top-view and 3D topograph of the (f) bare-Li and (g) gLi-100 anodes. [Reprinted with permission from Ref. [287].

process could be also applicable for the production of solar panels and optically transparent devices. Synthesized graphene also offers very high conductivity, chemical and thermal stability along with transferability between substrates [61]. Barcenas et al. developed a new modified technique for the production of graphene. In this method, N_2 (90%):H_2 (10%), C_2H_2 and electrolytic copper are used as a precursor. In the process, a discontinuous flow system was used at atmospheric pressure instead of a continuous flow system with vacuum. It optimized the consumption of gas and hence reduced the production of waste and pollution gases. It was evaluated the growth of graphene films under different gas flow rates was also evaluated. The process presents many advantages such as; (1) a reduction of the number of parameters (2) the

synthesis time is shorter than in traditional methods (3) electrolytic technical grade copper was used instead of mono crystalline copper which reduced the cost, (4) explosive risk is reduced due to mixture of N_2/H_2 instead of H_2. In general, the produced graphene shows very good quality as like mono-layer graphene hence it offers industrial applications [7].

2.2. Properties of graphene & its derived materials

Graphene has numerous qualities connected to increased sensitivity because of its enormous surface-to-volume ratio. These characteristics, in particular, make it an appealing material with a lot of potential for use in a range of sectors and technologies. The properties of graphene are briefly described in the next section.

2.2.1. Electronic properties

Novoselov et al. first explored the electrical and electronic features of graphene [35]. They found that the electrical as well as electronic features of graphene are sensitive to the number of layers of graphene sheets. Furthermore, the application of graphene in transistors was studied showing that the charge carrier concentration variation from holes to electrons is only applicable for single layer graphene sheet, and not for multilayer sheets due to the screening effect of electric field applied by other layers. Zhang et al. explored the quantum hall effect on electron besides hole carriers for graphene, showing that this effect results in higher mobility of electron at several temperatures plus exposure of magnetic field [62]. For mechanically synthesized graphene, the mobility can exceed 2000 $cm^2V^{-1}s^{-1}$. Characteristically, the classical integer quantum Hall effect occurs at $4e^2/h$, where e is the electron charge and *h* is the Planck's constant, but due to the unique band structure of graphene, the quantum hall effect for graphene is only half integers. Bolotin et al. found that the mobility of electrons for graphene not only depends on temperature but also depends on the substrate. To date, the largest mobility of any semiconductor is more than 200,000 $cm^2V^{-1}s^{-1}$, when graphene is suspended and annealed on Si/SiO_2.

2.2.2. Mechanical properties

Materials based on carbon usually show outstanding mechanical features. For example, diamond is the world hardest known natural material, while carbon nanotubes are known to have the highest tensile strength. In this regard, graphene was characterized by Lee et al. obtaining a tensile strength of 130 GPa, meanwhile the breaking stress was 200 times more than steel and the Young's modulus of 1 TPa. Though, the strength is highly dependent on the impurities present in the graphene sheet [64]. Alternatively, suspended graphene layer exhibits Young's modulus of 0.5 TPa [62]. Dikin et al. prepared and explored the characteristics of graphene oxide paper obtaining a modulus of elasticity nearly to 32 GPa and a fracture strength of around 120 MPa [65]. In the direction of progressing the mechanical features, Park et al. introduced divalent ions and polyallylamine between the layers of graphene [66]. Further, when the thickness of the graphene layers increase, the mechanical strength decreases.

2.2.3. Optical properties

The absorption of white light of graphene linearly increases with cumulative number of sheets, the absorption of each layer can be calculated by formula $A = 1\text{-}T = \pi\cdot\alpha$, where α is the fine structure constant and it is nearly equal to 1/37. Bae et al. found that one atom thick graphene is capable of absorbing 2.3% of white light while bilayer graphene absorbs up to 4.6% [49]. For UV light, the absorption ability of graphene is maximum observed for 270 nm. Sharma et al. explored the effects of the thickness of graphene by optical microscopy on a Si/SiO_2 substrate. Furthermore, the contrast of microscopy depends on the thickness of the sample where, multilayer samples present higher contrast [68].

2.2.4. Thermal properties

Zhu et al. found that the thermal conductivity of graphene was conquered through phonon transport, i.e. ballistic conductivity in addition to propagation at high as well as low temperatures, respectively [69]. Nonetheless, the electronic thermal transport of pure graphene is negligible as a result of low carrier density [70]. Besides, the intrinsic thermal conductivity is about 2000–6000 $Wm^{-1}K^{-1}$ for suspended graphene sheets at room temperature and 600 $Wm^{-1}K^{-1}$for suspended graphene on SiO_2 substrates [71,72].

The thermal conductivity is also reliant on the faults in graphene such as edge scattering, isotopic doping, plus sample fabrication residues [71,73–75]. Consequently, graphene produced by micromechanical cleavage present higher thermal conductivity attributable to high quality of the sheets. In addition, Balandin et al. produced suspended graphene by mechanical exfoliation and measured the thermal conductivity. They found that it is in the range of 4800–5300 $Wm^{-1}K^{-1}$ that is greater than that of natural diamond (2200 $Wm^{-1}K^{-1}$), 3000 $Wm^{-1}K^{-1}$ for multi-wall, besides 3500 $Wm^{-1}K^{-1}$ aimed at single wall carbon nanotubes at room temperature, respectively [75–77]. Cai et al. compared the thermal conductivity of suspended and supported graphene produced by CVD and they found that it is nearly 3000 $Wm^{-1}K^{-1}$, which is less than the graphene produced by mechanical exfoliation [78]. Due to the excellent thermal conductivity of graphene, it can be used for manufacturing in heat dissipaters, thermal sensors, and composites.

2.3. Battery application of graphene & its derived material

2.3.1. Graphene as anode material for Li ion battery

For large-scale production in addition to application, low cost and easy methods for prepairing graphene are developed. Graphene has attracted attention in the area of energy storage, in particular because of its large specific surface, which makes graphene suitable as electrode material for Li ion batteries. Li can be attached to both the surfaces of graphene and form Li_2C_6 stoichiometry, which increases the theoretical capacity of graphene 744 $mAhg^{-1}$ [313]. However, from in-situ Raman spectroscopy of CVD-grown single-layer plus multi-layer graphene, it was found that the LiC_6 stoichiometry could not be formed with single-layer graphene. This problem occurs because the binding energy of Li to carbon atoms is lower than the repulsive force between Li atoms on the contrary edges of the surface. The low surface coverage (about 5% Li) showed on a single layer graphene is corresponding to LiC_{20} stoichiometry and hence leads to a very low specific capacity [79, 314–316]. Uthaiser et al. found that defects increase on the conversion of polar form to coordinate form as the Li ion adsorbs and diffuses, reducing its accumulation. These findings allow to improve the electrochemical act of LIB [80,81]. Besides, Pan et al. explored the effect of disordering in graphene in the electrochemical performance of LIB anodes. It was found that defects and sites play an important role for Li storage [82]. Samples that shown more disorder reveal superior capacity, suggesting that storage in defects sites is the core appliance of Li ion storage in these materials. Xiang et al. also investigated the effects of layers of graphene and multilayer graphene with few defects plus found that both have a comparable electrochemical absorption actions for Li^+ interacted graphite [83]. One other thing to observe is how many edge sites there are, and how this increases the contact surface between the electrolyte and anode electrode, makes them unsuitable for battery use (see Fig. 4 b-f) . It also leads to further formation of solid electrolyte interphase (SEI) and low coulumbic efficiency at first discharge. Fang et al. synthesized a mesoporous graphene material leading to remarkable electrochemical properties. Lithium ion battery anodes made of these mesoporous graphene nanosheets exhibited a high reversible capacity of 770 $mAhg^{-1}$ at 100 mAg^{-1} [84]. A detailed comparison of graphene, doped graphene, and derived materials used as anodes and their first charged and discharged cycle and efficiency for Li-ion and other ion technology (Na, K) are shown in Tables 1 and 2, respectively.

Table 1
First cycle charge/discharged capacity, rate life and cycling performance of graphene as well as doped graphene aimed at Li-ion battery anodes.

2-D Material	First cycle charge/ discharge	Capacity	Cyclingperformance	Ref.
Graphene sheets, of ~ 4 layer thickness	1264/2035 $mAhg^{-1}$	718 $mAhg^{-1}$ at 500mAg^{-1}	54% once 20 cycles	[93]
Graphene (hydrazine nanosheet reduced rGO)	650/945 $mAhg^{-1}$	650 $mAhg^{-1}$ at 372mAg^{-1}	70% once 100 cycles	[94]
N-doped graphene	0.05/0.255 $mAhcm^{-2}$	0.03 $mAhcm^{-2}$ at 100 $mAcm^{-2}$	66% once 50 cycles	[94]
Thermally exfoliated graphene at 1050^{0}C	1264/2035 $mAhg^{-1}$	1264 $mAhg^{-1}$ at 100mAg^{-1}	67% once 40 cycles	
Thermally exfoliated graphene at 700^{0}C with N doping	1123/2800 $mAhg^{-1}$	241 $mAhg^{-1}$ at 20 Ag^{-1}	No significant decay over 50 cycles	[96]
Thermally exfoliated graphene at 700^{0}C	848/2000 $mAhg^{-1}$	112 $mAhg^{-1}$ at 20Ag^{-1}	87% once 50 cycles	[96]
S-doped graphene	870/1700 $mAhg^{-1}$	870 $mAhg^{-1}$ at 374 mAg^{-1}	52% over500cycles	[97]
Thermally exfoliated graphene at 105^{0}C	672/1233 $mAhg^{-1}$	672 $mAhg^{-1}$ at 0.2 $mAcm^{-2}$	74% over 30 cycles	[98]
rGO reduced in a H_2/Ar atmosphere at 300^{0}C	1540/2274 $mAhg^{-1}$	1540 $mAhg^{-1}$ at 50 mAg^{-1}	97% over 50cycles	[99]
Microwave-assisted exfoliation of graphene oxide (GO) at 1000^{0}C	414/600 $mAhg^{-1}$	250 $mAhg^{-1}$ at 1C	65% over 60cycles	[100]
H-graphene reduced under 60 Co-gamma ray irradiation	1570/3404 $mAhg^{-1}$	490 $mAhg^{-1}$ at 1000mAg^{-1}	80% over 550 cycles	[101]
Thermally reduced rGO at 105^{0}C	835/2381 $mAhg^{-1}$	835$mAhg^{-1}$ at 50 mAg^{-1}	50% over 25cycles	[102]
Holey graphene	889/2207 $mAhg^{-1}$	486 $mAhg^{-1}$ at 1C	93% over 30 cycles	[103]
S-doped graphene	1400/2520 $mAhg^{-1}$	280 $mAhg^{-1}$ at 20 Ag^{-1}	increasing over500 cycles	[104]
N-doped graphene	1043/2128 $mAhg^{-1}$	200 $mAhg^{-1}$ at 20 Ag^{-1}	42% over 30cycles	[86]
B-doped graphene	1549/2786 $mAhg^{-1}$	250 $mAhg^{-1}$ at 20 Ag^{-1}	47% over 30 cycles	[86]
N and S-doped graphene	1016/2157 $mAhg^{-1}$	250.1 $mAhg^{-1}$ at20 A g^{-1}	35% over 70 cycles	[105]
HighlyN-doped porous graphene	640/1279 $mAhg^{-1}$	317 $mAhg^{-1}$ at 150 mA g^{-1}	Remains same after 200 cycle at the rate of 400 mAg^{-1}	[32]
Sn/N-doped rGO nanocomposites	1200/2028 $mAhg^{-1}$	535 $mAhg^{-1}$ at 2C	76% over 30 cycles	[54]

Table 2
First cycle capacity, cycling life and performance of graphene and doped graphene for Na/K/Mg-ion battery anodes.

Battery	Appellation	First cycle charge/ discharge capacity	Rate performance	Cycle life	Ref.
Na-ion	N-doped graphene sheet	371.5/ 1186.6 $mAhg^{-1}$	155.8 $mAhg^{-1}$ at 500 mA g^{-1}	58% after 600 cycles	[55]
Na-ion	Solvothermal derived S-doped graphene	500/900 $mAhg^{-1}$	217 $mAhg^{-1}$ at 3200 mAg^{-1}	1000% after 900 cycles	[56]
Na-ion	B-dopped AGNR	833 $mAhg^{-1}$	NA	NA	[298]
Na-ion	Twin-graphene	496.2 $mAhg^{-1}$	NA	NA	[302]
K-ion	B-doped graphene	546 $mAhg^{-1}$	NA	NA	[57]
Mg-ion	Graphene like BSi	2749 $mAhg^{-1}$	NA	NA	[299]
Mg-ion	Antimonene/ graphene hetrostructure	735 $mAhg^{-1}$	NA	NA	[300]
Mg-ion	Pentagraphene	1653 $mAhg^{-1}$	NA	NA	[301]

The efficiency of graphene material as anode is typically around 50%, making difficult its use in a full cell. Wang et al. discovered that doping graphene sheets with heteroatoms improves the interaction between the Li-ion and the active sites, resulting in a slight increase in the efficiency of the first coulombic cycle, according to the findings [85].

Doping with B, N, S and F also allows to improve cycle performance and first cycle coulombic efficiency [86–90]. For graphene-based Li ion batteries to function better, a new synthesis technique is required. This is because graphene materials can only be efficiently distributed in a coating solvent at extremely low concentrations below 2–3% by weight, which is insufficient for good performance. Even with advanced manufacturing techniques, it is still difficult to achieve high packing densities of graphene materials. Up to now, nanocarbon based materials could not achieve the volumetric capacity of graphite electrodes (330–430 $mAhcm^{-2}$) [91].

2.3.2. *Graphene doped anode material for Li-ion battery*

Since surface modification enhances the Li adsorption capacity of carbon materials, the specific capacity of doped graphene material as anodes for Li ion batteries has been explored. Since atomic size of B and N are closest to the size of carbon atoms, doping of these atoms on carbon materials have been investigated. Sun et al. synthesized N-doped graphene nanosheet (N-GNS). In this approach, graphene nanosheet (GNS) was prepared from graphite by Hummers' method and rapidly exfoliated via thermal treatment at 1050 °C in the presence of nitrogen gas. Finally, GNS was further annealed in the presence of ammonia gas to obtain N-GNS. The produced N-GNS showed superior electrochemical performance, the specific capacity increasing with increasing charge/ discharge cycles, e. g 452 $mAhg^{-1}$ after 100 cycles in addition to 684 $mAhg^{-1}$ after 500 cycles. The significant improvement is attributed to the nitrogen insertion in the graphene level, which directed to an rise in the amount of fault places as well aspositions as Li^+ active sites above the apparent of GNS [88]. Wang et al. produced nitrogen doped graphene by using GO prepared by Hummers and Offeman methods. The obtained GO was then dried out in a vacuum oven at 600 °C for 4 h and then heated for 2 h in the presence of ammonia. The obtained N-GNS shows a great rescindable capacity of 900 $mAhg^{-1}$ at the rate of 0.05C plus 250 $mAhg^{-1}$ at a current density of 2.1 Ag^{-1} [87]. Reddy et al. prepared one to few layer N-GNS on Cu substrates by using CVD, by means of hexane in addition to acetonitrile as precursors, N-doped graphene sheet were obtained exhibiting an specific capacity of ~0.06 mA h cm^{-2} at the rate of 1 A cm^{-2} after 20 cycles [92].

Wu et al. also demonstrated that graphene improves when doped with nitrogen (N) or boron (B). It was found that the reversible capacity greater than 1040 $mAhg^{-1}$ at a low rate of 50 mAg^{-1}, with a charge-discharge time of 1 h to numerous tens of seconds, as well as extraordinary rate competency in addition to brilliant long term cyclability. Results indicate that B-doped graphene behaves better than N-doped graphene with a capacity of 235$mAhg^{-1}$ and 199 $mAhg^{-1}$ at 25 Ag^{-1}, respectively [86]. Ma et al. investigated the specific capacity of N-doped graphene as anode materials for Li ion batteries using first principle methods according to three different defect models of graphene; graphitic, pyridinic and pyrrolic, respectively. It was found that

pyridinic graphene is furthermost appropriate for Li storage as the specific capacity can reach up to 1262 $mAhg^{-1}$ [106]. Haung et al. synthesized N and B double-doped graphene sheets, the obtained NBGs-1000 exhibiting high reversible capacity of 909 $mAhg^{-1}$ and excellent discharge capacity 877 $mAhg^{-1}$ after 125 cycles. It has also shown a large capacity 429 $mAhg^{-1}$ at 1 Ag^{-1} and 318 $mAhg^{-1}$ at the rate of $2Ag^{-1}$ in contrast of graphite which shows 50 $mAhg^{-1}$ at 1 Ag^{-1} [107].

With the help of a sandwich-structured nanocomposite of N-doped graphene, Wen et al. created monodisperse Fe_3O_4 nanoparticles for use in solar energy conversion. Through interactions between N dopants, surfactant molecules, and iron precursors, N-doped graphene not only provides a conducting framework for the self-assembled structure, but also controls Fe_3O_4 nucleation. The unique sandwich-structure delivers a large conductivity and extraordinary reversible capacity of ~ 1227 $mAhg^{-1}$in addition to retains 96.8% capacity after 1000 cycles at a rate of 3 Ag^{-1} [108]. Young et al. synthesized sulfur doped graphene based nanosheets by using thermal treatment of elemental lyophilized GO mixtures. The reversible capacity of the produced S-GNS is two times the one of pristine GNS at a current density of 372 mAg^{-1} and three times at the rate of 11600 mAg^{-1}. Cyclic stability is constant up to 500 cycle at a high rate of 4C [97]. Zhan et al. synthesized fluorine doped GNS (F-GNS) by liquid exfoliation method of commercially available F-graphite powders via a sonication.

The resulted F-GNS exhibited a very large reversible capacity of 780 $mAhg^{-1}$ at a rate of 50 mAg^{-1} after 70 cycles in contrast of fluorinated graphite ~ 400 $mAhg^{-1}$ [109]. Zhan et al. synthesized iodine doped GNS (I-GNS) through facile heat treatment method and found that it exhibits large reversible capacity 1690 $mAhg^{-1}$ at the rate of 100 mAg^{-1}as compared to 593 $mAhg^{-1}$ of fluorine doped graphite [110]. Luan et al. prepared a nitrogen and phosphorous doped multilayer graphene (NPG) by using arc discharge method. The synthesized NPG shows large reversible capacity of 798 $mAhg^{-1}$ at the rate of 1 Ag^{-1} and with a coulombic efficiency of 98.6% after 1000 cycles [111]. Hu et al. premeditated the theoretical specific capacity of Germanium doped graphene by using first principle calculation method and it was found that Germagraphene exhibits a reversible capacity of 1734 $mAhg^{-1}$ that is four times the one of graphite. It was also investigated the diffusibility of Li-ion on germagraphene along with found that the dispersal obstacle of Li-ion is nearly equal to 0.151 eV. Therefore, Li-ion gets fastly diffused on Germagraphene surface [112]. Sui et al. arranged a novel heavily N-doped porous graphene material (NPGM), when applied as anode for Li-ion batteries; it exhibits a discharge capacity of 672 $mAhg^{-1}$ at a current density of 100 mAg^{-1}. NPGM also exhibits superior cycling stability, keeping its capacity value constant after 200 cycles at a current density of 400 mAg^{-1} [32].

2.3.3. Graphene active material composites

$Li_4Ti_5O_{12}$ (LTO) is currently applied as an anode material in commercial cells. Since the insertion of electrons and Li ions produces a small change in lattice dimensions, LTO exhibits a long cycle life through its probable platform at 1.5 V versus Li/Li^+. Nevertheless, the electrical conductivity of LTO is less than $10^{-13}Scm^{-1}$. One simple approach to improve the electrical conductivity is the fabrication of composites with carbon materials. In this regard, Shi et al. created LTO composites containing 5% rGO using a simple mixing process. Besides, the derived hybrid material achieved a specific capacity of 122 $mAhg^{-1}$ at a charge/discharge rate of 30C associated with 172 $mAhg^{-1}$ at 1C. Additionally, after 300 cycles at 20C charge/discharge rate, the capacity only reduced by 6% [113–118]. Ding et al. discussed about the size consequence of the synthesized LTO/rGO composites and it was concluded that the nano LTO anchored with rGO provides a capacity of 120 $mAhg^{-1}$ at a higher current density of 1600 mAg^{-1} [83]. Cai et al. explored the capacity of TiO_2 nanoparticles when attached on rGO sheets in two dissimilar potential windows: 1.0–3.0 V and 0.01–3.0 V. It was found that in the extended voltage window (0.1–3.0 V), TiO_2/rGO shows a specific capacity of 499 $mAhg^{-1}$while it has the same capacity as bare TiO_2 (200 $mAhg^{-1}$) in the 1.0–3.0 V potential window. When tested from 0.01 to 3 V, the coulombic efficiency was 45% in the first cycle, which is lower than for TiO_2 (71.8%). It was suggested that the excessive amount of SEI formed and the irreversible Li ion insertion have bigger influence when discharge occurs at lower cut-off voltage [118]. Sun et al. arranged a Sn/Nitrogen-doped reduced graphene oxide (Sn@N-G) composites. When implemented as anode for LIBs, it exhibits specific capacity of 535 $mAhg^{-1}$ at the current rate of 2C and it exhibits cycling stability up to 300 cycles at the rate of 0.5C [54].

2.3.4. Alloying anode materials

Caused by the high specific capacity, alloying materials are used as a potential anode for LIB. However, their enormous volume expansion throughout charging/discharging reduces their cycle life. To overcome this problem, composites of graphene and alloying material have been used to enhance mechanical integrity and electrical conductivity. Because of its great capacity (4000 $mAhg^{-1}$) and low cost, Si is applied as a new type of alloying anode material for Li ion batteries, but low conductivity and high volume expansion (300%) after lithiation limits its use. Jeong et al. synthesized a composite material of Si nanoparticles exceedingly distributed in the middle of graphene sheets as well as supported through a graphite sheet designed via altering sections of graphene stacks, improving Li ion storage capacity in addition to cycling stability. The storage capacity was more than 2200 $mAhg^{-1}$ after 50 cycles and more than 1500 $mAhg^{-1}$ after 200 cycles. The storage capacity decreases by ~0.5% per cycles, maintaining the same coulombic efficiency when prepared at 550 °C and 850 °C [119]. Tang et al. synthesized a composite of porous Si/rGO films by evaporation. Furthermore, the prepared composite film deliver an extraordinary reversible capacity and high rate capability of 1500 $mAhg^{-1}$ after 50 cycles plus 1261 $mAhg^{-1}$ after 70 cycles [120]. To improve the cycle stability free standing Si/graphene paper was prepared with an initial capacity of 1650 $mAhg^{-1}$ in addition to retained 150 $mAhg^{-1}$ even after 100 cycles [121]. Chang et al. prepared a Si based architecture, alternating Si/rGO layers on Ni substrates, improving the mechanical stability and exhibiting outstanding reversible capacity of 2300 $mAhg^{-1}$ at 0.05C plus 700 $mAhg^{-1}$ at the rate of 10C, respectively. It also showed good cycling stability, 6300 $mAhg^{-1}$ at a rate of 10C after 152 cycles and 780 $mAhg^{-1}$with a rate of 3C after 300 cycles. Although the electric and ionic conductivity of Geanatase is better than Si, it also has a large specific capacity but large volume expansion during charging and discharging [122]. Li et al. prepared CGe/graphene composite, with an equal distribution of very fine Ge nanoparticles of size 20–30 nm. Due to the insertion of the Ge between the graphene sheet and the carbon layers, this structure prevents the volume change showing initial specific capacity of 1600 $mAhg^{-1}$ at a rate of 1C which negligibly drop during charging when the rate increase from 0.2 to 5C. The capacity of C/Ge/G composites remains 992.8 $mAhg^{-1}$ after 160 cycles at the rate of 1C, which corresponds to 86.4% of the 2^{nd}cycle, while the Ge/G sample retain 643.9 $mAhg^{-1}$ at the 160th cycle, only retained 64% of the capacity [123]. Kein et al. synthesized graphene on Ge nanowires via using a metal catalyst free CVD route at 7600 °C. The synthesized alloy composite that exhibits a high specific capacity of 1059 $mAhg^{-1}$ after 200 cycles at a rate of 4.0C, which is three times larger than the bare Ge nanowire without graphene coating [124].

Nanomaterial based on SnO_2 also engrossed research courtesy as a potential anode material, because of its specific capacity 1494 $mAhg^{-1}$ that it is almost four times greater than graphite. The well-established reaction involved in SnO_2 depending electrodes is:

$$SnO_2 + 4Li^+ + 4e^- \rightarrow Sn + 2Li_2O \quad (1)$$

$$Sn + xLi^+ + xe^- \rightarrow Li_xSn\ (0 \leq x \leq 4.4) \quad (2)$$

For bulk SnO_2, the Sn produced in a first step is usually reported as irreversible but being reversible for nano-sized particles. Nevertheless,

during Li alloying/dealloying, the volume changes by more than 300% and a very thick SEI is formed in the course of cycling, foremost to a reduction of the electrodes as well as the development of Li_2O, which is an inactive electrochemically. Regarding particle size, Wang et al. and Zhou et al. synthesized SnO_2/RGO (see Fig. 5) and a SnO_2 nanocrystal/nitrogen doped rGO hybrid material (SnO_2NC@N-RGO), respectively, with uniformly distributed SnO_2 in graphene sheets [125,290]. Considering the fabrication methods, Zhang et al. prepared SnO_2/rGO composite using a hydrothermal technique without reducing agent obtaining a specific capacity of 757 $mAhg^{-1}$ after 150 cycles at 200 mAg^{-1} [126]. Li et al. used atomic layer deposition (ALD) technique for the deposition of SnO_2 on graphene nanosheetsthat exhibits a specific capacity after 154 cycles with almost 100% charging efficiency [127]. Table 3 summarized the electrochemical act of composites depending in their formation on graphene as anode materials aimed at Li-ion and Na-ion energy storage technology.

2.3.5. Conversion anode material

In conversion-type electrodes, the active material is totally replaced by Li and produced a Li encompassing compound as well as metal. These materials are usually oxides, sulphides, phosphides, nitrides, and carbides of transition metal. The electrochemical reactions for adaptation response can be inscribed as;

$$Li + M_aX_b \rightarrow aM + bLi_nX \quad (3)$$

Where, M is a transition metal ion with valency n and X is an anion. During conversion reaction, more electrons are there which increased its specific capacity. However, its cycle life is reduced by different factors, such as the formation of unstable SEI and volume changes during cycling as well as its electrical conductivity due to agitation of oxide nanoparticle [151]. In order to avoid the consequences that entails the formation of a SEI, a reduction of the material size produces a heterogeneous phase conversion [152]. Although it is not fully understood that the conversion electrode requires large over-potential to drive the conversion reaction [90], the polarization can be dependent on the electrode fabrication technique [153,154]. Su et al. fabricated 2-D core shell nanostructured (G@Fe_3O_4@C). Having double protection, this structure improves the storage capacity of MO in lithium storage. Because the presence of graphene, it possess high electrical conductivity, large aspect ratio and also tackle the deformation of metal oxide nanoparticles during charging and discharging while overall electrode are highly conductive and active in lithium storage. Remarkably, the material displays excellent rate performance for lithium storage 920 $mAhg^{-1}$ at the rate of 200 mAg^{-1} after 100 cycles [155,156]. Accordingly, to previous sections, the application of this kind of conversion materials can also be extended to Na-ion technology. Table 4 displays the electrochemical performance of graphene-based conversion anode material aimed at Na-ion batteries.

2.3.6. Some 2D carbon allotropes

Not only graphene carbon allotropes also used as anode materials for battery application, these allotropes are graphyne, graphdiyne, graphenylene, Phographene, T-Graphene, Xgraphene, Ψ-Graphene, Pentagraphene etc. 'Graphyne' is a class of two dimensional graphene like materials consisting of one atom thick planar sheets of sp and sp^2 linked carbon organized in a crystal lattice. According to the proportion of acetylene linkages (sp carbon atoms) between carbon bonds (sp^2) in the graphene structure, the graphyne may be one of three distinct (α, β and γ) types. Thus, the structures of α, β and γ graphyne contain 100%, 66.67%, and 33.33% acetylene links, respectivel [322]. In 1997, Haley et al. synthesized graphdiyne substructures, it is planar polymeric networks consist of sp and sp^2 carbon atoms [323]. Linjie et al. reported the effective synthesis of large area graphdiyne films on the surface of copper through a cross-coupling process using hexaethnylbenzene by modifying the Glaser-Hay coupling reaction [324,325]. There are 33.3% sp^2-and 66.7% sp-carbon atoms in graphdiyne, making it a 2D flexible developing carbon allotrope material. The DFT (Local Density Approximation) simulation predicts a bandgap of 0.46 eV for this semiconductor with a direct bandgap of 1.22 eV [326,327]. While the electrons of C═C double bonds are delocalized in graphene, they are

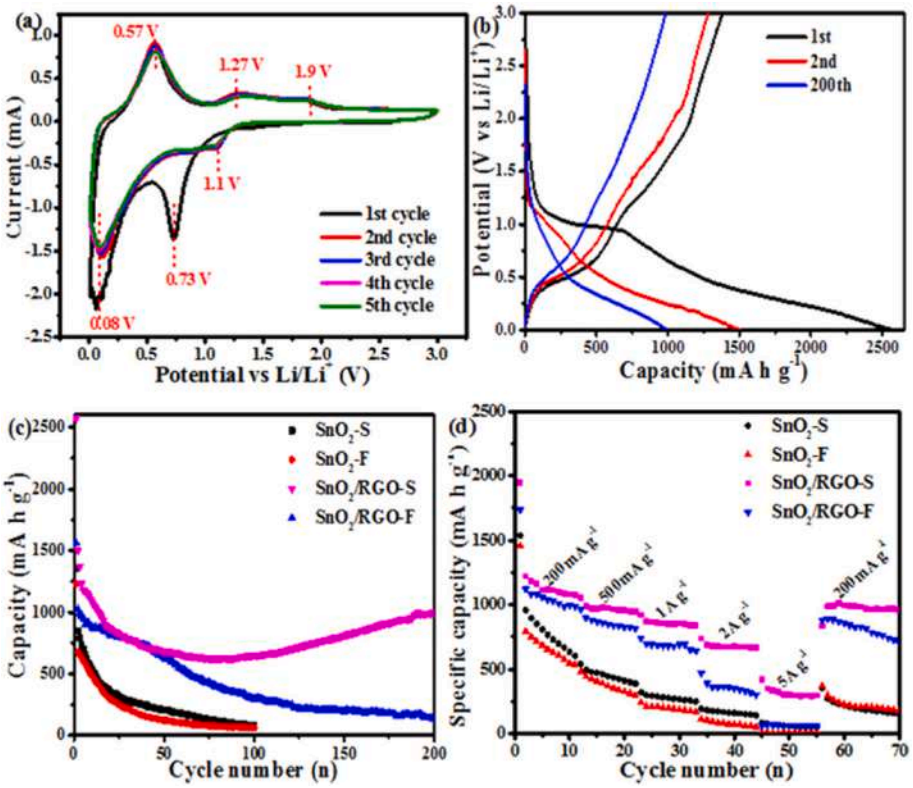

Fig. 5. (a) CV curves of the as-synthesized SnO_2/RGO-S electrode at a scan rate of 0.2 mV s^{-1} in a voltage window of 0.01–3 V aimed at the first five cycles. (b) Galvanostatic charge/discharge curves of SnO_2/RGO-S cycled at a current density of 200 mAg^{-1} at different cycles. (c) Cycling performance of SnO_2–F, SnO_2–S, SnO_2/RGO-F, and SnO_2/RGO-S electrodes at 200 mAg^{-1}(d) Comparison of the rate capability of SnO_2–F, SnO_2–S, SnO_2/RGO-F, and SnO_2/RGO-S electrodes at various current densities. Reprinted with permission from Ref. [290].

Table 3
Electrochemical performance of graphene based composite recently used as anode for Li/Na battery.

Type of Battery	Composite materials	Electrochemical capacity ($mA{\cdot}h{\cdot}g^{-1}$)	Current density ($mA{\cdot}g^{-1}$)	No. of cycles	Ref.
Li-ion	Si@crumpled graphene	940	1000	250	[92]
Li-ion	FeS@reduced graphene oxide	978	100	40	[128]
Li-ion	Sn@N-doped reduced graphene oxide	481	100	100	[129]
Li-ion	Cobalt sulphides/graphene nanosheet	950	100	50	[130]
Li-ion	Si–rGO stratum structure	1500	1350	100	[131]
Li-ion	$NiCo_2O_4$/graphene nanosheets	1267	100	10	[132]
Li-ion	Silicon-nanowire@graphene sheath@reduced graphene overcoat	1650	840	50	[132]
Li-ion	Co_3Sn_2@Co–N-doped graphene	1615	250	100	[133]
Li-ion	Carbon nanofibersbers/silicon nanoparticles@reduced graphene oxide	1048	890	200	[133]
Li-ion	Sn@porous graphene networks	682	2000	1000	[134]
Li-ion	Si/reduced graphene oxide	780	7200	300	[122]
Li-ion	TiO_2 nanotube/N-doped graphene	369	100	180	[135]
Li-ion	Defect-free graphene/Co_3O_4	900	1000	200	[136]
Li-ion	Si/templated carbon-bridged oriented graphene	1390	2000	200	[137]
Li-ion	Graphene–Si	1989	100	200	[138]
Li-ion	Sandwich-structured metal sulfide@reduced graphene oxide	1345	500	400	[139]
Li-ion	Room-temperature synthesized ZnO@GOnanocomposites	660	0.1	100	[140]
Li-ion	10 RGO/Si-600 composite	728	2000	100	[141]
Li-ion	SnO_2–SnS_2@C/NG	944.3	1000	950	[142]
Li-ion	Reduced graphene oxide (RGO)/hexagonal boron nitride (h-BN) nanocomposites (1500C)	~200	1240	100	[143]
Na-ion	FlakyCoS_2andgraphene nanocomposite	192	1000	1000	[144]
Na-ion	FeO_3/gC_3N_4–graphene	980	50	50	[145]
Na-ion	SnO_2–reduced graphene oxide	330	150	150	[146]
Na-ion	Phosphorus/graphene hybrid	1706	260	60	[147]
Na-ion	SbO_x–reduced graphene oxide	409	1000	100	[148]
Na-ion	$NaTi_2(PO_4)_3$ embedded in 3D graphene networks	77	1330	1000	[149]
Na-ion	Sb/multi-layer graphene	405	100	200	[149]
Na-ion	N-doped modified graphene/Fe_2O_3 nanocomposites	428.3	500	100	[150]

Table 4
Electrochemical performance of graphene-based conversion anode material for Na-ion batteries.

Battery	Composite used as anode	First cycle charge/ dischage capacity	High rate Performance	Cycle	Ref.
Na-ion	SnS_2 quantum dots uniformly dispersed on S-doped graphene	795/1141.6 $mAhg^{-1}$	236 $mAhg^{-1}$ at 27 A g^{-1}	92% after 50 cycles	[157]
Na-ion	SnS_2 NC/ EDA–RGO nanosheets	~700 at 1000 mA h g^{-1}	480 $mAh{\cdot}g^{-1}$ at 1000 mA g^{-1}	85% after 1000 cycles	

localised in the thermodynamically stable structure of graphenylene. Through ab-initio Molecular Dynamics (AIMD) simulations, Brunetto et al. verify the viability of synthesizing this graphenylene by selective dehydrogenation of porous graphene. Electronic and physical features (pore structure) could be able to help store atoms and molecules for energy storage devices [324,328]. Both Mandal et al. and Sharma et al. anticipated the existence of 2D carbon allotropes formed of the 5–6–8 carbon rings. These carbon allotropes are referred to as phographenes. These constructions include rings of pentagons, hexagons, and octagon [329,330]. The experimental investigations of defect chains in graphene have shown that it is possible to readily generate polygons such as 5–7 (the Stone–Wales defect) and 5–8 by introducing defects into the graphene. Among all of the several configurations of phographene (α, β, γ, δ, and ε), α, -phographene is the most stable one. It is even more stable than Phagraphene, and its Young's modulus and Poisson's ratio values are comparable to those of graphene. Phographene is metallic in nature and has outstanding thermal and dynamical stabilities even at extremely high temperatures [331–334]. First-principles calculations were used by Liu and his colleagues to theoretically indicate the existence of an energetically metastable (up to 700 K) and dynamically stable 2D tetrasymmetrical carbon with tetra-rings termed T-graphene. Both the planar and buckled descriptions are applicable to it. These two systems have formation energies that are equivalent to graphite. The negative formation energies of these two systems are 8.73 and 8.41 eV per atom, respectively [335,336].

3. Transition metal dichalcogenides

Based on the interesting physical in addition to chemical features of graphene, various two-dimensional (2D) materials, for instance, hexagonal BN, transition metal dichalcogenides (TMD), silicene, germanene, or phosphorene have been also investigated. Among them, TMDs become potential candidates for energy storage devices because of their high surface-to-volume ratio as well as internal surface areas. TMDs are of the form of MX_2, in which M is a transition metal, and X is a dichalcogenides. TMD materials are composed of many stacked layers, which are connected by weak Vander Waal forces. Consequently, exfoliation or CVD process is common techniques to synthesize single or few layers TMDs. They present excellent properties including electrical, magnetic, optical, and mechanical, suitable for different applications.

Herein, we have explored the different fabrication techniques, properties as well as applications of TMDs as anode for different metal ions batteries.

3.1. Synthesis method of TMD and its derived materials

In general there are four method used for synthesis of TMD and its derived materials. These methods are as follows: Mechanical exfoliation method, Liquid exfoliation method, Sulfurization (or selenization) of metal (or metal oxide) thin film, Vaporization of metal oxide with chalcogen precursor, and Femtosecond laser irradiation method.

3.1.1. Mechanical exfoliation method

Yin et al. used mechanical exfoliation method to fabricate the single layer MoS_2 for phototransistor. In this method a single layer of MoS_2 deposited on the substrate of Si/SiO_2 using scotch-tape mechanical exfoliation process [308].

3.1.2. Liquid exfoliation method

Large amounts of TMDs nanosheets are required to fully realize the tremendous potential of these stacked materials. A solution processing technique would be more ideal for obtaining large volumes of single- or few-layer TMDs nanosheets. Zeng et al. prepared high yield, single layer TMDs using electrochemical lithiation process. In this process they have used TMDs bulk materials as cathode in electrochemical cell and intercalation of Li is controlled during discharge process. After getting the intercalated compound, to produce high-grade TMDs single-layer materials in large quantities, the intercalated compounds can be ultrasonicated and exfoliated in water or ethanol [309].

3.1.3. Sulfurization (or selenization) of metal (or metal oxide) thin film

TMDs materials must be grown on a huge scale for real device applications. To apply TMDs materials to real devices, their large scale growth is essential. The most efficient approach to achieve large-area growth is by chemical vapor deposition (CVD). This approach is divided into two types first one is sulfurization (or selenization) of metal thin films and second is vapor phase reaction of metal oxides with chalcogen precursor. Song et al. used this approach for synthesis of WS_2 nanosheets. In this method WS_2 nanosheet fabricated on SiO_2 substrate by using sulfurization of WO_3 film. Here, WO_3 film prepared by atomict layer deposition method. Number of layers of produced WS_2 nanosheets is controlled by the number of cycles of sulfurization of WO_3 [310].

3.1.4. Vaporization of metal oxide with chalcogen precursor

Nazmaei et al. synthesized MoS_2 nanosheets using vapor phase deposition using MoO_3 metal oxide and sulfur as precursore and reactant materials. To control the thickness layers of MoS_2, concentration of MoO_3 nanoribbons varied on a substrate however, other parameters taken as constant [311].

3.1.5. Femtosecond laser irradiation method

An et al. used the same process to fabricate the high quality few layer of TMDs by femtosecond laser irradiation. This method indicates that TMDs can be exfoliated from bulk to few layers (up to 3 layers). This method is very fast and significantly easier than other method [312].

The examination of MoS_2 nanosheets using transmission electron microscopy (TEM) and high-resolution transmission electron microscopy (HRTEM) is shown in Fig. 6.

Xia et al. synthesized ultrathin MoS_2/N-graphene composites by using simple and facile technique. Fabricated ultrathin nanosheet of MoS_2 is uniformly distributed on the N-dopped graphene by using reduction and functionalization process [160]. Microstructures of MoS_2nanosheet are observed by HRTEM are founded in Fig. 7.

3.2. Properties of TMDs

3.2.1. Composition of TMDs

A transition metal from groups 4–10 (M) and chalcogens (X = S, Se, and Te) make up TMD materials. A layered structure is generally found in TMD comprised of metals from groups 4 to 7, while metals from groups 8 to 10 are non-layered. There are six to seven layers of TMDs, each of which is a hexagonally packed layer of metal atoms surrounded by weak van Der Waals forces [161]. For the TMD bonding states, transition metal atoms provide four electrons and chalcogen atoms provide two electrons. For TMD, the bonding length is between 3.15 and 4.03 Å, depending on the size of the transition metal and the chalcogen

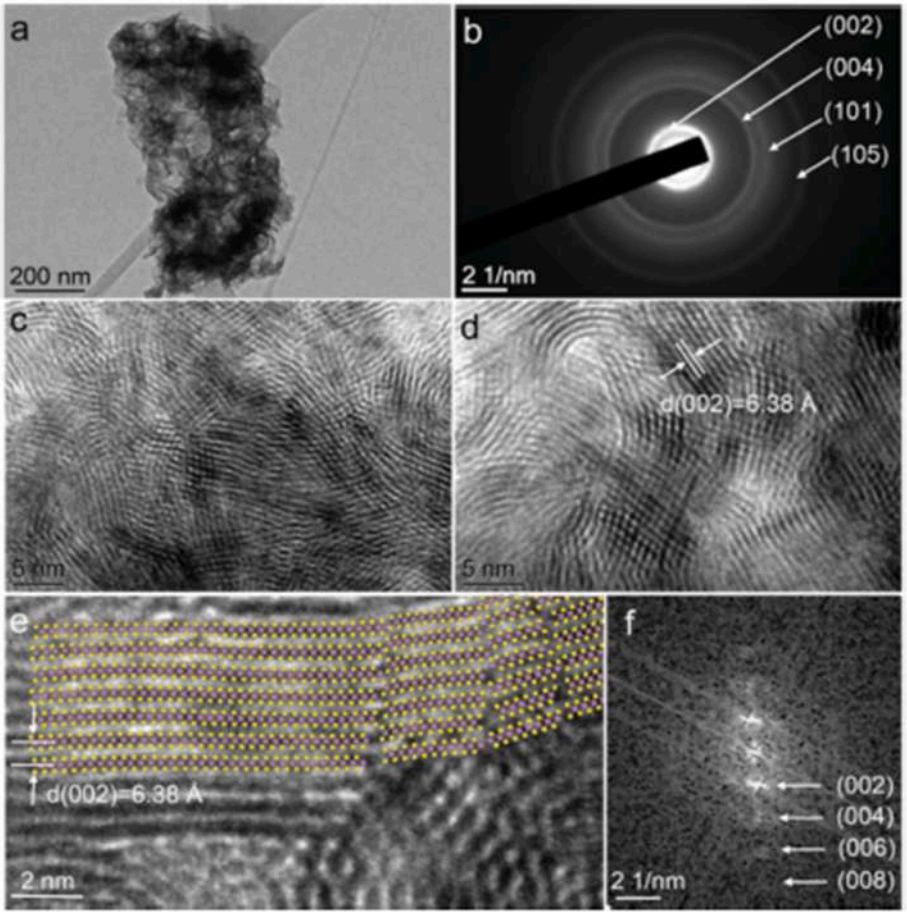

Fig. 6. (a) Low magnification image of MoS_2 nanosheets, (b) selected area electron diffraction pattern, (c, d) are magnified image of MoS_2 nanosheet, (e) HRTEM image of resolved lattice, (f) fast fourier transform of MoS_2 nanosheet. Reprinted with permission from Ref. [159].

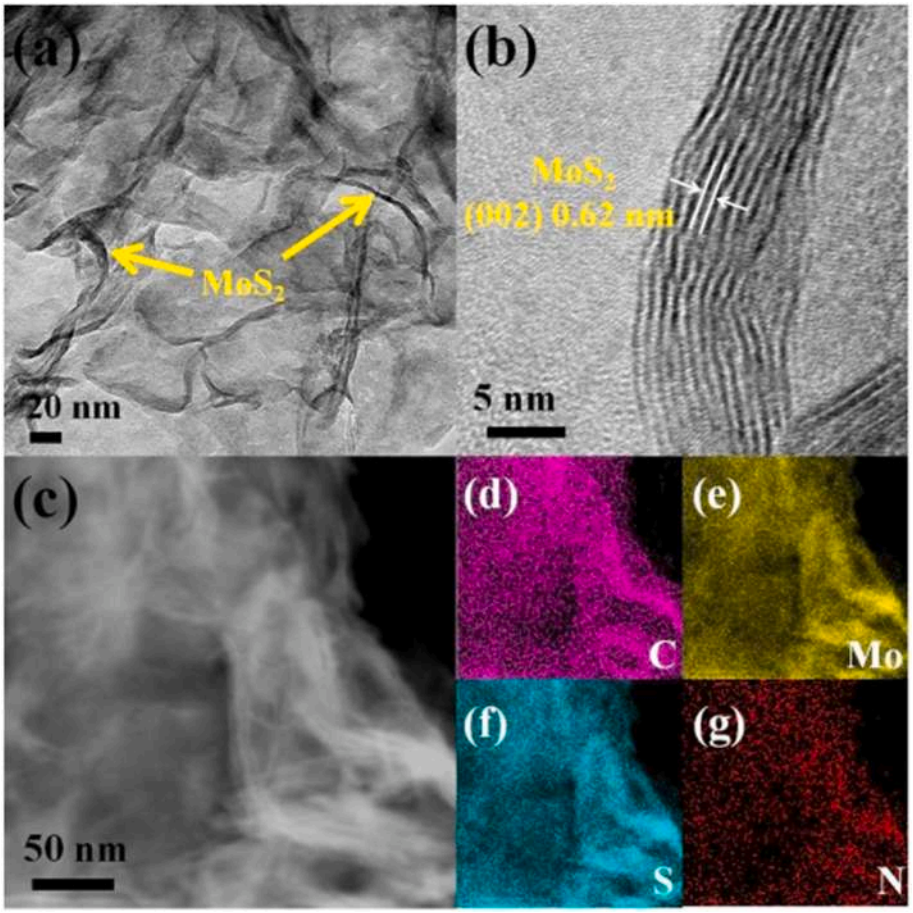

Fig. 7. (a) As well as (b) show the HRTEM appearance of MoS_2 nanosheet, (c) STEM image, in addition to (d)–(g) elemental mapping of anchoring MoS_2 nanosheet anchoring on N-dopped graphene nanoshete. Reprinted with permission from Ref. [160].

atoms utilized.

3.2.2. Mechanical properties

Castellanos-Gomez et al. investigated the elastic features of MoS_2 containing 5–25 layers, showing that the Young's modulus lies between 0.33 ± 0.07 TPa [162]. Bertolazzi et al. also calculated the breaking strength and stiffness ofsingle and bilayer of MoS_2 produced by exfoliation method, the stiffness constant and the Young's modulus of elasticity being 180 ± 60 Nm and 270 ± 100 GPa, respectively. It was also reported that the strength of the monolayer membrane was 11% of the Young's modulus. This crystalline and almost defect-free materials is suitable aimed at a diversity of tenders as well as especially for flexible electronic devices [163].

3.2.3. Electrical structure and optical properties

TMDs show different electronic properties depending onthe substantial of non-bonding d-bands as of the group of 4–10 elements while it shows the metallic properties when its d band is partially filled. Although chalcogen atoms do no contribute to the electronic properties when compared to the metal, it reductions the bandgap when the atomic number of chalcogen increases [161]. TMDs in bulk show an indirect bandgap [164,165], showing negligible photo-luminescence (PL) signal when MoS_2 was explored irradiated by white light. However, few layers of MoS_2 presents a pronounced emission at ~670 and ~627 nm [166], depending the intensity of PL signal on the number of layers present in TMDs [166,167]. Besides, two main peaks are perceived for Si/SiO_2--sustained MoS_2 at 1.85 eV (670 nm) in addition to at 1.98 eV (627 nm), respectively. Benameur et al. used broadband green illumination to differentiate the single, bi and tri-layer of MoS_2 and WSe_2 on a 90/270 nm SiO_2 through gauging the contrast [168]. The same technique was also applied via Li et al. to distinguish the single to tri-layer MoS_2 nanosheets fabricated on 300 nm SiO_2 substrate by using optical microscopy [165]. Some researchers also used the intensity difference method to investigate the number of layers between the MoS_2 nanosheets and SiO_2 layers.

3.3. Transition metal dichalcogenides as anodes for Li, Na and K ion batteries

According to the aforementioned properties, TMDs have strained noteworthy curiosity by way of a latent chemically active materials as compared to the standard carbon based anode material (graphite) [169]. Su et al. prepared ultrathin few layer MoS_2 nanosheets of thickness nearly equal to10 nm. For the synthesis, a simple and scalable exfoliation technique was used [159]. TMDs exhibits Li ion storage capacity (~800–1000 $mAhg^{-1}$) in contrast of graphite anode (372 $mAhg^{-1}$) [170,171]. Among all possible options, MoS_2 and WS_2 are the most attractive anode materials aimed at Li-ion battery. The layered structure of MoS_2 is similar to graphite, with a double theoretical capacity in addition to outstanding cycle stability. In addition, for Li ion intercalation/deintercalation interlayer distance is ~ 0.6 nm that is larger than in graphite [172]. Nanostructured MoS_2shows better capacity than bulk MoS_2 because it has more storage holes for Li ions over a larger surface area [173–177]. Farabi et al. prepared MoS_2 nanopowder (MoS_2-NP) via the so-called self-propagating high-temperature synthesis (SHS) investigating the electrochemical properties. Jing et al. explored the adsorption plus diffusion characteristics of Li ion on VS_2 monolayers. It was concluded that VS_2 exhibits an electrochemical capacity of 466

$mAhg^{-1}$ with an open circuit voltage of 0.9 V [176]. Chang et al. synthesized MoS_2/graphene nanosheet composites with a specific capacity of ~1300 $mAhg^{-1}$ for LIBs. MoS_2/GNS composites show a charge/discharge capacity of 2200/1300 $mAhg^{-1}$with a large reversible specific capacity of 1290 $mAhg^{-1}$ after 50 cycles in comparison to the free electrode of MoS_2 after 50 cycles [178]. It has also been proved as MoS_2/GNS composites have large capacity (1040 $mAhg^{-1}$) at 1000 mAg^{-1}. It also shows extraordinary cycling performance, when current changes from 1000 mAg^{-1} to 100 mAg^{-1}, the specific capacity of the MoS_2composite revenues to 1300 $mAhg^{-1}$ [178].

Darwin et al. investigated the monolayer VS_2 polytypes as potential material for Na ion battery using DFT and found that VS_2 does not change its structure during phase transition in cycles of charging and discharging hence providing better stability than other TMDs. It was also found that V top and H center sites of VS_2 polytypes are both favorable adsorption sites for Na and it was found that 1H phase is stronger. Finally, it was reported that 1H phase has specific capacity of 232.91 $mAhg^{-1}$and 1-T phase has 116.45 $mAhg^{-1}$ also, 1H phase has better OCV [199]. Zhang et al. used first principle technique to explore the capacity of VS_2 and TiS_2 as potential candidates for anode material for potassium ion battery (KIBs) with optimal open circuit voltage (1.2–1.34 eV v/s. K^+/K) of electrochemical capacity of 278 $mAhg^{-1}$ in addition to 282 $mAhg^{-1}$, respectively [179].

Due to large density of active sites and auspicious supplement and abandonment of Li/Na ions sideways the planar route and governor on the crystal structure, TMD exhibits stable cycling performance. Zhang et al. synthesized MoS_2 nanobelts and found that they present large active sites, short ions diffusion distances and stable structure during charging and discharging. When used for LIBs, it is found that they exhibit 820 $mAhg^{-1}$ and 480 $mAhg^{-1}$ at the rate of 1 and 20 Ag^{-1}, respectively after 100 cycles. Nevertheless, for SIBs they exhibit 520 $mAhg^{-1}$ and 380 $mAhg^{-1}$ at the rate of 1 and 20 Ag^{-1} after 100 cycles, respectively [180]. Ning et al. synthesized Molybdenum ditelluride nanosheets encapsulated in a few layers of graphene by using simple heating method by using Te and Mo powder subsequently ball milling with graphite. The prepared $MoTe_2$/FLG exhibits excellent reversible capacity 596.5 $mAhg^{-1}$ at 100 mAg^{-1} and 334.5 $mAhg^{-1}$ at the rate of $2Ag^{-1}$. Moreover, the capacity remains constant after 400 cycles at a rate of 0.5 Ag^{-1} [181]. Cao et al. synthesized a novel heterogeneous nanowire array of TiO_2–B@VS_2 on Ti foil by using two-step hydrothermal process and used as additives-free anodes for LIBs. This structure exhibits reversible capacity of 365.4 $mAhg^{-1}$ at the rate of 1C after 500 cycles [182,183]. Zhang et al. discovered the electrochemical potential of 2D MoN as anode material for Li ion battery using first principle theory, concluding that for single Li ion, the adsorption energy is −4.04 eV and it exhibits maximum capacity 406 $mAhg^{-1}$ [184]. Table 5 demonstrates the electrochemical performance of the transition metal dichalcogenides as anode material aimed at Li/Na/K-ion batteries.

Table 5
Electrochemical performance of the transition metal dichalcogenides as anode material aimed at Li/Na/K-ion batteries.

Battery	Composite	Capacity ($mAhg^{-1}$)	Current density	Cycle	Ref
Na-ion	MoS_2/rGO composite	512	1844.1	83% after 20 cycles	[185]
Na-ion	$MnTe_2$	130	–	–	[184]
Li-ion	MoS_2Embedded in Carbon Nanofiber	985	100	–	[183]
Li-ion	Defects-rich few layers nanocomposites	1000	0.5	Remains constant after 100 cycles	[186]
Na-ion	$MoS_{2(1-x)}Se_{2x}$ MoS_2@LEGr heterostructures few layer	387	100	–	[187]
Na-ion	ZnSe/MWCNT	447	500	83% after 80 cycles	[188]
Li-ion	(NiSe/rGO)	1125	50	Gradualy increases for first 50 cycles	[189]
Na-ion	Decorated NiSe nanoparticles reduced graphene oxides (NiSe/rGO)	423	50	89.4% after 50 cycles	[189]
LI-ion	ZnS–TiC–C	613	100	~85% after 600 cycles	[190]
K-ion	WS_2	60	500	~90% after 400 cycle	[191]
K-ion	VS_2 and TiS_2	278/282	–	–	[179]

4. MXene synthesis, properties & battery applications

At Drexel University, 2D transition metal nitrides and carbides called as MXene were developed [26]. In 2011 Naguib et al. prepared the first 2D titanium carbide (Ti_3C_2Tx) leadingto the MXenes family [33,192]. In general, MXene was prepared through discerning etching of "A" layers from MAX stage. Furthermore, the general formula of MAX phase is $M_{n+1}AX_nT_x$ where (n = 1–3). "M" is used for early transitional metal (such as Ti, V, Mo, Sc, Nb, etc.), "A" is an element of group IIIA or IVA (such as Al, Ga, Si or Ge), "X" represents the carbon/nitrogen ratio and "T" represents the surface functional group which are attached on the surface during selective etching process such as O, OH and/or F. Although it has been also reported the MXene having surface termination of Cl [27,28].

However, MAX phases can also be synthesized by using solid solutions of "M", "A" and "X", such as $(Ti,Nb)_2AlC$ [29], $Ti_3(Al_{0.5}Si_{0.5})C_2$ [30] and $Ti_2Al(C_{0.5}N_{0.5}$ [31]. Efforts are being deboted to prepare fluorine free MXene. Tengfi et al. reported an alkali assisted hydrothermal method to prepare $Ti_3C_2T_x$ (T = –OH, –O) where the whole method is free from fluorine [194].

4.1. Synthesis of MXenes

To produce high quality and controlled structure, CVD is used in bottom up approach. However, CVD is not suitable for MXenes preparation because it produces thin layers instead of a single layer. Xu et al. used CVD to yield thin films of Mo_2C, Tungsten carbide (WC) in addition to tantalum carbide (TaC), finding that the thinnest Mo_2C presented having six layers [195]. Top-down approaches are divided into mechanical strips and chemical strips [193]. Therefore, top-down approaches for MXenes mainly consists of (i) Etching (ii) Exfoliation.

4.1.1. Top-down approaches

4.1.1.1. Etching. Almost all-2D material undergo exfoliation processes when extracted from bulk layer materials, as they present a robust in-plane bond besides weak out-of-plane bond [196–198]. In general, 2-D materials as graphene, dichalcogenides, or boron nitride have been produced by mechanical approaches such as ball milling, scotch tape shearing, etc. In 2013, Nicolosi et al. used mechanical exfoliation to synthesize MXene from MAX phase, however they could not able to break the metallic bonds M-A [199]. Therefore, the wet chemical etching procedure for MXene synthesis from their MAX phase is preferred. In 2011, Naguib et al. produced the first MXene, titanium carbide (Ti_3C_2) by using hydrofluoric acid (HF) selective etching to remove the Al from its precursor Ti_3AlC_2 (MAX) [33]. Generally, fluoride based etchant is used for selective etching of A due to its selectivity to etch the A element from its MAX phase. In general, the produced MXene surface is not pristine, functionalization depending on the synthesis approach and etchant used for selective etching [33,200–202]. Properties of MXene such as band structure, chemical reactivity and optical absorption depends on the surface functionalization of Fluorine (F), hydroxyl (OH), and oxygen (O) [203–206]. To date, about 70

MXene have been reported, although it is predicted that in future MXene becomes one of the mostly evolving family of 2D material [199,204,207,208].

HF Etchants: Naguib et al. first used HF etchant of concentration 50% on a layered precursor (e.g. Ti_3AlC_2) to the M–A metallic bonds resulting in etching of the Al layer from Ti_3AlC_2 [33]. For selective etching with fluorine-containing etchants the involved reaction is

$$Ti_3AlC_2 + 3HF \rightarrow AlF_3 + (3/2)\ H_2 + Ti_3C_2 \quad (4)$$

During this reaction, the aluminum layer between the individual Ti_3C_2 layers is removed, which results in the defeat of metal bonds among Ti as well as Al [209]. Besides, the coverage time of Ti_3AlC_2 in HF varying from few hours to days plus the temperature changing from (220–500 °C) depending on the precursors [207]. Since many coated forerunners exist with dissimilar constructions in addition to configurations, not only etching time, concentration and temperature varied, synthesis via selective etching of Al is also varied. Mashtailer et al. used HF as an etchant for the extraction of Al from Ti_3AlC_2, and it was found that less than 2 h of exposure time is sufficient [210]. Moreover, Sang et al. concluded that the concentration of HF also affects the defect concentration of the synthesized materials [211]. In general, thinner $M_{n+1}AX_n$ requires less exposure time to HF etchant as compared to the thicker counterparts. Zhou et al. and Tao et al. synthesized new MXene (Hf_3C_2 and $Mo_{1.33}C$) from its MAX phase $Hf_3(AlSi)_4C_6$ and $(Mo_{0.67}Sc_{0.33})_2AlC$ using HF as an etchant [212,213]. Wang et al. showed that the MXene produced by selective etching with HF acid shows large exteriors completed with –F and –OH compared to –O groups and it does not depend on the concentration of HF [214].

HF-Forming Etchants: Since HF is harmful and dangerous to the atmosphere, new substitutes to reduce the amount of HF are being explored. HF can be shaped by reaction of fluoride salts with acid or by the hydrolysis of alkaline biflouride salts. Feing et al. used sodium and potassium bifluoride and ammonium bifluoride to form HF as an etchant for discerning design of Al as of its MAX phase precursor Ti_3AlC_2 to synthesize the Ti_3C_2 [215]. Ghidiu et al. used LiF with HCl to synthesize Ti_3C_2 [216]. When HF is used as etchant, the produced MXene exhibits smaller interlayer spacing, however when HF-forming etchants are used, it shows large interlayer spacing due to intercalation of cation of salts which is used for the preparation of etchants. However, this route has taken less time to achieve delamination but the major issue comes at the time of scalability, since produced MXene contains unetched MAX phase [208,216].

HF-Containing Etchants: Shahzad et al. used etchants aimed at the creation of MXene depending on acid mixtures of HF/HCl instead of LiF/HCl which contains a lesser attentiveness of HF (5–10 wt%) to synthesize Mo_2TiC_2 and $Mo_2Ti_2C_3$ from Mo_2TiAlC_2 and $Mo_2Ti_2AlC_3$MAX phases, respectively [217]. Also, addition of tetrabutylammonium hydroxide solution (TBAOH) inside Mo_2TiC_2 and $Mo_2Ti_2C_3$ MXenes, results a stable colloidal solution of MXene [217]. This method is more controllable and more beneficial, however it requires less amount of etching ingredients than etching with HF alone.

Alkaline and/or Hydrothermal Treatment: Since alkali's formed strong bonds with Al, alkaline etchants may be used for the etching of Ti_3AlC_2 or other layered precursors. In some cases, higher temperature and pressure are also required due to the strong affinity of alkalis with third group elements. Xuang et al. etched Ti_3AlC_2 powders for 30 min in little concentrated (10–20 wt %) HF solution, then they immersed the resulted Ti_3AlC_2 in tetramethylammonium hydroxide solution (TMAOH), which produced the Ti_3C_2 [218–220]. It was also found that the formed Ti_3C_2 surface is terminated with aluminium oxide/hydroxide layers; therefore it was required additional steps to clean the surface. Liu et al. used the hydrothermal process for the fabrication of Nitrogen-doped Nb_2CT_x MXene. The fabrication of N–Nb_2CT_x was divided in two steps; first, the layered Nb_2CT_x MXene was fabricated by immersing Nb_2AlC MAX powder into a concentrated solution of HF under continuously stirring for 90 h at room temperature and a pH value up to 6. The produced Nb_2CT_x suspension was washed, centrifuged, filtered and dried at room temperature under vacuum condition. The c lattice parameters for $NeNb_2CT_x$, Nb_2CT_x MXene and Nb_2AlC MAX are 34.78 Å, 22.32 Å, and 13.88 Å, concluding that the interlayer spacing increases with nitrogen doping [221].

Thermal-assisted electrochemical etching: Sin et al. established a thermal-assisted electrochemical etching (E-etching) process, which can be considereda safer and more gentler method than the traditional HF etching. After the preparation of MXene (Ti_2CT_x) with the E-etching method with diluted HCl, it was found that the structural and surface properties of the prepared MXene varied with varying etching condition. This method is also used to produce MXenes (e.g. V_2CT_x and Cr_2CT_x up to 25 nm and a flower-like architecture.

Selective etching of Ga, Si, and other A elements: Since Al has the lowest reduction potential compared to additional A elements: Si, Ga and Ge, most of theMXene are derived from Al containing MAX phase in HF containing solution. Due to the limited quantity of Ti_3AlC_2 and costly manufacturing, Ti_3SiC_2 is the most studied MAX phase due to its availability in large quantities and less expensive than Ti_3AlC_2. At the first stage 80 mL of colloidal black solution of exfoliated MXene is taken, (if diluted its colour is green) collected after centrifugation at 3500 rpm (4500 g) for 30 min.

4.1.1.2. Exfoliation. The exfoliation techniques used to exfoliate the MXene depend on two factors (i) Etching method (ii) Composition of MXene. Naguib et al. found that exfoliation using direct sonication of multilayer MXene produced by HCl/LiF results in small yields [33]. The yield has been increased by using liquid exfoliation followed by intercalation of molecules, which results in 20 mg mL^{-1} of MXenes [222–224]. M. Ghidiu et al. used alkylammonium cations for the intercalation to obtain single nanosheets on large scale [223]. Anasori et al. and Mastalir et al. used polar organic molecule dimethyl sulfoxide (DMSO) as an intercalant in the direction of exfoliating $Ti_3C_2T_z$ and $(Mo_{2/3}Ti_{1/3})_3C_2T_z$ [224,225]. In addition, the d-spacing is further increased to 22.4 Å with the co-intercalation of water. The use of DMSO is only restricted to the two compositions aforementioned, in the case of Nb_2CT_z, the exfoliation takes place by using intercalation of isopropylamine [226]. Naguib et al. proved that the exfoliation using tetrabutylammonium hydroxide are frequently applied as intercalant for the other 2D material by producing V_2CT_z and Ti_3CNT_z [227]. In this method, TBA^+ ions intercalate in the space and increase the d−spacing. This method is also used to exfoliate $(Mo_{2/3}Ti_{1/3})_3C_2T_z$ and $(Mo_{1/2}Ti_{1/2})_4C_3T_z$, $Ti_4N_3T_z$, Mo_2CT_z [33].

Mashtalir et al. found that TBAOH did not exfoliate $Ti_3C_2T_z$ but TMAOH [226]. HCl/LiF etching methods are used not only to reduce the concentration HF along with its hazardous effect, it also increases the interlayer spacing due to the intercalation of Li^+ ion combined with its shell hydration between the interlayer space which helps in exfoliation also. M. Ghiddu et al. found that the after etching, the d-spacing between interlayer in dry condition is close to 13 Å which is 3 Å more than the multilayers etched with HF alone [216]. The same group observed that the co-intercalation of water in between the wet multilayer increases the d spacing up to 16.5 Å and exfoliate each layer separately [222]. Furthermore, spontaneous exfoliation is observed with washed and etched via HCl/LiF solution at 6 pH value [216]. Sonication also increases the produced amount. Maleski et al. explored the dispersion behaviour of $Ti_3C_2T_z$ in organic solvent and it was found that for dispersing of $Ti_3C_2T_z$, the polar solvents are better than the non-polar ones [228]. Commonly, colloids and centrifuging process are used to exfoliate the multilayers sheet. Once the colloidal suspension of monolayer or multilayer sheet is obtained, it can be treated in various ways for the fabrication of thick films (typically it is in the range of few microns). Spray or spin coating is also used to obtain the thin films (below 100 nm) [229–232]. Collini et al. applied electrophoretic deposition to form thick

films [233]. Fig. 8 depicts the schematic of the fabrication of Ti_3C_2 (MXene) by selective etching of silicon from its layered MAX phase [288].

4.1.2. Bottom-up preparation of 2D transition metal carbides as well as nitrides

For the mass production of synthesis of pristine MXene, functionalized carbide and nitrides top-down approach is used. However, during etching process, MXene surface is completed with several well-designed groups such as –O, –OH as well as –F introducing defects [207]. Mechanical vibration or sonication also reduces the size, which results in more defective structures. These chemical and mechanical damages to MXene hampered research into the unique properties of 2D TMC and TMN. It is found that the only M_2X, M_3X_2, and M_4X_3 structures are produced by using top-down method [207]. Synthesis of TMC and TMN based MX structures such as MoC, MoN, NbC, and NbN, etc. are not possible with top-down synthesis methods. The excellent properties exhibited by bulk MX structures based on TMC and TMN make them suitable for potential application as superconductors. Moreover, WC exhibits semi metallic property with Dirac cone [234]. As consequence, researchers are working to improve the quality of 2D TMC and TMN family by developing various synthesis approaches.

In contrast to the top-down synthesis approach, the bottom-up approach is suitable for synthesizing large areas of great superiority 2D material. In addition, this technique is more flexible and can be used for the growth of 2D material based heterostructures. Moreover, these methods also allowed the growth of non-layered materials. Various bottom-up approaches have been aimed at the fabrication of diverse 2D TMCs in addition to TMNs through CVD, template approaches, and plasma chemical vapor deposition methods (e.g. PEPLD).

Chemical Vapor Deposition: Xu et al. first described high-quality ultra-thin 2D TMC crystals. Two ultra-thin metal foils of Cu and Mo were used as a substrate. First, both metal foils are stacked and heated to more than 1085 °C in presence of H_2. During this step, Mo diffuses on the surface of Cu. After that, CH_4 in very low concentration was introduced to provide the C atom, which results in 2D Mo_2C crystals on the Cu [195]. 2D crystals produced by this method exhibit 10 μm in lateral size with thickness 3–20 nm. They have found that the thickness in addition to lateral size of the created 2D α-Mo_2C crystals depends on the growth time and temperature. Importantly, produced 2D crystal can be transferred to the other substrate by using 0.2 M $(NH_4)_2S_2O_8$ as etchant. Geng et al. used the similar procedure to fabricate 2D Mo_2C crystals of different shapes by changing temperature (1100 °C), thickness of copper foil (50 m), and concentrations of CH_4 [235]. It was found that when the concentration of CH_4 was 0.1 sccm, fabricated Mo_2C crystals have fractal shape. When the concentration of CH_4 increases, the shape of the crystal changes from fractal to hexagonal. When the thickness of the copper foil increases, thinner crystals of Mo_2C are obtained [236]. Qi et al. used the same method to fabricate a mono-atomic layer of rhenium carbide (ReC). Re (0001) was used as a substrate with C_2H_4 as carbon source under ultrahigh vacuum condition. After the formation of graphene at 903 K, it begins to decompose when the substrates are heated to 953–1113 K. Then the decomposed carbon atoms melted in Re throughout the cooling route, forms 2-D ReC crystals with a periodic "flower-like" superstructure [237].

Chemical Vapor Deposition Growth of Graphene/2D TMC Heterostructures: Since CVD technique is generally applied for preparation of high-quality graphene films on copper foils, there are two methods of growth of graphene/2D TMC structures (i) Direct or one step method and (ii) two-step process. Deng et al. used the direct method shown in Fig. 9 aimed at the growth of vertical graphene (top)/2D α-Mo_2C (bottom) heterostructures [238].

It was found that this method required more concentration of $CH_4$for the growth of 2D TMCs. Geng et al. used one-step CVD method for the fabrication of 2D α-Mo_2C graphene heterostructures [239]. Similarly, Xu et al. manufactured vertical graphene α-Mo_2C heterostructure via two-step CVD method with high purity. In a first step, graphene was developed on the Cu/Mo substrates at the temperature (1070 °C), less than the melting point of Cu [195]. It was also found that the 2D α-Mo_2C crystals plus graphene exhibits the similar crystal lattice. Zeng et al. also used the same technique to obtain the 2D in-plane WC–graphene (i-WC-G) heterostructures. Droplet of Ga was used in place of Cu foil in addition to CH_4 as a carbon basis at 980–1020 °C and based on AFM measurements dimension of the 2D i-WC-G heterostructure were ~1 0.36 nm thick [240].

Template Method: Along with CVD, template routine is additionally applied for the progress of 2D TMCs and TMNs, being the one that produces large yields. In this system, 2D transition metal oxides (TMOs) nanosheets are applied as templates, that are carbonized or nitride according to the TMO based TMCs and TMNs structure [241,242]. Hexagonal MoN, (h-MoN) nanosheets have been synthesized using salt-templated method as shown in Fig. 9. In this method, TMO coated with NaCl are synthesized by annealing of Mo at 280 °C as depicted in Fig. 9(a) Similarly, to synthesize the 2D MoN@NaCl powders, MoO_3@NaCl crystals initially ammoniated by NH_3 at 650 °C. Finally, to obtain the 2D MoN nanosheets (NS), NaCl is washed out by deionized water. From (XRD) patterns it is found that the 2D MoN NSs have hexagonal lattice structure with lattice constants a = b = 5.75 Å and c = 5.62 Å (Fig. 9(b)). Similar to the etching method, it can be also discrete in water faster by Tyndall effect, as shown in Fig. 9(c). It was concluded that the obtained 2D MoN nanosheet is laterally uniform of thickness 71 nm (Fig. 9(d) and (e)). This method is also used for the synthesis of 2D WN and VN NSs. Joshi et al. synthesized 2D layered δ-MoN NSs via applying a two-step method exposed in (Fig. 9(f)). In first step, hot-filament CVD (HFCVD) process was used to synthesize highly aligned 2D layered MoO_3 nanosheet. In the second step, produced MoO_3 NSs is ammoniated in presence of Ar at 700 °C for 8 h resulting in 2D δ-MoN NSs. When 2D layered MoO_3 NSs ammoniated, due to nitridation changes from bluish to dark blue. It was found that the produced 2D δ-MoN NSs have lateral size 20–30 m and a thickness of 5–40 nm as

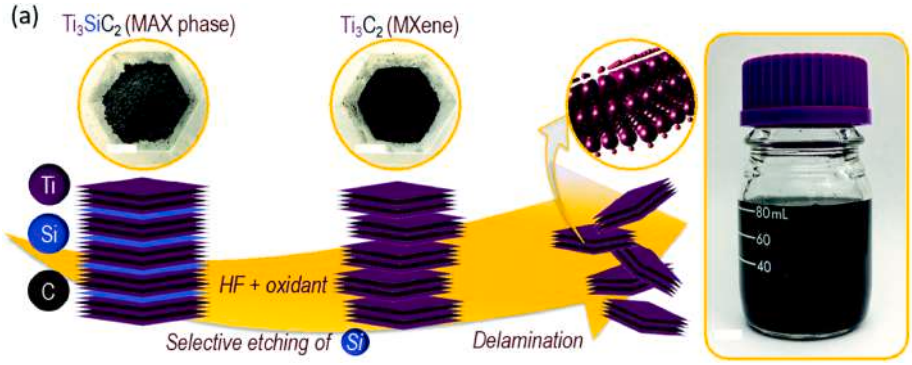

Fig. 8. Schematic representation of the synthesis of Ti_3C_2 (MXene): Synthesis of MXene was achieved via selective etching of silicon from its layered MAX phase (Ti_3SiC_2) by using etching solution which consists of HF and an oxidizing agent (H_2O_2 or $(NH_4)_2S_2O_8$ or HNO_3 or $KMnO_4$ or $FeCl_3$). The precursor MAX powder exhibits a grayish-to-silverish color (top left). Reprinted with permission from Ref. [288]. (For interpretation of the references to color in this figure legend, the reader is referred to the Web version of this article.)

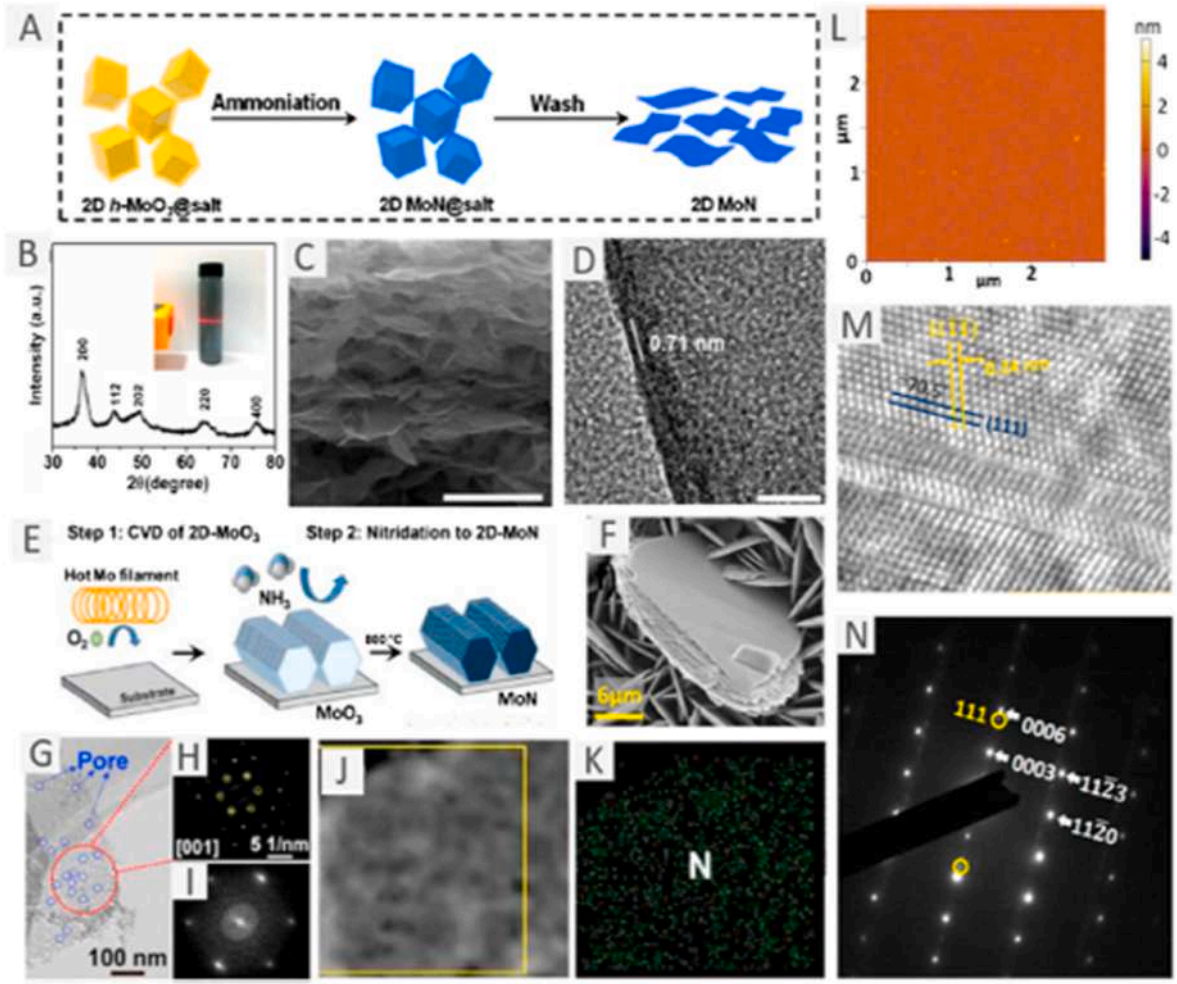

Fig. 9. 2D MoN as well as N-doped Mo_2C prepared via template scheme. (a) Representation of combination process of 2D MoN, (b) XRD pattern of 2D MoN powder, the inset displays the Tyndall effect of the 2D MoN colloidal dispersion in water, (c) SEM image of 2D MoN NSs. The scale bar is 500 nm, (d) HRTEM image of the edge of a 2D MoN nanosheet. The scale bar is 5 nm, (e) Schematic representation of the two-step procedure for synthesizing 2D layers of δ-MoN, (f) Photographs of MoO_3 and δ-MoN grown on a FTO-coated glass substrate, (g) Top-down SEM images of vertically aligned 2D layers of δ-MoN synthesized on FTO substrates, (h) SEM images of MoO_2 NSs (top) and N–Mo_2C NSs (bottom). (i) Thicknesses characterized by AFM and crystal models of N–Mo_2CNSs. (j)–(l) TEM image (j), the corresponding electron diffraction pattern (k), and fast Fourier transform (l)–(n) of N–Mo_2CNSs. (Panels (a)–(d) are reprinted with permission from Ref. [241], Panels (e)–(f) are reprinted with permission from Ref. [243], Panels (g)–(k) are reprinted with permission from Ref. [242]. Panels (l)–(n) are reprinted with permission from Ref. [245].

shown in Fig. 9(g) [243]. Instead of MoO_3 NS, MoO_2 NS can also be used as template for synthesizing of N-doped Mo_2C (N–Mo_2C) and consequently N–Mo_2 NSs. Jia et al. used MoO_2NSs as a template and dicyandiamide ($C_2H_4N_4$) used to provide the C and N atom by heating at 450 °C for 2 h and then 750 °C for 2 h. From SEM images it is clear that the N–Mo_2C NSs have same morphology as MoO_2 NSs as shown in (Fig. 9 (h)), providing a solid proof of the effectiveness of template synthesis. It was found that the thickness of N–Mo_2C NSs is a little less than the thickness of the MoO_2template as well as the interplanar spacing of MoO_2 NSs (0.241 nm) is slightly larger than the N–Mo_2C NSs (0.237 nm) as shown in (Fig. 9(i)). The quality of obtained crystalline N-doped Mo_2C nanosheets is poor due to many nanopores observed on it (Fig. 9(j)–(l)). By using same approach, pure Mo_2C NSs can also be synthesized by using glucose instead of dicyandiamide.

Further, Fig. 10(a) displays the graphic of heterostructures of 2D TMCs with graphene fabricated by two-step CVDprogressionaimed at the production of graphene (top)/2D α-Mo_2C (bottom) vertical heterostructure. Fig. 10(b) demonstrates the optical appearance of graphene/2D α-Mo_2C heterostructures grown on Cu/Mo substrate, Fig. 10(c) demonstrate Raman spectra taken from a pure 2D α-Mo_2C crystal, Fig. 10(d) typicalHAADF-STEM image taken from a 2D α-Mo_2C crystal in heterostructure. As shown in Fig. 10(e), an optical picture of the G peak point is shown in Fig. 10(f). 2D crest location as depicted in Fig. 10(g), strain domains can be clearly seen in the graphene and 2D -Mo2C heterostructure. Figures (b–d) show the 5 μm scale bars.

Plasma-Enhanced Pulsed Laser Deposition: Zhang et al. used plasma-enhanced pulsed laser deposition (PEPLD) technique to synthesize a large-area high-quality 2D face-cantered cubic (FCC)-structured Mo_2C crystal on sapphire (0001) substrate. In this method, modified pulsed laser deposition system is used for generating CH_4 plasma. To provide Mo atom metal, a KrF laser of 248 nm the target was impinged. Fig. 11(a) and **11(b)** show the XRD patterns of the grown samples at 700 °C. It was concluded that the ionized CH_4 is essentially required for deposition, as Mo_2C ionized CH_4 plasma plays an important role in the deposition of 2D FCC-structure Mo_2C crystal. The 2D Mo_2C film dumped through PEPLD technique presents a smooth surface (Fig. 11(c)) [245] and the thickness of 2D Mo_2C film can be optimize from 2 nm to 25 nm. Although the crystal quality degrades when deposition temperature decreases [246], it can be fabricated a high quality single crystal when Mo_2C film grown at 700 °C, as shown in Fig. 11(e). However, the resulting film has lower quality of crystal when compared it with CVD growth sample, and numerous stacking defects

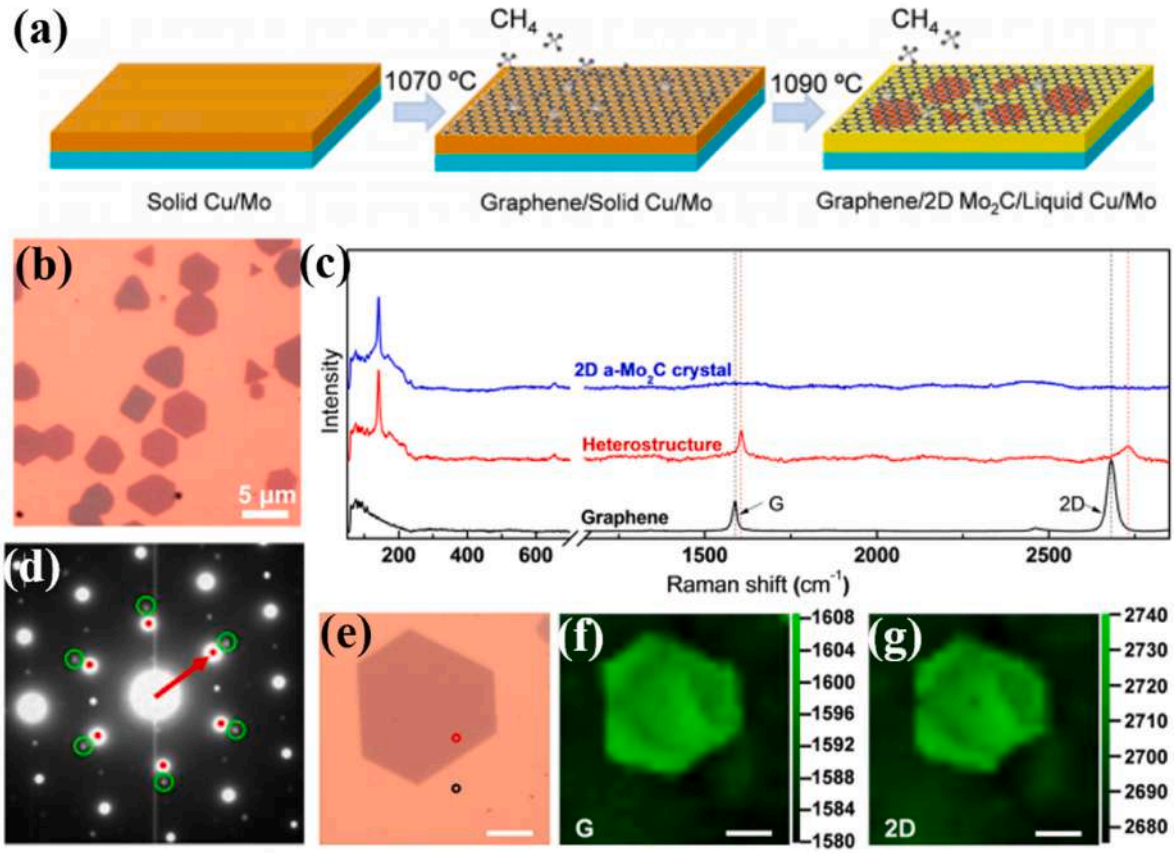

Fig. 10. Schematic of heterostructures of 2D TMCs with graphene prepared viaCVD method (a) representation diagram of the two-step CVD route aimed at the fabrication of graphene (top)/2D α-Mo_2C (bottom)vertical heterostructure, (b)optical image of graphene/2D α-Mo_2C heterostructures grown on Cu/Mo substrate, (c) Raman spectra taken from a pure 2D α-Mo_2C crystal, (d) typical HAADF-STEM image for a 2D α-Mo_2C crystal in heterostructure. (e, f) The graphene (indicated by black circle) and heterostructure (indicated by red circle) in (e), showing the graphene is compressed in the heterostructure. (e)–(g) Optical image (e) and the corresponding G peak position (f) and 2D peak position (g) mappings of a CVD-grown graphene/2D α-Mo_2C heterostructure, showing clear strain domains. Scale bars in (B–D) are 5 μm. Reproduced with permission from Ref. [244]. (For interpretation of the references to color in this figure legend, the reader is referred to the Web version of this article.)

were observed on the cross-sectional TEM images (Fig. 11(f)). It suggested that unlike other crystal structures, the formation of the FCC structure is due to the alignment association as well as little lattice disparity between {111} Mo_2C and {0003} sapphire.

4.2. Properties of exfoliated MXenes

MXenes show remarkable features, for instance, high Young's modulus, thermal in addition to electrical conductivity and tunable band gaps. In this section, the potential properties of exfoliated MXene are presented.

4.2.1. Electronic and electrical features

Electronic as well as electrical features of MXenes can be adjusted via functional group modification, stoichiometry, or solid solution formation. It has been well established that the electrical conductivities of pressed disc of MXene are similar as for multi-layered graphene and higher than for carbon nanotubes and rGO materials [216,247]. In addition, Naguib et al. found that the resistivity of MXene growths according to the number of layers and functional groups [192,224,248]. As a result, experimental conductivity is generally higher than reported according to simulation technique [249,250]. Since electrical conductivity based on numerous aspects as the concentration of defect, surface functional groups, delamination yield, d−spacing between MXene flakes and the lateral size induced by each etching process, these effects on MXene have been addressed. H. wang et al. prepared highly conductive MXene (Ti_3C_2) nanosheets by using layered Ti_3AlC_2 in aqueous solution of HF and alkalizate and calcinate the samples to remove the functional groups. It was found that the conductivity of Ti_3C_2 nanosheets increased from 850 Scm^{-1} to 2410 Scm^{-1} by calcination at 600 °C for 1 h, because of elimination of OH functional groups in addition to reduction of conduction paths [251]. Jhang et al. prepared a transparent film, by spin-casting the $Ti_3C_2T_x$ nanosheet colloidal solution, and then vacuum-annealed it at 200 °C. It was found that the electrical conductivity of transparent films nearly equal to 9880 Scm^{-1} [61]. Maleski et al. fabricated the Mxene by using lower concentration of HF and etching times, showing that MXene with larger lateral size present higher conductivity ~5000 Scm^{-1}, whereas the films collected of the minimum flakes displayed the lower most conductivity ~1000 Scm^{-1} [182,200]. Muckley et al. remarked the influence of humidity on the conductivities, pointing its application towards humidity sensing [252,253]. Surface modification by heat treatment and alkaline treatment also improved the electrical properties, as proven by the alteration and/or exclusion of functional groups (especially–F) [248,251,254–257].

4.2.2. Mechanical properties

Because of the toughest bonds between M − C as well as M − N, it attracted more interest towards mechanical properties of MXenes. Kurtoglue et al. explored the elastic constants (c11) of MXene by using simulation techniques. Results shown that the c11 value of MXene is two times greater than for its MAX phases [258] in addition to other 2D

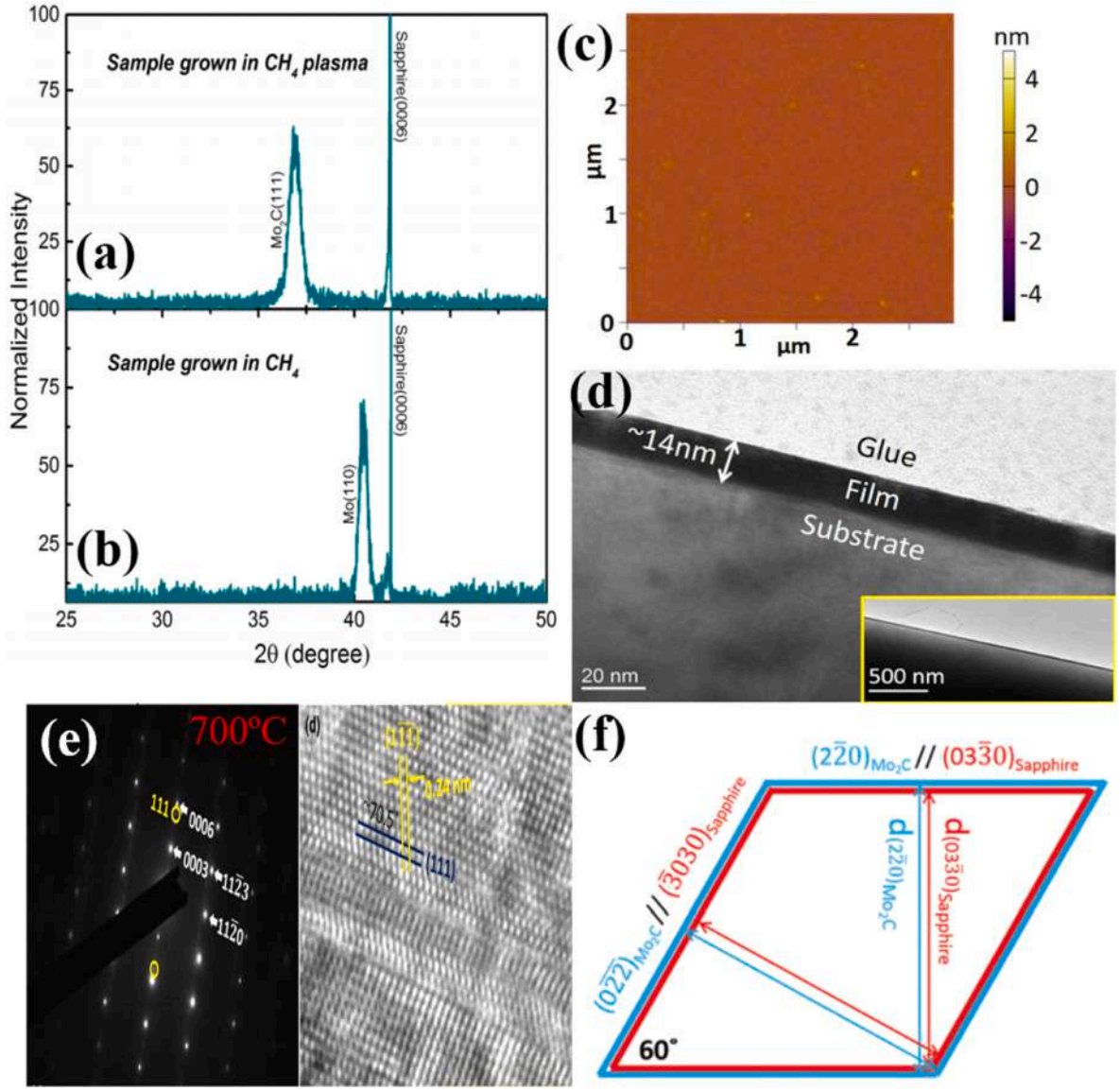

Fig. 11. FCC-structured Mo_2C film invented through PEPLD. (a),(b) show the XRD pattern of the grown sample (a) in ionized CH_4 plasma, (b) non-ionized CH_4, (c) AFM image of as-grown thin film of Mo_2C, (d) enlarged cross-sectional TEM image and the inset showing a low-magnification TEM image of Mo_2C film grown on the sapphire substrate, (e) high-resolution TEM image and SAED pattern taken from the cross section of the Mo_2C film grown at 700 °C, (f) It shows the schematic of coherence of the atomic planes at sapphire substrate and FCC-structured Mo_2C interface. (Panels (a)–(e) are reprinted with permission from Ref. [245]. Panels (f) are reprinted with permission from Ref. [246].

materials, such by means of MoS_2, while it is 2–4 times lower than graphene (1060 GPa) [259,260]. Nevertheless, bending stiffness of MXene is high [33,216,258,261], indicating its potential as a reinforcing material for composites. Feng et al. discovered the effect of alloying on mechanical properties of MXene. It was determined that when Ti is replaced by V, the elastic constant increases and $(Ti_{0.25}V_{0.75})_2CO_2$ shows the largest mechanical strength, with an elastic constant c11 of 425 GP. However, when Ti is replaced by Sc, the composition of Sc increases, resulting in a lower lowest c11 of 104 GPa [262]. Zha et al. explored the effect of functionalization on mechanical features of the carbide M_2CT_2. It was proven that the use of oxygen improves the mechanical strength (example W_2CO_2 shows the highest mechanical strength with c11 equivalent to 592.7 GPa) compared to functionalized MXene by fluorine or hydroxyl groups [263]. Zhang et al. determined by DFT that the elastic properties of $Ti_{n+1}C_n$ decreases when thickness increase, i.e. in the demand of $Ti_2C > Ti_3C_2 > Ti_4C_3$ with standards of 601 GPa, 473 GPa, and 459 GPa, respectively [264]. Lipatove et al. performed mechanical characterization of single layer flakes of $Nb_4C_3T_x$ MXene showing that the effective Young's modulus of $Nb_4C_3T_x$ monolayers was 386 ± 13 GPa, which is higher than for $Ti_3C_2T_x$ MXene [216,263].

4.2.3. *Thermal properties*

Due to the continuous miniaturization of electronics and energy storage devices, thermoelectric properties play an increasingly relevant role. Zha et al. discovered the thermal properties of oxide fictionalized MXene flake of 5 μm. It was found that at room temperature, thermal conductivity of Hf_2CO_2 is 86.25$Wm^{-1}K^{-1}$ exceeding the values of MoS_2 and phosphorene [265]. Luo et al. analyzed the effect of fluoride on $Sc_3(CN)F_2$, concluding that the thermal conductivity is nearly equal to the conductivity of MoS_2 and phosphorene. They also found that when lateral size of flakes increases, the thermal conductivity also increases [266]. Zha et al. explored the effect of surface termination on carbide MXene. When the surface is functionalized with –OH and –F, the thermal conductivity increases according to the flake's length [267]. In the case of oxidized carbide MXene, the thermal conductivity increases with the atomic number of metal "M" [256,268]. Kim et al. presented a pioneer

work regarding the thermoelectric conductivity of Mo-based MXenes such as Mo_2CT_x, $Mo_2TiC_2T_x$, and $Mo_2Ti_2C_3T_x$. It was found that these MXenes show high conductivity and n-type Seebeck coefficient after heating to 800 K. As an example, Mo_2TiC_2Tx MXene the thermoelectric power reaches 3.09 × 10^{-4} $Wm^{-1}K^{-2}$ at 803 K [218].

4.2.4. Magnetic properties

Since MAX phases show magnetic properties, the magnetic features of MXene have been explored. A number of pristine MXene such as Ti_4C_3 [269], Ti_3CN [244], Fe_2C [270], Cr_2C, Ti_3N_2 [271,272], Ti_2N [273], Zr_2C, and Zr_3C_2 [274] possess magnetic moments. However, functionalization could vanish in some cases their magnetic response. Urbankowski et al. explored the magnetic properties of pristine and functionalized MXene and it was found that pristine Ti_4N_3 MXene exhibits a magnetic moment of 7.0 μB per unit cell while terminated Ti_3CNT_x and $Ti_4C_3T_x$ show zero magnetic moment [218]. Khajaei et al. explored MXenes such as Cr_2CF_2, $Cr_2C(OH)_2$, Cr_2NF_2, $Cr_2N(OH)_2$, in addition to Cr_2NO_2 which are ferromagnetic in ground state [203] while Mn_2NT_x is ferromagnetic [275].

4.2.5. Optical properties

Optical properties of MXene are important for photocatalysts, photoelectrons, photoelectrons, and transparent conductive electrode devices. Zhang et al. fabricated transparent films of $Ti_3C_2T_x$ via spin casting of colloidal solutions, followed by annealing in vacuum condition at 200 °C, obtaining transmittance values of 93% and 29% with a thickness of 4 nm as well as 88 nm, respectively [276]. Adsorption properties of MXene depend on the thickness of the film, showing a strong and wide absorption band around 700–800 nm, resulting in a pale greenish film color [230]. Hantanasirisakul et al. fabricated transparent conductive homogeneous films of thickness 5–70 mm by spray coating of delaminated Ti_3C_2 MXene flakes with a transmittance of 40%–90%. According to the optoelectronic properties, Ying et al. explored V_2CT_x MXene into flexible transparent films. They used tetrabutylammonium hydroxide as an etchent (TBAOH) for the fabrication of V_2CT_x MXene films from aqueous colloidal suspensions. It was obtained an absorption coefficient of 1.22 ± 0.05 × 10^5 cm^{-1} at a wavelength of 550 nm which is twice the $Ti_3C_2T_x$. Further, by ion intercalation the optical properties are also optimized. Regarding the solvent used, Hydrazine, Urea, and DMSO decrease the transmittance of $Ti_3C_2T_x$ film meanwhile tetramethylammonium hydroxide (NMe_4OH) improved it from 74.9 to 92.0% [277]. In this context, Berdiyorov et al. discovered the consequence of functional groups on the optical features of MXene. It was found that when the sample is oxidized its absorption features increases, but when sample is fluorinated, absorption features decreases. For the ultraviolet energy range, all functional groups enhance both reflectivity and absorption properties of the MXene [278]. Malesky et al. initiate that when lateral size reduced the absorption in the visible range [182]. Due to the metallic conductivity and optical transparency in visible range the MXene are potential candidate for flexible transparent electrode application. Whereas due to high resistivity in the ultraviolet region it can be used as ultraviolet filter coating materials. Li et al. found that the light to heat conversion efficiency of Ti_3C_2 is nearly equal to 100.

4.3. Battery application of MXene as anodes

Naguib et al. exfoliated the Ti_2C produced by HF treatment of Ti_2AlC powder. Used for Li-ion batteries, the produced Ti_2C exhibits specific capacity of 80 $mAhg^{-1}$ at the rate of 3C after 120 cycles and 70 $mAhg^{-1}$ at the rate of 10C after 200 cycles [279]. Tang et al. reported the effect of functionalities when MXenes are used as anodes in Li ion batteries. In particular, pristine Ti_3C_2 exhibits a specific capacity of 320 $mAhg^{-1}$ and when Ti_3C_2 terminated with F/OH, capacity drastically falls down to 130/67 $mAhg^{-1}$ [272]. Mashtalior et al. synthesized a binder-free MXene after filtering the aforementioned colloidal solution through a membrane. The produced binding free MXene 'paper' exhibits a specific capacity of 410 $mAhg^{-1}$ at the rate of 1C and 110 $mAhg^{-1}$ at the rate of 36C [224]. Sun et al. synthesized 2D Ti_3C_2 by etching $Ti_3AlC_2$with concentrated HF. Then, in order to increase the d-spacing, intercalation process was used with dimethyl sulfoxide (DMSO), increasing the storage of Li, and consequently the specific capacity. It was found that the intercalated Ti_3C_2 exhibits a first charge capacity of 107.2 $mAhg^{-1}$ and 118.7 $mAhg^{-1}$ after 75 cycles, which means a capacity retain of 96% [224]. Wang et al. explored the electrochemical capacity of single layer Ti_2N and surface functionalized Ti_2NT_2 (where T = O, F, in addition to OH) using first principle for Mg^{2+} ions battery. Results exhibited a specific capacity more than 2000 $mAhg^{-1}$ because of the two electron reactions as well as unique multilayer adsorption behavior of Mg^{2+} ion [280]. Naguib et al. synthesized two new MXene Nb_2CT_x and V_2CT_x by simple HF treatment of Nb_2AlC and V_2AlC powders. Nb_2T_x and V_2CT_x exhibit specific capacity of 110 $mAhg^{-1}$ and 125 $mAhg^{-1}$ at the rate of 10C after 150 cycles, respectively. They also found that Nb_2CT_x exhibits reversible capacity of 170 mAg^{-1} at the rate of 1C at lower lithiation voltage while V_2CT_x exhibits larger capacity 210 $mAhg^{-1}$ at the rate of 1C at higher lithiation voltage [281]. The electrochemical capacity of titanium carbonitride Mxene (Ti_3CNT_z) for potassium ion batteries was also explored. Although, it exhibits first cycle specific capacity of 710 $mAhg^{-1}$ at 20 mAg^{-1} it dropped to 275 $mAhg^{-1}$ after second cycle. After 100 charge/discharge cycles it exhibits reversible capacity 75 $mAhg^{-1}$ at the rate of 10 mAg^{-1} [282]. Zhou et al. explored the electrochemical properties of Hf_3C_2Tz as an anode material for Li and Na ion batteries. After 200 cycles, it exhibits reversible volumetric capacities of 1567 mAh cm^{-3} and 504 mAh cm^{-3} at the rate 200 mAg^{-1} for Li and Na ions batteries, respectively [213]. Zhou et al. prepared a 2D $Nb_4C_3T_x$ for Li ion batteries finding that its charging/discharging capacity increases from 310 to 380 $mAhg^{-1}$ at 0.1 $mAg^{-1}$and from 116 to 320 $mAhg^{-1}$ at 1Ag^{-1} after 100 cycles [283]. Yang et al. investigated the electrochemical performance of 2D Hf based MXene Hf_3C_2, its derivative and hybrid passivated: $Hf_3C_2FxO_{2-x}$ and $Hf_3C_2O_x(OH)_{2-x}$ [x = 1.0,1.5] as anode material for Li/Na ion battery by using first principle theory. It was determined that Hf_3C_2monolayer exhibits excellent characteristics like good conductivity, high specific capacity, low diffusion energy barrier and low open circuit voltage (for Li ion battery 1034.70 $mAhg^{-1}$ and for Na ion battery 444.90 $mAhg^{-1}$) [284]. Meng et al. investigated the electrochemical characteristics of S-functionalized Ti_3C_2 monolayer MXene using first principle calculations. Comparing the specific capacity of $Ti3C_2S_2$, Ti_3C_2 and $Ti_3C_2O_2$ for Na ion battery, maximum capacities of 320, 268 and 463 $mAhg^{-1}$, respectively, were found. Dong et al. prepared Ti_3C_2 MXene derived ultrathin nanoribbons of sodium titanate (M-NaTO) and potassium titanate (M-KTO). M-NaTO and M-KTO exhibit reversible specific capacity of 191 $mAhg^{-1}$at the rate of 200 mAg^{-1} for Na ion battery and 151 $mAhg^{-1}$ at the rate of 50 mAg^{-1} for K ion battery respectively. M-KTO also shows high rate capacity of 88 $mAhg^{-1}$at 300 mAg^{-1} after 900 cycles [285]. Shukla et al. investigated the electrochemical characteristic of S-functionalized Nitride Mxenes V_2NS_2 and Ti_2NS_2 as anode materials by first principle method for Li/Na ion batteries. They found that the V_2NS_2 and Ti_2NS_2 exhibits the specific capacity of 308.28 and 299.52 $mAhg^{-1}$ for Li ion batteries and 84.76 and 99.8 $mAhg^{-1}$ for Na ion batteries respectively [286]. Zho et al. investigated the VS_4 carbon coated VS_4@Ti_3C_2/C nanosheet as anode material for Mg-ion battery, it exhibits discharge capacity of 492 $mAhg^{-1}$ at 50 mA g^{-1} [291]. Li et al. investigated the electrochemical properties of VS_2/Ti_2CO_2 and VS_2/Ti_2CS_2 for Li, Mg, K and Na ion battery and they have found that VS_2/Ti_2CO_2 and VS_2/Ti_2CS_2 shows strong adsorption, low diffusion barrier, high capacity and low open circuit voltage for Mg-ion batteries and VS_2/Ti_2CS_2 shows good for Na-ion batteries [292]. Zhang et al. prepared a free-standing COF derived porous N-doped carbon/MXene paper for Li–S batteries and they have found that it shows good storage capacity with excellent cyclic stability 584 $mAhg^{-1}$ after 100 cycle [293]. Wei et al. prepared a flexible and freestanding MXene/COF framework for Li–S batteries and found that it does not raise issue regarding Li dendrites, high chemical reactivity, large volume

changes, and unstable SEI [294]. Fan et al. investigated the electrochemical potential of V_3C_2 as an electrode material for metal-ion (such as Li, Na, K, and Ca) battery application. Calculation shows that V_3C_2 shows excellent storage capacity 606.42 $mAhg^{-1}$ for both Li and Na ions battery compared to 269.86 $mAhg^{-1}$ for K and 539.71 $mAhg^{-1}$ for Ca ion batteries [317]. Fan et al. also investigated the electrochemical potential of phosphorous carbide monolayer (PC_x, x = 2, 5, and 6) as anode material for Li ion battery. From nudged elastic band calculation it was found that for single Li atom diffusion barrier for PC_2 is 0.18 eV and it was 0.44 eV for PC_6 [318].

5. Other 2D materials used as an anode

Ma et al. investigated the new phases of two dimensional transition metal borides and named as (MBenes) for Mg-ion battery they have taken Sc_2B, Ti_2B and V_2B materials as electrode for MIBs and found that these shows the capacity of 3192.81 $mAhg^{-1}$, 3018.41 $mAhg^{-1}$and 2853.95 $mAhg^{-1}$ respectively [295]. Yuan et al. investigated the electrochemical properties of MoS_2/M_2CS_2 (M = Ti, V) heterostructures for metal ion batteries they have found that it shows storage capacity of 400 $mAhg^{-1}$ for NIBs and 320 $mAhg^{-1}$ for LIBs. This indicate that MoS_2/M_2CS_2 (M = Ti, V) heterostructures is more suitable for NIBs rather than other metal ion batteries [296].

He et al. calculated the storage capacity of 1T-MoS_2 monolayer for metal ion battery and they have found that Li, Na, Mg shows more adsorption and it formed up to 7 layers for Li on 1-T MoS_2. The capacity exhibits by MoS_2 for Li ion is largest (1172 $mAhg^{-1}$) compare to other metal ions such as Na-ion (335 $mAhg^{-1}$) [297].

Xu et al. investigated the electrochemical potential of single layer silicene nanosheet and found that it exhibits storage capacity up to 1196 $mAhg^{-1}$ without breaking of Si–Si bonds [303]. Zhu et al. investigated the electrochemical potential of freestanding silicone, graphene-silicene-graphene and graphene-silicine hetrostructure for Na-ion batteries they have found that free standing silicene shows good storage capacity (954 $mAhg^{-1}$) compared to graphene-silicene superlattice (760 $mAhg^{-1}$) [304]. Teng et al. synthesized the ultrathin ZnO nanosheet covered by a carbon coating of 5 nm (C–ZnO). Synthesis of C–ZnO nanosheet achieved by hydrothermal method followed by CVD process where C_2H_2 used as a source of carbon. When it is used as anode for Li ion batteries it exhibits reversible storage capacity of 804 $mAhg^{-1}$ at the rate of 1 Ag^{-1} after 200 cycles and when used for Na-ions batteries it exhibits 100 $mAhg^{-1}$ at the rate of 100 mAg^{-1} after 200 cycles [305].

6. Limitations of conventional 2D materials

To some extent, all traditional 2D materials suffer from their open structure and nanoscale morphology. Many 2D materials have significant redox activity in intercalation processes and shows good performance when used as anode for energy storage devices however, they all have some drawbacks. Large specific surface area of 2D materials provide more interaction with electrolyte which improve the ions transfer but it results in more consumption of electrolyte and forming SEI layer causing irreversible capacity in first cycle. Common limitation of 2D materials is as follows: Fabrication of controlled 2D materials is very difficult, Doping amount and position of doped material are less controllable, Mature fabrication techniques of 2D materials is not there, Bulk production are not feasible, Buckled structure etc. Furthermore, 2D materials often have a significant number of active sites for ion intercalation, resulting in parasitic electrolyte decomposition [306,307]. To overcome these limitations researcher uses different techniques which control the doping concenteration as well as doping position, Kawai et al. synthesized the atomically controlled boron doped armchair graphene nanoribbons of width 7, 14 and 21 [337]. Intermediate assisted grinding exfoliation techniques used by Zhang et al. for mass production of 2D materials using this method control both the lateral size and thickness [338].

7. Basic Requirements of 2D promising anode materials in battery application

Anode materials required some basic characteristics for battery application. These characteristics are excellent porosity, conductivity, durability, light weight, low cost, and voltage compatibility with selected cathode. 2D materials improve the electrical conductivity of the electrodes. 2D materials often provide the ability to add increased gravimetric and volumetric capacities while fine-tuning the electrical characteristics [319]. These substances may increase the surface area of the electrodes and the amount of active material that is available [320]. Pulverization of high-capacity electrodes owing to volume expansion and stress buildup during cycling reduces battery cycle life and performance. A network of 2D materials enveloping electrode particles may avoid cracking and increase electrochemical as well as thermal stability. 10–60 wt % of active materials are employed to improve electrode mechanical and electrochemical performance [321].

8. Conclusions and outlook

The synthesis, modification techniques and important properties of graphene/composites of graphene and other 2D structures such as TMDs and MXene have been summarized, as well as theis applicability for Li, Na and K ion batteries. In contrast to bulk material, the unique physical and chemical properties of 2D materials, with high surface to volume ratio, make them suitable candidates for applications in metal ions batteries. Significant improvement in synthesis techniques and in performance of electrochemical capacity has been described with the engagement of these graphene related 2D materials. N-graphdiyne shows specific capacity of 600–900 $mAhg^{-1}$ for Na-ion battery, while T-graphene exhibits 2232 $mAhg^{-1}$, it is three times larger than its capacity for Li-ion battery. Till now reported capacity for K ion battery are 1871 $mAhg^{-1}$ when N-TpG used as anode. MoO_2 shows very high storage capacity for Li ion battery nearly equal to 2513 $mAhg^{-1}$. MoO_2 shows ultrahigh capacity for Na storage capacity of 857 $mAhg^{-1}$. ReS_2 shows a high storage capacity for Na-ion battery 428 $mAhg^{-1}$ in comparisons of MoS_2 and VS_2 .VS_2 and TS_2 shows good storage capacity for K-ion battery, it is nearly equal to 278 and 282 $mAhg^{-1}$ respectively. $TiCP_2$ and V_2CP_2 show storage capacity 1264 and 1220 $mAhg^{-1}$ and very high storage capacity 1767 and 1592 $mAhg^{-1}$ for Ti_2CSi_2 and V_2CSi_2 for Li ion battery. Zr_2C shows highest Na-storage capacity among all MXene and it is nearly equal to 546 $mAhg^{-1}$. Although a significant evolvement has been accomplished in the field of synthesis of 2D materials for its directions as anode for metal ion battery, reliable mass production with high quality is still a big challenge. Furthermore, it desires to be also handled the production of freestanding 2D materials like Germanene, Borophene and Tellurene, etc. Chemical exfoliation method may be used for the construction of large-scale 2D material with high quality. Nevertheless, when 2D materials such as MXene and TMDs are employed in Li ion batteries, a detailed surface chemistry of MXene and reaction mechanisms of TMDs are still not fully understood. Therefore, computational techniques would contribute to untangle the final structure, electrochemical properties and mediated reactions. By using density functional theories researchers can be able to developed some new 2D materials and realize their physical and chemical properties without fabrication and when the characteristics of the predicted 2D materials shows excellent property required for anode materials then suitable fabrication technique used for synthesis. Kawai et al. synthesized the atomically controlled boron doped armchair graphene nanoribbons of width 7, 14 and 21 [337]. After synthesis of para-boron doped AGNR, Liu et al. investigated the Li adsorption, diffusion barrier and open circuit voltage and predicted that it can be used as anode material for Li ion battery [339]. The large volume-to-mass ratio exhibited by 2D materials results in low volumetric energy density for Li/Na ion batteries as electrode material. For example, graphene can be easily re-stacked during charging/discharging, resulting in inferior cycling stability.

Moreover, the formation of SEI took places due to large surface area, contributing to a poor electrochemical capacity. In order to overcome those problems, composites based on graphene, TMDs and MXene are being explored.

Functionalization as well as different etching materials have been used in the synthesis of pristine MXene to reduce, safety hazards, by-products and to develop the electrochemical capacity of those materials. To overcome the charging and discharging rate problems, researchers used hetroatom doped 2D materials, it improve the chemical potential as well as diffusion barriers of metal ions. 2D materials contain large surface areas and lots of active spots, which can be utilized to hold several insulated active compounds, like S, red P, and Si. 2D materials stabilized the active sites, reduced volume expand and provide suitable path for metal ions diffusion.

The application of graphene, TMDs and MXene or their composites for Li/Na/K ion battery are in early stage in addition to the current research are far from industrial application. In the near future, it will be expected that the challenges mentioned above are tackled with the purpose of developing the capacity, cycle life as well as manufacturing for industrial application.

Declaration of competing interest

The authors declare that they have no known competing financial interests or personal relationships that could have appeared to influence the work reported in this paper.

Data availability

No data was used for the research described in the article.

Acknowledgements

The authors would like to acknowledge the department of Electronics and Communication, NIT Patna for utilization of resources of Microelectronics and VLSI Lab. Furthermore, AES would like to thank the National Research grants from MINECO, Spain, ‘‘Juan de la Cierva’’ [FJCI-2018-037717]. Further authors thank support from the Basque Government Industry Department under the ELKARTEK programs.

References

[1] B. Dunn, H. Kamath, J.-M. Tarascon, Electrical energy storage for the grid: a battery of choices, Science 334 (2011) 928–935.
[2] H. Shevchenko, M. Petrushenko, B. Burkynskyi, N. Khumarova, Sdgs andthe ability to manage change within the european green deal: the case of Ukraine, Probl. Perspect. Manag. 19 (2021). Art. no. 53.
[3] A.G. Pandolfo, A.F. Hollenkamp, Carbon properties and their role insupercapacitors, J. Power Sources 157 (2006) 11–27.
[4] A. Oh, Y.J. Sa, H. Hwang, H. Baik, J. Kim, B. Kim, S.H. Joo, K. Lee, Rational design of Pt–Ni–Co ternary alloy nanoframe crystals as highly efficient catalysts toward the alkaline hydrogen evolution reaction, Nanoscale 8 (2016) 16379–16386.
[5] N. Danilovic, R. Subbaraman, K.C. Chang, S.H. Chang, Y. Kang, J. Snyder, A. P. Paulikas, D. Strmcnik, Y.T. Kim, D. Myers, V.R. Stamenkovic, N.M. Markovic, Using surface segregation to design stable Ru-Ir oxides for the oxygen evolution reaction in acidic environments, Angew. Chem. 126 (2014) 14240–14245.
[6] J. Yoon, J. Park, Y.J. Sa, Y. Yang, H. Baik, S.H. Joo, K. Lee, Synthesis of bare Pt_3Ni nanorods from PtNi@Ni core–shell nanorods by acid etching:one-step surfactant removal and phase conversion for optimal electrochemical performance toward oxygen reduction reaction, CrystEngComm 18 (2016) 6002–6007.
[7] L. Yang, M.B. Vukmirovic, D. Su, K. Sasaki, J.A. Herron, M. Mavrikakis, S. Liao, R. R. Adzic, Tuning the catalytic activity of Ru@Pt core–shell nanoparticles for the oxygen reduction reaction by varying the shell thickness, J. Phys. Chem. C 117 (2013) 1748–1753.
[8] H. Jin, K.W. Lee, N.T. Khi, H. An, J. Park, H. Baik, J. Kim, H. Yang, K. Lee, Rational synthesis of heterostructured M/Pt (M=Ru or Rh) octahedral nanoboxes and octapods and their structure-dependent electrochemical activity toward the oxygen evolution reaction, Small 11 (2015) 4462–4468.
[9] M.K. Debe, Electrocatalyst approaches and challenges for automotive fuelcells, Nature 486 (2012) 43–51.
[10] H.A. Gasteiger, S.S. Kocha, B. Sompalli, F.T. Wagner, Activity benchmarks and requirements for Pt, Pt-alloy, and non-Pt oxygen reduction catalysts for PEMFCs, Appl. Catal. B Environ. 56 (2005) 9–35.
[11] Y. Yan, B.Y. Xia, B. Zhao, X. Wang, A review on noble-metal-free bi-functional heterogeneous catalysts for overall electrochemical water splitting, J. Mater. Chem. 4 (2016) 17587–17603.
[12] M.S. Burke, L.J. Enman, A.S. Batchellor, S. Zou, S.W. Boettcher, Oxygen evolution reaction electrocatalysis on transition metal oxides and (oxy) hydroxides: activity trends and design principles, Chem. Mater. 27 (2015) 7549–7558.
[13] B.M. Hunter, H.B. Gray, A.M. Muller, Earth-abundant heterogeneous water oxidation catalysts, Chem. Rev. 116 (2016) 14120–14136.
[14] J. Wang, F. Xu, H. Jin, Y. Chen, Y. Wang, Non-noble metal-based carbon composites in hydrogen evolution reaction: fundamentals to applications, Adv. Mater. 29 (2017), 1605838. Art. no.
[15] C. Jin, F. Lin, K. Suenaga, S. Iijima, Fabrication of a freestanding boronnitride single layer and its defect assignments, Phys. Rev. Lett. 102 (2009), 195505. Art. no.
[16] H. Zeng, C. Zhi, Z. Zhang, X. Wei, X. Wang, W. Guo, Y. Bando, D. Golberg, White graphenes": boron nitride nanoribbons via boron nitride nanotubeunwrapping, Nano Lett. 10 (2010) 5049–5055.
[17] Z. Zeng, Z. Yin, X. Huang, H. Li, Q. He, G. Lu, F. Boey, H. Zhang, Single-layer semiconducting nanosheets: high-yield preparation and device fabrication, Angew. Chem. 123 (2011) 11289–11293.
[18] K.-G. Zhou, N.-N. Mao, H.-X. Wang, Y. Peng, H.-L. Zhang, A mixed-solvent strategy for efficient exfoliation of inorganic graphene analogues, Angew. Chem. 123 (2011) 11031–11034.
[19] K.-G. Zhou, N.-N. Mao, H.-X. Wang, Y. Peng, H.-L. Zhang, A mixed-solvent strategy for efficient exfoliation of inorganic graphene analogues, Angew. Chem. 123 (2011) 11031–11034.
[20] P. Vogt, P. De Padova, C. Quaresima, J. Avila, E. Frantzeskakis, M.C. Asensio, A. Resta, B. Ealet, G. Le Lay, Silicene: compelling experimental evidence for graphene like two-dimensional silicon, Phys. Rev. Lett. 108 (2012), 155501. Art. no.
[21] E. Bianco, S. Butler, S. Jiang, O.D. Restrepo, W. Windl, J.E. Goldberger, Stability and exfoliation of germanane: a germanium graphane analogue, ACS Nano 7 (2013) 4414–4421.
[22] H.O. Churchill, P. Jarillo-Herrero, Phosphorus joins the family, Nat. Nanotechnol. 9 (2014) 330–331.
[23] H. Liu, Y. Du, Y. Deng, D.Y. Peide, Semiconducting black phosphorus:synthesis, transport properties and electronic applications, Chem. Soc. Rev. 44 (2015) 2732–2743.
[24] Y. Jing, X. Zhang, Z. Zhou, Phosphorene: what can we know from computations? Wiley Interdiscip. Rev. Comput. Mol. Sci. 6 (2016) 5–19.
[25] S.Z. Butler, S.M. Hollen, L. Cao, Y. Cui, J.A. Gupta, H.R. Gutierrez, T.F. Heinz, S. S. Hong, J. Huang, A.F. Ismach, et al., Progress, challenges, and opportunities in two-dimensional materials beyond graphene, ACS Nano 7 (2013) 2898–2926.
[26] J.N. Coleman, M. Lotya, A. O'Neill, S.D. Bergin, P.J. King, U. Khan, K. Young, A. Gaucher, S. De, R.J. Smith, I.V. Shvets, S.K. Arora, G. Stan- ton, H.-Y. Kim, K. Lee, G.T. Kim, G.S. Duesberg, T. Hallam, J.J. Boland, J.J. Wang, J.F. Donegan, J.C. Grunlan, G. Moriarty, A. Shme- liov, R.J. Nicholls, J.M. Perkins, E. M. Grieveson, K. Theuwissen, D.W. McComb, P.D. Nellist, V. Nicolosi, Two-dimensional nanosheets produced by liquid exfoliation of layered materials, Science 331 (2011) 568–571.
[27] W. Sun, S. Shah, Y. Chen, Z. Tan, H. Gao, T. Habib, M. Radovic, M. Green, Electrochemical etching of Ti_2AlC to Ti_2CTx (MXene) in low-concentration hydrochloric acid solution, J. Mater. Chem. 5 (2017) 21663–21668.
[28] S. Yang, P. Zhang, F. Wang, A.G. Ricciardulli, M.R. Lohe, P.W. Blom, X. Feng, Fluoride-free synthesis of two-dimensional titanium carbide (MXene) using a binary aqueous system, Angew. Chem. 130 (2018) 15717–15721.
[29] I. Salama, T. El-Raghy, M. Barsoum, Synthesis and mechanical propertiesof Nb_2AlC and (Ti, $Nb)_2AlC$, J. Alloys Compd. 347 (2002) 271–278.
[30] H. Zhang, Y. Zhou, Y. Bao, M. Li, J. Wang, Intermediate phases in synthesisof Ti_3SiC_2 and $Ti_3Si(Al)C_2$ solid solutions from elemental powders, J. Eur. Ceram. Soc. 26 (2006) 2373–2380.
[31] M. Barsoum, T. El-Raghy, M. Ali, Processing and characterization of Ti_2AlC, Ti_2AlN, and $Ti_2AlC_{0.5}N_{0.5}$, Metall. Mater. Trans. 31 (2000) 1857–1865.
[32] Z.-Y. Sui, C. Wang, Q.-S. Yang, K. Shu, Y.-W. Liu, B.-H. Han, G.G. Wallace, A highly nitrogen-doped porous graphene an anode material for lithium ion batteries, J. Mater. Chem. 3 (2015) 18229–18237.
[33] M. Naguib, M. Kurtoglu, V. Presser, J. Lu, J. Niu, M. Heon, L. Hultman, Y. Gogotsi, M.W. Barsoum, Two-dimensional nanocrystals produced by exfoliation of Ti_3AlC_2, Adv. Mater. 23 (2011) 4248–4253.
[34] M.A. Shannon, P.W. Bohn, M. Elimelech, J.G. Georgiadis, B.J. Marinas, A. M. Mayes, Science and technology for water purification in the coming decades, Nanoscience and technology: a collection of reviews from, Nat. J. (2010) 337–346.
[35] K.S. Novoselov, A.K. Geim, S.V. Morozov, D. Jiang, Y. Zhang, S.V. Dubonos, I. V. Grigorieva, A.A. Firsov, Electric field effect in atomically thin carbon films, Science 306 (2004) 666–669.
[36] M.D. Stoller, S. Park, Y. Zhu, J. An, R.S. Ruoff, Graphene-based ultracapacitors, Nano Lett. 8 (2008) 3498–3502.
[37] R.S. Edwards, K.S. Coleman, Graphene synthesis: relationship to applications, Nanoscale 5 (2013) 38–51.
[38] I.E. Abbott's, Graphene: exploring carbon flatland, Phys. Today 60 (2007), 35. Art. no.
[39] M. Aliofkhazraei, Advances in Graphene Science, BoD–Books on Demand, 2013.

[40] A. Dato, V. Radmilovic, Z. Lee, J. Phillips, M. Frenklach, Substrate-free gas-phase synthesis of graphene sheets, Nano Lett. 8 (2008) 2012–2016.
[41] A. Reina, X. Jia, J. Ho, D. Nezich, H. Son, V. Bulovic, M.S. Dresselhaus, J. Kong, Large area, few-layer graphene films on arbitrary substrates by chemical vapor deposition, Nano Lett. 9 (2009) 30–35.
[42] R. Verdejo, M.M. Bernal, L.J. Romasanta, M.A. Lopez-Manchado, Graphene filled polymer nanocomposites, J. Mater. Chem. 21 (2011) 3301–3310.
[43] S. Park, R.S. Ruoff, Chemical methods for the production of graphenes, Nat. Nanotechnol. 4 (2009) 217–224.
[44] S. Amini, J. Garay, G. Liu, A.A. Balandin, R. Abbaschian, Growth of large-area graphene films from metal-carbon melts, J. Appl. Phys. 108 (2010), 094321.
[45] P.W. Sutter, J.-I. Flege, E.A. Sutter, Epitaxial graphene on ruthenium, Nat. Mater. 7 (2008) 406–411.
[46] I. Pletikosi'c, M. Kralj, P. Pervan, R. Brako, J. Coraux, A. N'diaye, C. Busse, T. Michely, Dirac cones and minigaps for graphene on Ir (111), Phys. Rev. Lett. 102 (2009), 056808.
[47] K.S. Kim, Y. Zhao, H. Jang, S.Y. Lee, J.M. Kim, K.S. Kim, J.-H. Ahn, P. Kim, J.-Y. Choi, B.H. Hong, Large-scale pattern growth of graphene films for stretchable transparent electrodes, Nature 457 (2009) 706–710.
[48] Y. Zhang, L. Zhang, C. Zhou, Review of chemical vapor deposition of graphene and related applications, Acc. Chem. Res. 46 (2013) 2329–2339.
[49] S. Bae, H. Kim, Y. Lee, X. Xu, J.-S. Park, Y. Zheng, J. Balakrishnan, T. Lei, H. R. Kim, Y.I. Song, et al., Roll-to-roll production of 30-inch graphene films for transparent electrodes, Nat. Nanotechnol. 5 (2010) 574–578.
[50] J. Rafiee, X. Mi, H. Gullapalli, A.V. Thomas, F. Yavari, Y. Shi, P.M. Ajayan, N. A. Koratkar, Wetting transparency of graphene, Nat. Mater. 11 (2012) 217–222.
[51] P. Sutter, How silicon leaves the scene, Nat. Mater. 8 (2009) 171–172.
[52] T. Ohta, A. Bostwick, J.L. McChesney, T. Seyller, K. Horn, E. Rotenberg, Interlayer interaction and electronic screening in multilayer graphene investigated with angle-resolved photoemission spectroscopy, Phys. Rev. Lett. 98 (2007), 206802. Art. no.
[53] A. Chakrabarti, J. Lu, J.C. Skrabutenas, T. Xu, Z. Xiao, J.A. Maguire, N. S. Hosmane, Conversion of carbon dioxide to few-layer graphene, J. Mater. Chem. 21 (2011) 9491–9493.
[54] Q. Sun, Y. Huang, S. Wu, Z. Gao, H. Liu, P. Hu, L. Qie, Facile synthesisof Sn/nitrogen-doped reduced graphene oxide nanocomposites with superb lithium storage properties, Nanomaterials 9 (2019), 1084. Art. no.
[55] G. Ma, K. Huang, Q. Zhuang, Z. Ju, Superior cycle stability of nitrogen-doped graphene nanosheets for Na-ion batteries, Mater. Lett. 174 (2016) 221–225.
[56] B. Quan, A. Jin, S.-H. Yu, S.M. Kang, J. Jeong, H.D. Abruna, L. Jin, Y. Piao, Y.-E. Sung, Solvothermal-derived S-doped graphene as an anode ma- terial for sodium-ion batteries, Adv. Sci. 5 (2018), 1700880. Art. no.
[57] S. Gong, Q. Wang, Boron-doped graphene as a promising anode material for potassium-ion batteries with a large capacity, high rate performance, and good cycling stability, J. Phys. Chem. C 121 (2017) 24418–24424.
[58] X. Li, W. Cai, J. An, S. Kim, J. Nah, D. Yang, R. Piner, A. Velamakanni, I. Jung, E. Tutuc, L. Banerjee, K. Sanjay, R.S. Colombo, Rouf, Large- area synthesis of high-quality and uniform graphene films on copper foils, Science 324 (2009) 1312–1314.
[59] Y. Li, Z. Peng, E. Larios, G. Wang, J. Lin, Z. Yan, F. Ruiz-Zepeda, M. Jose-Yacaman, J.M. Tour, Rebar graphene from functionalized boron nitride nanotubes, ACS Nano 9 (2015) 532–538.
[60] E. Irissou, J.-G. Legoux, A.N. Ryabinin, B. Jodoin, C. Moreau, Review on cold spray process and technology: part I—intellectual property, J. Therm. Spray Technol. 17 (2008) 495–516.
[61] X. Wang, L. Zhi, K. Mullen, Transparent, conductive graphene electrodes for dye-sensitized solar cells, Nano Lett. 8 (2008) 323–327.
[62] Y. Zhang, Y.-W. Tan, H.L. Stormer, P. Kim, Experimental observation ofthe quantum hall effect and berry's phase in graphene, Nature 438 (2005) 201–204.
[64] C. Lee, X. Wei, J.W. Kysar, J. Hone, Measurement of the elastic properties and intrinsic strength of monolayer graphene, Science 321 (2008) 385–388.
[65] D.A. Dikin, S. Stankovich, E.J. Zimney, R.D. Piner, G.H. Dommett, G. Evmenenko, S.T. Nguyen, R.S. Ruoff, Preparation and characterization of graphene oxide paper, Nature 448 (2007) 457–460.
[66] S. Park, K.-S. Lee, G. Bozoklu, W. Cai, S.T. Nguyen, R.S. Ruoff, Grapheneoxide papers modified by divalent ions-enhancing mechanical properties via chemical cross-linking, ACS Nano 2 (2008) 572–578.
[68] R. Sharma, J.H. Baik, C.J. Perera, M.S. Strano, Anomalously large reactivity of single graphene layers and edges toward electron transfer chemistries, Nano Lett. 10 (2010) 398–405.
[69] C. Zhu, D. Du, Y. Lin, Graphene and graphene-like 2D materials for optical biosensing and bioimaging: a review, 2D Mater. 2 (2015), 032004. Art. no.
[70] C. Yu, L. Shi, Z. Yao, D. Li, A. Majumdar, Thermal conductance and ther-mopower of an individual single-wall carbon nanotube, Nano Lett. 5 (2005) 1842–1846.
[71] J.H. Seol, I. Jo, A.L. Moore, L. Lindsay, Z.H. Aitken, M.T. Pettes, X. Li, Z. Yao, R. Huang, D. Broido, N. Mingo, R.S. Ruoff, L. Shi, Two-dimensional phonon transport in supported graphene, Science 328 (2010) 213–216.
[72] A.A. Balandin, Thermal properties of graphene and nanostructured carbon materials, Nat. Mater. 10 (2011) 569–581.
[73] D. Nika, E. Pokatilov, A. Askerov, A. Balandin, Phonon thermal conduction in graphene: role of umklapp and edge roughness scattering, Phys. Rev. B 79 (2009), 155413. Art. no.
[74] J.-W. Jiang, J. Lan, J.-S. Wang, B. Li, Isotopic effects on the thermal conductivity of graphene nanoribbons: localization mechanism, J. Appl. Phys. 107 (2010), 054314.
[75] M.T. Pettes, I. Jo, Z. Yao, L. Shi, Influence of polymeric residue on the thermal conductivity of suspended bilayer graphene, Nano Lett. 11 (2011) 1195–1200.
[76] T. Anthony, W. Banholzer, J.F. Fleischer, L. Wei, P. Kuo, R. Thomas, R. Pryor, Thermal diffusivity of isotopically enriched c 12 diamond, Phys. Rev. B 42 (1990), 1104. Art. no.
[77] L. Shi, J. Zhou, P. Kim, A. Bachtold, A. Majumdar, P.L. McEuen, Thermalprobing of energy dissipation in current-carrying carbon nanotubes, J. Appl. Phys. 105 (2009), 104306. Art. no.
[78] W. Cai, A.L. Moore, Y. Zhu, X. Li, S. Chen, L. Shi, R.S. Ruoff, Thermal transport in suspended and supported monolayer graphene grown by chemical vapor deposition, Nano Lett. 10 (2010) 1645–1651.
[79] E. Pollak, B. Geng, K.-J. Jeon, I.T. Lucas, T.J. Richardson, F. Wang, R. Kostecki, The interaction of Li $^{+}$ with single-layer and few-layer graphene, Nano Lett. 10 (2010) 3386–3388.
[80] C. Uthaisar, V. Barone, Edge effects on the characteristics of Li diffusion ingraphene, Nano Lett. 10 (2010) 2838–2842.
[81] L.-J. Zhou, Z. Hou, L.-M. Wu, First-principles study of lithium adsorptionand diffusion on graphene with point defects, J. Phys. Chem. C 116 (2012) 21780–21787.
[82] D. Pan, S. Wang, B. Zhao, M. Wu, H. Zhang, Y. Wang, Z. Jiao, Li storage properties of disordered graphene nanosheets, Chem. Mater. 21 (2009) 3136–3142.
[83] H. Xiang, B. Tian, P. Lian, Z. Li, H. Wang, Sol-gel synthesis and electro-chemical performance of $Li_4Ti_5O_{12}$/graphene composite anode for lithium-ion batteries, J. Alloys Compd. 509 (2011) 7205–7209.
[84] Y. Fang, Y. Lv, R. Che, H. Wu, X. Zhang, D. Gu, G. Zheng, D. Zhao, Two-dimensional mesoporous carbon nanosheets and their derived graphene nanosheets: synthesis and efficient lithium ion storage, J. Am. Chem. Soc. 135 (2013) 1524–1530.
[85] H. Wang, T. Maiyalagan, X. Wang, Review on recent progress in nitrogen-doped graphene: synthesis, characterization, and its potential applications, ACS Catal. 2 (2012) 781–794.
[86] Z.-S. Wu, W. Ren, L. Xu, F. Li, H.-M. Cheng, Doped graphene sheets as anode materials with superhigh rate and large capacity for lithium ion batteries, ACS Nano 5 (2011) 5463–5471.
[87] H. Wang, C. Zhang, Z. Liu, L. Wang, P. Han, H. Xu, K. Zhang, S. Dong, J. Yao, G. Cui, Nitrogen-doped graphene nanosheets with excellent lithium storage properties, J. Mater. Chem. 21 (2011) 5430–5434.
[88] X. Li, D. Geng, Y. Zhang, X. Meng, R. Li, X. Sun, Superior cycle stability of nitrogen-doped graphene nanosheets as anodes for lithium ion batteries, Electrochem. Commun. 13 (2011) 822–825.
[89] D. Sun, J. Yang, X. Yan, Hierarchically porous and nitrogen, sulfur-codopedgraphene-like microspheres as a high capacity anode for lithium ion batteries, Chem. Commun. 51 (2015) 2134–2137.
[90] X. Cai, L. Lai, Z. Shen, J. Lin, Graphene and graphene-based composites as Li-ion battery electrode materials and their application in full cells, J. Mater. Chem. 5 (2017) 15423–15446.
[91] J. Zhang, H. Cao, X. Tang, W. Fan, G. Peng, M. Qu, Graphite/grapheneoxide composite as high capacity and binder-free anode material for lithium ion batteries, J. Power Sources 241 (2013) 619–626.
[92] J. Luo, X. Zhao, J. Wu, H.D. Jang, H.H. Kung, J. Huang, Crumpled graphene-encapsulated Si nanoparticles for lithium ion battery anodes, J. Phys. Chem. Lett. 3 (2012) 1824–1829.
[93] E. Yoo, J. Kim, E. Hosono, H.-s. Zhou, T. Kudo, I. Honma, Large reversible Li storage of graphene nanosheet families for use in rechargeable lithium ion batteries, Nano Lett. 8 (2008) 2277–2282.
[94] G. Wang, X. Shen, J. Yao, J. Park, Graphene nanosheets for enhanced lithium storage in lithium ion batteries, Carbon 47 (2009) 2049–2053.
[96] P. Lian, X. Zhu, S. Liang, Z. Li, W. Yang, H. Wang, Large reversible capacityof high quality graphene sheets as an anode material for lithium-ion batteries, Electrochim. Acta 55 (2010) 3909–3914.
[97] Y.S. Yun, V.-D. Le, H. Kim, S.-J. Chang, S.J. Baek, S. Park, B.H. Kim, Y.-H. Kim, K. Kang, H.-J. Jin, Effects of sulfur doping on graphene-based nanosheets for use as anode materials in lithium-ion batteries, J. Power Sources 262 (2014) 79–85.
[98] P. Guo, H. Song, X. Chen, Electrochemical performance of graphenenanosheets as anode material for lithium-ion batteries, Electrochem. Commun. 11 (2009) 1320–1324.
[99] T. Li, L. Gao, A high-capacity graphene nanosheet material with capacitive characteristics for the anode of lithium-ion batteries, J. Solid State Electrochem. 16 (2012) 557–561.
[100] S. Petnikota, N.K. Rotte, V.V. Srikanth, B.S. Kota, M. Reddy, K.P. Loh, B. Chowdari, Electrochemical studies of few-layered graphene as an anode material for Li ion batteries, J. Solid State Electrochem. 18 (2014) 941–949.
[101] W. Chen, Z. Zhu, S. Li, C. Chen, L. Yan, Efficient preparation of highly hydrogenated graphene and its application as a high-performance anode material for lithium ion batteries, Nanoscale 4 (2012) 2124–2129.
[102] H. Xiang, Z. Li, K. Xie, J. Jiang, J. Chen, P. Lian, J. Wu, Y. Yu, H. Wang, Graphene sheets as anode materials for Li-ion batteries: preparation, structure, electrochemical properties and mechanism for lithium storage, RSC Adv. 2 (2012) 6792–6799.
[103] Z. Jiang, B. Pei, A. Manthiram, Randomly stacked holey graphene anodes for lithium ion batteries with enhanced electrochemical performance, J. Mater. Chem. 1 (2013) 7775–7781.
[104] Y. Yan, Y.-X. Yin, S. Xin, Y.-G. Guo, L.-J. Wan, Ionothermal synthesisof sulfur-doped porous carbons hybridized with graphene as superior anode materials for lithium-ion batteries, Chem. Commun. 48 (2012) 10663–10665.

[105] D. Cai, C. Wang, C. Shi, N. Tan, Facile synthesis of N and S co-doped graphene sheets as anode materials for high-performance lithium-ion batteries, J. Alloys Compd. 731 (2018) 235–242.

[106] C. Ma, X. Shao, D. Cao, Nitrogen-doped graphene nanosheets as anode ma-terials for lithium ion batteries: a first-principles study, J. Mater. Chem. 22 (2012) 8911–8915.

[107] S. Huang, L. Zhang, J. Zhu, P.K. Shen, et al., Crumpled nitrogen-and boron-dual-self-doped graphene sheets as an extraordinary active anode material for lithium ion batteries, J. Mater. Chem. 4 (2016) 14155–14162.

[108] W. Qi, X. Li, H. Li, W. Wu, P. Li, Y. Wu, C. Kuang, S. Zhou, X. Li, Sandwich-structured nanocomposites of N-doped graphene and nearly monodisperse Fe_3O_4 nanoparticles as high-performance Li-ion battery anodes, Nano Res. 10 (2017) 2923–2933.

[109] L. Zhan, S. Yang, Y. Wang, Y. Wang, L. Ling, X. Feng, Fabrication of Fully fluorinated graphene nanosheets towards high-performance lithium storage, Adv. Mater. Interfac. 1 (2014), 1300149. Art. no.

[110] Y. Zhan, B. Zhang, L. Cao, X. Wu, Z. Lin, X. Yu, X. Zhang, D. Zeng, F. Xie, W. Zhang, et al., Iodine doped graphene as anode material for lithium ion battery, Carbon 94 (2015) 1–8.

[111] Y. Luan, R. Hu, Y. Fang, K. Zhu, K. Cheng, J. Yan, K. Ye, G. Wang, D. Cao, Nitrogen and phosphorus dual-doped multilayer graphene as universal anode for full carbon-based lithium and potassium ion capacitors, Nano-Micro Lett. 11 (2019) 1–13.

[112] J. Hu, C. Ouyang, S.A. Yang, H.Y. Yang, Germagraphene as a promis-ing anode material for lithium-ion batteries predicted from first-principles calculations, Nanoscale Horizons 4 (2019) 457–463.

[113] Y. Shi, L. Wen, F. Li, H.-M. Cheng, Nanosized $Li_4Ti_5O_{12}$/graphene hybrid materials with low polarization for high rate lithium ion batteries, J. Power Sources 196 (2011) 8610–8617.

[114] A. Naserieh, T. Gholami, M. Ghiyasiyan-Arani, M. Salavati-Niasari, Insight into effects of graphene and zinc oxide in $Li_4Ti_5O_{12}$ as anode materials forLi-ion full-cell battery, Int. J. Hydrogen Energy 45 (2020) 27705–27712.

[115] H.-C. Tao, L.-Z. Fan, X. Yan, X. Qu, In situ synthesis of Tio_2–graphenenano sheets composites as anode materials for high-power lithium ion batteries, Electrochim. Acta 69 (2012) 328–333.

[116] Y. Qiu, K. Yan, S. Yang, L. Jin, H. Deng, W. Li, Synthesis of size-tunableanatase TiO_2 nanospindles and their assembly into anatase@titanium oxyni-tride/titanium nitride-graphene nanocomposites for rechargeable lithium ion batteries with high cycling performance, ACS Nano 4 (2010) 6515–6526.

[117] T. Hu, X. Sun, H. Sun, M. Yu, F. Lu, C. Liu, J. Lian, Flexible free-standing graphene–TiO_2 hybrid paper for use as lithium ion battery anode materials, Carbon 51 (2013) 322–326.

[118] D. Cai, P. Lian, X. Zhu, S. Liang, W. Yang, H. Wang, High specific capacity of TiO_2-graphene nanocomposite as an anode material for lithium-ion batteriesin an enlarged potential window, Electrochim. Acta 74 (2012) 65–72.

[119] J.K. Lee, K.B. Smith, C.M. Hayner, H.H. Kung, Silicon nanoparticles–graphene paper composites for Li ion battery anodes, Chem. Commun. 46 (2010) 2025–2027.

[120] H. Tang, Y. Zhang, Q. Xiong, J. Cheng, Q. Zhang, X. Wang, C. Gu, J. Tu, Self-assembly silicon/porous reduced graphene oxide composite film as a binder-free and flexible anode for lithium-ion batteries, Electrochim. Acta 156 (2015) 86–93.

[121] H. Jiang, X. Zhou, G. Liu, Y. Zhou, H. Ye, Y. Liu, K. Han, Free-standing Si/graphene paper using Si nanoparticles synthesized by acid-etching Al-Si alloy powder for high-stability Li-ion battery anodes, Electrochim. Acta 188 (2016) 777–784.

[122] J. Chang, X. Huang, G. Zhou, S. Cui, P.B. Hallac, J. Jiang, P.T. Hurley, J. Chen, Multilayered Si nanoparticle/reduced graphene oxide hybrid as a high-performance lithium-ion battery anode, Adv. Mater. 26 (2014) 758–764.

[123] D. Li, K.H. Seng, D. Shi, Z. Chen, H.K. Liu, Z. Guo, A unique sandwich-structured C/Ge/graphene nanocomposite as an anode material for high power lithium ion batteries, J. Mater. Chem. 1 (2013) 14115–14121.

[124] H. Kim, Y. Son, C. Park, J. Cho, H.C. Choi, Catalyst-free direct growth ofa single to a few layers of graphene on a germanium nanowire for the anode material of a lithium battery, Angew. Chem. 125 (2013) 6113–6117.

[125] X. Zhou, L.-J. Wan, Y.-G. Guo, Binding SnO_2 nanocrystals in nitrogen-doped graphene sheets as anode materials for lithium-ion batteries, Adv. Mater. 25 (2013) 2152–2157.

[126] C. Zhang, X. Peng, Z. Guo, C. Cai, Z. Chen, D. Wexler, S. Li, H. Liu, Carbon-coated SnO_2/graphene nanosheets as highly reversible anode materials forlithium ion batteries, Carbon 50 (2012) 1897–1903.

[127] X. Li, X. Meng, J. Liu, D. Geng, Y. Zhang, M.N. Banis, Y. Li, J. Yang, R. Li, X. Sun, M. Cai, M.W. Verbrugge, Tin oxide with controlled morphology and crystallinity by atomic layer deposition onto graphene nanosheets for enhanced lithium storage, Adv. Funct. Mater. 22 (2012) 1647–1654.

[128] L. Fei, Q. Lin, B. Yuan, G. Chen, P. Xie, Y. Li, Y. Xu, S. Deng, S. Smirnov, H. Luo, Reduced graphene oxide wrapped FeS nanocomposite for lithium-ion battery anode with improved performance, ACS Appl. Mater. Interfaces 5 (2013) 5330–5335.

[129] X. Zhou, J. Bao, Z. Dai, Y.-G. Guo, Tin nanoparticles impregnated innitrogen-doped graphene for lithium-ion battery anodes, J. Phys. Chem. C 117 (2013) 25367–25373.

[130] G. Huang, T. Chen, Z. Wang, K. Chang, W. Chen, Synthesis and electro-chemical performances of cobalt sulfides/graphene nanocomposite as anode material of Li-ion battery, J. Power Sources 235 (2013) 122–128.

[131] F. Sun, K. Huang, X. Qi, T. Gao, Y. Liu, X. Zou, X. Wei, J. Zhong, Arationally designed composite of alternating strata of Si nanoparticles and graphene: a high-performance lithium-ion battery anode, Nanoscale 5 (2013) 8586–8592.

[132] Y. Chen, J. Zhu, B. Qu, B. Lu, Z. Xu, Graphene improving lithium-ionbattery performance by construction of $NiCo_2O_4$/graphene hybrid nanosheet arrays, Nano Energy 3 (2014) 88–94.

[133] N. Mahmood, C. Zhang, F. Liu, J. Zhu, Y. Hou, Hybrid of Co_3Sn_2@Conanoparticles and nitrogen-doped graphene as a lithium ion battery anode, ACS Nano 7 (2013) 10307–10318.

[134] J. Qin, C. He, N. Zhao, Z. Wang, C. Shi, E.-Z. Liu, J. Li, Graphene networksanchored with Sn@graphene as lithium ion battery anode, ACS Nano 8 (2014) 1728–1738.

[135] Y. Li, Z. Wang, X.-J. Lv, N-doped TiO_2 nanotubes/N-doped graphene-nanosheets composites as high performance anode materials in lithium-ion battery, J. Mater. Chem. 2 (2014) 15473–15479.

[136] K.H. Park, D. Lee, J. Kim, J. Song, Y.M. Lee, H.-T. Kim, J.-K. Park, Defect-free, size-tunable graphene for high-performance lithium ion battery, Nano Lett. 14 (2014) 4306–4313.

[137] M. Zhou, X. Li, B. Wang, Y. Zhang, J. Ning, Z. Xiao, X. Zhang, Y. Chang, L. Zhi, High-performance silicon battery anodes enabled by engineering graphene assemblies, Nano Lett. 15 (2015) 6222–6228.

[138] I.H. Son, J. Hwan Park, S. Kwon, S. Park, M.H. Rummeli, A. Bachmatiuk, H. J. Song, J. Ku, J.W. Choi, J.-M. Choi, S.-G. Doo, H. Chang, Silicon carbide-free graphene growth on silicon for lithium-ion battery with high volumetric energy density, Nat. Commun. 6 (2015) 1–8.

[139] J. Huang, D. Liu, C. Gu, J. Liu, General approach for preparing sandwich-structured metal sulfide@reduced graphene oxide as highly reversible Li-ion battery anode, Mater. Res. Lett. 6 (2018) 307–313.

[140] Y. Qi, C. Zhang, S. Liu, Y. Zong, Y. Men, Room-temperature synthesisof ZnO@GO nanocomposites as anode for lithium-ion batteries, J. Mater. Res. 33 (2018) 1506–1514.

[141] L. Liu, X. Li, G. Zhang, Z. Zhang, C. Fang, H. Ma, W. Luo, Z. Liu, Enhancedstability lithium-ion battery based on optimized graphene/Si nanocomposites by templated assembly, ACS Omega 4 (2019) 18195–18202.

[142] H. Li, B. Zhang, X. Wang, J. Zhang, T. An, Z. Ding, W. Yu, H. Tong, Heterostructured SnO_2-SnS_2@C embedded in nitrogen-doped graphene asa robust anode material for lithium-ion batteries, Front. Chem. 7 (2019), 339.

[143] Y. Mussa, F. Ahmed, M. Arsalan, E. Alsharaeh, Two dimensional (2D)reduced graphene oxide (RGO)/hexagonal boron nitride (h-BN) based nanocomposites as anodes for high temperature rechargeable lithium-ion bat- teries, Sci. Rep. 10 (2020) 1–13.

[144] Z. Li, W. Feng, Y. Lin, X. Liu, H. Fei, Flaky CoS_2 and graphene nanocomposite anode materials for sodium-ion batteries with improved performance, RSC Adv. 6 (2016) 70632–70637.

[145] M. Shi, T. Wu, X. Song, J. Liu, L. Zhao, P. Zhang, L. Gao, Active Fe_2O_3 nanoparticles encapsulated in porous gC_3N_4/graphene sandwich-type nanosheets as a superior anode for high-performance lithium-ion batteries, J. Mater. Chem. 4 (2016) 10666–10672.

[146] Y.-X. Wang, Y.-G. Lim, M.-S. Park, S.-L. Chou, J.H. Kim, H.-K. Liu, S.-X. Dou, Y.-J. Kim, Ultrafine SnO_2 nanoparticle loading onto reduced graphene oxide as anodes for sodium-ion batteries with superior rate and cycling performances, J. Mater. Chem. 2 (2014) 529–534.

[147] J. Song, Z. Yu, M.L. Gordin, S. Hu, R. Yi, D. Tang, T. Walter, M. Regula, D. Choi, X. Li, A. Manivannan, D. Wang, Chemically bonded phosphorus/graphene hybrid as a high performance anode for sodium-ion batteries, Nano Lett. 14 (2014) 6329–6335.

[148] X. Zhou, X. Liu, Y. Xu, Y. Liu, Z. Dai, J. Bao, An SbO_x/reduced graphene oxide composite as a high-rate anode material for sodium-ion batteries, J. Phys. Chem. C 118 (2014) 23527–23534.

[149] C. Wu, P. Kopold, Y.-L. Ding, P.A. van Aken, J. Maier, Y. Yu, Synthesizing porous $NaTi_2(PO_4)_3$ nanoparticles embedded in 3D graphene networks for high-rate and long cycle-life sodium electrodes, ACS Nano 9 (2015) 6610–6618.

[150] Y. Chen, Z. Guo, B. Jian, C. Zheng, H. Zhang, N-doped modified graphene/Fe_2O_3 nanocomposites as high-performance anode material forsodium ion storage, Nanomaterials 9 (2019), 1770.

[151] J. Lu, Z. Chen, Z. Ma, F. Pan, L.A. Curtiss, K. Amine, The role of nanotechnology in the development of battery materials for electric vehicles, Nat. Nanotechnol. 11 (2016) 1031–1038.

[152] F. Lin, D. Nordlund, T.-C. Weng, Y. Zhu, C. Ban, R.M. Richards, H.L. Xin, Phase evolution for conversion reaction electrodes in lithium-ion batteries, Nat. Commun. 5 (2014) 1–9.

[153] N. Nitta, G. Yushin, High-capacity anode materials for lithium-ion batteries: choice of elements and structures for active particles, Part. Part. Syst. Char. 31 (2014) 317–336.

[154] S. Yang, X. Feng, S. Ivanovici, K. Mullen, Fabrication of graphene-encapsulated oxide nanoparticles: towards high-performance anode materials for lithium storage, Angew. Chem. Int. Ed. 49 (2010) 8408–8411.

[155] Y. Su, S. Li, D. Wu, F. Zhang, H. Liang, P. Gao, C. Cheng, X. Feng, Two-dimensional carbon-coated graphene/metal oxide hybrids for enhanced lithium storage, ACS Nano 6 (2012) 8349–8356.

[156] Y. Sun, X. Hu, W. Luo, F. Xia, Y. Huang, Reconstruction of conformal nanoscale MnO on graphene as a high-capacity and long-life anode material for lithium ion batteries, Adv. Funct. Mater. 23 (2013) 2436–2444.

[157] S. Jin, X. Sun, S. Cai, J. Guo, A. Fan, N. Zhang, H. Wu, C. Zheng, SnS_2 quantum dots uniformly anchored on dispersed S-doped graphene as high-rate anodes for sodium-ion batteries, Ceram. Int. 46 (2020) 14416–14424.

[159] D. Su, S. Dou, G. Wang, Ultrathin MoS_2 nanosheets as anode materials forsodium-ion batteries with superior performance, Adv. Energy Mater. 5 (2015), 1401205.
[160] S. Xia, Y. Wang, Y. Liu, C. Wu, M. Wu, H. Zhang, Ultrathin MoS_2nanosheets tightly anchoring onto nitrogen-doped graphene for enhanced lithium storage properties, Chem. Eng. J. 332 (2018) 431–439.
[161] M. Chhowalla, H.S. Shin, G. Eda, L.-J. Li, K.P. Loh, H. Zhang, The chemistry of two-dimensional layered transition metal dichalcogenide nanosheets, Nat. Chem. 5 (2013) 263–275.
[162] A. Castellanos-Gomez, M. Poot, G.A. Steele, H.S. Van Der Zant, N. Agraıt, G. Rubio-Bollinger, Elastic properties of freely suspended MoS_2 nanosheets, Adv. Mater. 24 (2012) 772–775.
[163] S. Bertolazzi, J. Brivio, A. Kis, Stretching and breaking of ultrathin MoS_2, ACS Nano 5 (2011) 9703–9709.
[164] H. Zeng, J. Dai, W. Yao, D. Xiao, X. Cui, Valley polarization in MoS_2 monolayers by optical pumping, Nat. Nanotechnol. 7 (2012) 490–493.
[165] H. Li, G. Lu, Z. Yin, Q. He, H. Li, Q. Zhang, H. Zhang, Optical identification of single and few-layer MoS_2 sheets, Small 8 (2012) 682–686.
[166] A. Splendiani, L. Sun, Y. Zhang, T. Li, J. Kim, C.-Y. Chim, G. Galli, F. Wang, Emerging photoluminescence in monolayer MoS_2, Nano Lett. 10 (2010) 1271–1275.
[167] K.F. Mak, C. Lee, J. Hone, J. Shan, T.F. Heinz, Atomically thin MoS_2: a new direct-gap semiconductor, Phys. Rev. Lett. 105 (2010), 136805.
[168] M. Benameur, B. Radisavljevic, J. H'eron, S. Sahoo, H. Berger, A. Kis, Visibility of dichalcogenide nanolayers, Nanotechnology 22 (2011), 125706.
[169] F. Gustavsson, F. Svahn, U. Bexell, S. Jacobson, Nanoparticle based and sputtered WS_2 low-friction coatings differences and similarities with respect to friction mechanisms and tribo-film formation, Surf. Coating. Technol. 232 (2013) 616–626.
[170] H. Topsøe, B.S. Clausen, F.E. Massoth, Hydrotreating catalysis, in: Catalysis, Springer, 1996, pp. 1–269.
[171] A. Sobczynski, Molybdenum disulfide as a hydrogen evolution catalyst for water photodecomposition on semiconductors, J. Catal. 131 (1991) 156–166.
[172] Y. Yu, L. Gu, A. Dhanabalan, C.-H. Chen, C. Wang, Three-dimensional porous amorphous SnO_2 thin films as anodes for Li-ion batteries, Electrochim. Acta 54 (2009) 7227–7230.
[173] S. Goriparti, E. Miele, F. De Angelis, E. Di Fabrizio, R.P. Zaccaria, C. Capiglia, Review on recent progress of nanostructured anode materials for Li-ion batteries, J. Power Sources 257 (2014) 421–443.
[174] F. Bozheyev, A. Zhexembekova, S. Zhumagali, A. Molkenova, Z. Bakenov, MoS_2 nanopowder as anode material for lithium-ion batteries produced by self-propagating high-temperature synthesis, Mater. Today Proc. 4 (2017) 4567–4571.
[175] D. Chen, G. Ji, B. Ding, Y. Ma, B. Qu, W. Chen, J.Y. Lee, Double transition-metal chalcogenide as a high-performance lithium-ion battery anode material, Ind. Eng. Chem. Res. 53 (2014) 17901–17908.
[176] Y. Jing, Z. Zhou, C.R. Cabrera, Z. Chen, Metallic VS_2 monolayer: a promising 2D anode material for lithium ion batteries, J. Phys. Chem. C 117 (2013) 25409–25413.
[177] E. Yang, H. Ji, Y. Jung, Two-dimensional transition metal dichalcogenidemonolayers as promising sodium ion battery anodes, J. Phys. Chem. C 119 (2015) 26374–26380.
[178] K. Chang, W. Chen, In situ synthesis of MoS_2/graphene nanosheet composites with extraordinarily high electrochemical performance for lithium ion batteries, Chem. Commun. 47 (2011) 4252–4254.
[179] Z. Zhang, M. Yang, N. Zhao, L. Wang, Y. Li, Two-dimensional transitionmetal dichalcogenides as promising anodes for potassium ion batteries from first-principles prediction, Phys. Chem. Chem. Phys. 21 (2019) 23441–23446.
[180] Z. Zhang, S. Wu, J. Cheng, W. Zhang, MoS_2 nanobelts with (002) plane edges enriched flat surfaces for high-rate sodium and lithium storage, Energy Storage Mater. 15 (2018) 65–74.
[181] N. Ma, X.-Y. Jiang, L. Zhang, X.-S. Wang, Y.-L. Cao, X.-Z. Zhang, Novel 2D layered molybdenum ditelluride encapsulated in few-layer graphene as high-performance anode for lithium-ion batteries, Small 14 (2018), 1703680.
[182] K. Maleski, C.E. Ren, M.-Q. Zhao, B. Anasori, Y. Gogotsi, Size-dependent physical and electrochemical properties of two-dimensional MXene flakes, ACS Appl. Mater. Interfaces 10 (2018) 24491–24498.
[183] Y.-X. Li, D.B. Putungan, S.-H. Lin, Two-dimensional MTe_2 (M= Co, Fe,Mn, Sc, Ti) transition metal tellurides as sodium ion battery anode materials: density functional theory calculations, Phys. Lett. 382 (2018) 2781–2786.
[184] Q. Zhang, J. Ma, M. Lei, R. Quhe, Metallic Monolayer and its application as anode for lithium-ion batteries, Nanotechnology 29 (2018), 165402.
[185] S. Mukherjee, J. Turnley, E. Mansfield, J. Holm, D. Soares, L. David, G. Singh, Exfoliated transition metal dichalcogenide nanosheets for super-capacitor and sodium ion battery applications, R. Soc. Open Sci. 6 (2019), 190437.
[186] G. Cai, L. Peng, S. Ye, Y. Huang, G. Wang, X. Zhang, Defect-rich $MOs_{2(1-x)}Se_{2x}$ few-layer nanocomposites: a superior anode material for high-performance lithium-ion batteries, J. Mater. Chem. 7 (2019) 9837–9843.
[187] J. Li, H. Wang, W. Wei, L. Meng, Advanced MoS_2 and graphene heterostructures as high-performance anode for sodium-ion batteries, Nanotechnology 30 (2019), 104003. Art. no.
[188] C. Tang, X. Wei, X. Cai, Q. An, P. Hu, J. Sheng, J. Zhu, S. Chou, L. Wu, L. Mai, ZnSe microsphere/multiwalled carbon nanotube composites as high-rate and long-life anodes for sodium-ion batteries, ACS Appl. Mater. Interfaces 10 (2018) 19626–19632.
[189] Y. Liu, X. Wang, Reduced graphene oxides decorated NiSe nanoparticles as high performance electrodes for Na/Li storage, Materials 12 (2019), 3709.
[190] Q.H. Nguyen, T. Park, J. Hur, Enhanced cycle stability of zinc sulfide anode for high-performance lithium-ion storage: effect of conductive hybrid matrix on active ZnS, Nanomaterials 9 (2019), 1221.
[191] Y. Wu, Y. Xu, Y. Li, P. Lyu, J. Wen, C. Zhang, M. Zhou, Y. Fang, H. Zhao, U. Kaiser, et al., Unexpected intercalation-dominated potassium storage in WS_2 as a potassium-ion battery anode, Nano Res. 12 (2019) 2997–3002.
[192] M. Naguib, O. Mashtalir, J. Carle, V. Presser, J. Lu, L. Hultman, Y. Gogotsi, M. W. Barsoum, Two-dimensional transition metal carbides, ACS Nano 6 (2012) 1322–1331.
[193] M. Sokol, V. Natu, S. Kota, M.W. Barsoum, On the chemical diversity ofthe MAX phases, Trends Chem. 1 (2019) 210–223.
[194] L. Verger, C. Xu, V. Natu, H.-M. Cheng, W. Ren, M.W. Barsoum, Overview of the synthesis of MXenes and other ultrathin 2D transition metal carbides and nitrides, Curr. Opin. Solid State Mater. Sci. 23 (2019) 149–163.
[195] C. Xu, L. Wang, Z. Liu, L. Chen, J. Guo, N. Kang, X.-L. Ma, H.-M. Cheng, W. Ren, Large-area high-quality 2D ultrathin Mo_2C superconducting crystals, Nat. Mater. 14 (2015) 1135–1141.
[196] M. Xu, T. Liang, M. Shi, H. Chen, Graphene-like two-dimensional materials, Chem. Rev. 113 (2013) 3766–3798.
[197] H. Zhang, Ultrathin two-dimensional nanomaterials, ACS Nano 9 (2015) 9451–9469.
[198] V. Nicolosi, M. Chhowalla, M.G. Kanatzidis, M.S. Strano, J.N. Coleman, Liquid exfoliation of layered materials, Science 340 (2013), 1226419.
[199] M. Naguib, V.N. Mochalin, M.W. Barsoum, Y. Gogotsi, 25th anniversary article: MXenes: a new family of two-dimensional materials, Adv. Mater. 26 (2014) 992–1005.
[200] X. Tang, X. Guo, W. Wu, G. Wang, 2D metal carbides and nitrides (MXenes) as high-performance electrode materials for Lithium-based batteries, Adv. Energy Mater. 8 (2018), 1801897.
[201] M.A. Hope, A.C. Forse, K.J. Griffith, M.R. Lukatskaya, M. Ghidiu, Y. Gogotsi, C. P. Grey, NMR reveals the surface functionalisation of Ti_3C_2MXene, Phys. Chem. Chem. Phys. 18 (2016) 5099–5102.
[202] J. Halim, K.M. Cook, M. Naguib, P. Eklund, Y. Gogotsi, J. Rosen, M.W. Barsoum, X-ray photoelectron spectroscopy of select multi-layered transition metal carbides (mxenes), Appl. Surf. Sci. 362 (2016) 406–417.
[203] M. Khazaei, M. Arai, T. Sasaki, C.-Y. Chung, N.S. Venkataramanan, M. Estili, Y. Sakka, Y. Kawazoe, Novel electronic and magnetic properties of two-dimensional transition metal carbides and nitrides, Adv. Funct. Mater. 23 (2013) 2185–2192.
[204] M. Khazaei, A. Ranjbar, M. Arai, T. Sasaki, S. Yunoki, Electronic properties and applications of MXenes: a theoretical review, J. Mater. Chem. C 5 (2017) 2488–2503.
[205] Y. Xie, P. Kent, Hybrid density functional study of structural and electronicproperties of functionalized Ti $_{n+1}X_n$ (X = C,N) monolayers, Phys. Rev. 87 (2013), 235441.
[206] Y. Xie, M. Naguib, V.N. Mochalin, M.W. Barsoum, Y. Gogotsi, X. Yu, K.-W. Nam, X.-Q. Yang, A.I. Kolesnikov, P.R. Kent, Role of surface structure on Li-ion energy storage capacity of two-dimensional transition-metal carbides, J. Am. Chem. Soc. 136 (2014) 6385–6394.
[207] B. Anasori, M.R. Lukatskaya, Y. Gogotsi, 2D metal carbides and nitrides (MXenes) for energy storage, Nat. Rev. Mater. 2 (2017) 1–17.
[208] M. Alhabeb, K. Maleski, B. Anasori, P. Lelyukh, L. Clark, S. Sin, Y. Gogotsi, Guidelines for synthesis and processing of two-dimensional titanium carbide ($Ti_3C_2T_x$ MXene), Chem. Mater. 29 (2017) 7633–7644.
[209] M. Naguib, Y. Gogotsi, Synthesis of two-dimensional materials by selective extraction, Accounts Chem. Res. 48 (2015) 128–135.
[210] O. Mashtalir, M. Naguib, B. Dyatkin, Y. Gogotsi, M.W. Barsoum, Kinetics of aluminum extraction from Ti_3AlC_2 in hydrofluoric acid, Mater. Chem. Phys. 139 (2013) 147–152.
[211] X. Sang, Y. Xie, M.-W. Lin, M. Alhabeb, K.L. Van Aken, Y. Gogotsi, P.R. Kent, K. Xiao, R.R. Unocic, Atomic defects in monolayer titanium carbide ($Ti_3C_2T_x$) MXene, ACS Nano 10 (2016) 9193–9200.
[212] Q. Tao, M. Dahlqvist, J. Lu, S. Kota, R. Meshkian, J. Halim, J. Palisaitis, L. Hultman, M.W. Barsoum, P.O. Persson, et al., Two-dimensional $Mo_{1.33}$CMXene with divacancy ordering prepared from parent 3D laminate with in- plane chemical ordering, Nat. Commun. 8 (2017) 1–7.
[213] J. Zhou, X. Zha, X. Zhou, F. Chen, G. Gao, S. Wang, C. Shen, T. Chen, C. Zhi, P. Eklund, et al., Synthesis and electrochemical properties of two-dimensional hafnium carbide, ACS Nano 11 (2017) 3841–3850.
[214] H.-W. Wang, M. Naguib, K. Page, D.J. Wesolowski, Y. Gogotsi, Resolving the structure of $Ti_3C_2T_x$ MXenes through multilevel structural modeling of the atomic pair distribution function, Chem. Mater. 28 (2016) 349–359.
[215] A. Feng, Y. Yu, Y. Wang, F. Jiang, Y. Yu, L. Mi, L. Song, Two-dimensional MXene Ti_3C_2 produced by exfoliation of Ti_3AlC_2, Mater. Des. 114 (2017) 161–166.
[216] M. Ghidiu, M.R. Lukatskaya, M.-Q. Zhao, Y. Gogotsi, M.W. Barsoum, Conductive two-dimensional titanium carbide 'clay' with high volumetric capacitance, Nature 516 (2014) 78–81.
[217] F. Shahzad, M. Alhabeb, C.B. Hatter, B. Anasori, S. Man Hong, C.M. Koo, Y. Gogotsi, Electromagnetic interference shielding with 2D transition metal carbides (MXenes), Science 353 (2016) 1137–1140.
[218] P. Urbankowski, B. Anasori, T. Makaryan, D. Er, S. Kota, P.L. Walsh, M. Zhao, V. B. Shenoy, M.W. Barsoum, Y. Gogotsi, Synthesis of two-dimensional titanium nitride Ti_4N_3 (MXene), Nanoscale 8 (2016) 11385–11391.
[219] M. Wu, B. Wang, Q. Hu, L. Wang, A. Zhou, The synthesis process and thermal stability of V_2C MXene, Materials 11 (2018), 2112.

[220] J. Xuan, Z. Wang, Y. Chen, D. Liang, L. Cheng, X. Yang, Z. Liu, R. Ma, T. Sasaki, F. Geng, Organic-base-driven intercalation and delamination for the production of functionalized titanium carbide nanosheets with superior photothermal therapeutic performance, Angew. Chem. 128 (2016) 14789–14794.

[221] R. Liu, W. Cao, D. Han, Y. Mo, H. Zeng, H. Yang, W. Li, Nitrogen-doped Nb_2CT_x MXene as anode materials for lithium ion batteries, J. Alloys Compd. 793 (2019) 505–511.

[222] M. Ghidiu, J. Halim, S. Kota, D. Bish, Y. Gogotsi, M.W. Barsoum, Ion-exchange and cation solvation reactions in Ti_3C_2 MXene, Chem. Mater. 28 (2016) 3507–3514.

[223] M. Ghidiu, S. Kota, J. Halim, A.W. Sherwood, N. Nedfors, J. Rosen, V. N. Mochalin, M.W. Barsoum, Alkylammonium cation intercalation into Ti_3C_2(MXene): effects on properties and ion-exchange capacity estimation, Chem. Mater. 29 (2017) 1099–1106.

[224] O. Mashtalir, M. Naguib, V.N. Mochalin, Y. Dall'Agnese, M. Heon, M.W. Barsoum, Y. Gogotsi, Intercalation and delamination of layered carbides and carbonitrides, Nat. Commun. 4 (2013) 1–7.

[225] B. Anasori, Y. Xie, M. Beidaghi, J. Lu, B.C. Hosler, L. Hultman, P.R. Kent, Y. Gogotsi, M.W. Barsoum, Two-dimensional, ordered, double transition metals carbides (MXenes), ACS Nano 9 (2015) 9507–9516.

[226] O. Mashtalir, M.R. Lukatskaya, M.-Q. Zhao, M.W. Barsoum, Y. Gogotsi, Amine-assisted delamination of Nb_2C MXene for Li-ion energy storage de-vices, Adv. Mater. 27 (2015) 3501–3506.

[227] M. Naguib, R.R. Unocic, B.L. Armstrong, J. Nanda, Large-scale delamination of multi-layers transition metal carbides and carbonitrides "MXenes", Dalton Trans. 44 (2015) 9353–9358.

[228] K. Maleski, V.N. Mochalin, Y. Gogotsi, Dispersions of two-dimensional titanium carbide MXene in organic solvents, Chem. Mater. 29 (2017) 1632–1640.

[229] V. Natu, M. Clites, E. Pomerantseva, M.W. Barsoum, Mesoporous MXene powders synthesized by acid induced crumpling and their use as Na-ion battery anodes, Mater. Res. Lett. 6 (2018) 230–235.

[230] K. Hantanasirisakul, M.-Q. Zhao, P. Urbankowski, J. Halim, B. Anasori, S. Kota, C. E. Ren, M.W. Barsoum, Y. Gogotsi, Fabrication of $Ti_3C_2T_x$ MXene transparent thin films with tunable optoelectronic properties, Adv. Electron. Mater. 2 (2016), 1600050. Art. no.

[231] A.D. Dillon, M.J. Ghidiu, A.L. Krick, J. Griggs, S.J. May, Y. Gogotsi, M. W. Barsoum, A.T. Fafarman, Highly conductive optical quality solution-processed films of 2D titanium carbide, Adv. Funct. Mater. 26 (2016) 4162–4168.

[232] G. Ying, A.D. Dillon, A.T. Fafarman, M.W. Barsoum, Transparent, con-ductive solution processed spincast 2D Ti_2CT_x (MXene) films, Mater. Res. Lett. 5 (2017) 391–398.

[233] P. Collini, S. Kota, A.D. Dillon, M.W. Barsoum, A.T. Fafarman, Elec-trophoretic deposition of two-dimensional titanium carbide (MXene) thick films, J. Electrochem. Soc. 164 (2017), D573.

[234] J.-Z. Ma, J.-B. He, Y.-F. Xu, B. Lv, D. Chen, W.-L. Zhu, S. Zhang, L.-Y. Kong, X. Gao, L.-Y. Rong, et al., Three-component fermions with surface Fermi arcs in tungsten carbide, Nat. Phys. 14 (2018) 349–354.

[235] D. Geng, X. Zhao, L. Li, P. Song, B. Tian, W. Liu, J. Chen, D. Shi, M. Lin, W. Zhou, et al., Controlled growth of ultrathin Mo_2C superconducting crystals on liquid Cu surface, 2D Mater. 4 (2016), 011012.

[236] Z. Wang, V. Kochat, P. Pandey, S. Kashyap, S. Chattopadhyay, A. Samanta, S. Sarkar, P. Manimunda, X. Zhang, S. Asif, et al., Metal immiscibility route to synthesis of ultrathin carbides, borides, and nitrides, Adv. Mater. 29 (2017), 1700364.

[237] Y. Qi, C. Meng, X. Xu, B. Deng, N. Han, M. Liu, M. Hong, Y. Ning, K. Liu, J. Zhao, et al., Unique transformation from graphene to carbide on Re (0001) induced by strong carbon–metal interaction, J. Am. Chem. Soc. 139 (2017) 17574–17581.

[238] R. Deng, H. Zhang, Y. Zhang, Z. Chen, Y. Sui, X. Ge, Y. Liang, S. Hu, G. Yu, D. Jiang, Graphene/Mo_2C heterostructure directly grown by chemical vapor deposition, Chin. Phys. B 26 (2017), 067901.

[239] D. Geng, X. Zhao, Z. Chen, W. Sun, W. Fu, J. Chen, W. Liu, W. Zhou, K.P. Loh, Direct synthesis of large-area 2D Mo_2C on in situ grown graphene, Adv. Mater. 29 (2017), 1700072.

[240] M. Zeng, Y. Chen, J. Li, H. Xue, R.G. Mendes, J. Liu, T. Zhang, M.H.R. ummeli, L. Fu, 2D WC single crystal embedded in graphene for enhancing hydrogen evolution reaction, Nano Energy 33 (2017) 356–362.

[241] X. Xiao, H. Yu, H. Jin, M. Wu, Y. Fang, J. Sun, Z. Hu, T. Li, J. Wu, L. Huang, et al., Salt-templated synthesis of 2D metallic Mon and other nitrides, ACS Nano 11 (2017) 2180–2186.

[242] J. Jia, T. Xiong, L. Zhao, F. Wang, H. Liu, R. Hu, J. Zhou, W. Zhou, S. Chen, Ultrathin N-doped Mo_2C nanosheets with exposed active sites as efficient electrocatalyst for hydrogen evolution reactions, ACS Nano 11 (2017) 12509–12518.

[243] S. Joshi, Q. Wang, A. Puntambekar, V. Chakrapani, Facile synthesis of large area two-dimensional layers of transition-metal nitride and their use as insertion electrodes, ACS Energy Lett. 2 (2017) 1257–1262.

[244] C. Xu, S. Song, Z. Liu, L. Chen, L. Wang, D. Fan, N. Kang, X. Ma, H.-M. Cheng, W. Ren, Strongly coupled high-quality graphene/2D superconducting Mo_2C vertical heterostructures with aligned orientation, ACS Nano 11 (2017) 5906–5914.

[245] F. Zhang, Z. Zhang, H. Wang, C.H. Chan, N.Y. Chan, X.X. Chen, J.-Y. Dai, Plasma-enhanced pulsed-laser deposition of single-crystalline Mo_2C ultrathin superconducting films, Phys. Rev. Mater. 1 (2017), 034002.

[246] Z. Zhang, F. Zhang, H. Wang, C.H. Chan, W. Lu, J.-y. Dai, Substrate orientation-induced epitaxial growth of face centered cubic Mo_2C superconductive thin film, J. Mater. Chem. C 5 (2017) 10822–10827.

[247] R. Li, L. Zhang, L. Shi, P. Wang, MXene Ti_3C_2: an effective 2D light-to-heat conversion material, ACS Nano 11 (2017) 3752–3759.

[248] K. Wang, Y. Zhou, W. Xu, D. Huang, Z. Wang, M. Hong, Fabrication andthermal stability of two-dimensional carbide Ti_3C_2 nanosheets, Ceram. Int. 42 (2016) 8419–8424.

[249] M. Khazaei, M. Arai, T. Sasaki, M. Estili, Y. Sakka, Two-dimensional molyb-denum carbides: potential thermoelectric materials of the MXene family, Phys. Chem. Chem. Phys. 16 (2014) 7841–7849.

[250] X.-H. Zha, J. Yin, Y. Zhou, Q. Huang, K. Luo, J. Lang, J.S. Francisco, J. He, S. Du, Intrinsic structural, electrical, thermal, and mechanical properties of the promising conductor Mo_2C MXene, J. Phys. Chem. C 120 (2016) 15082–15088.

[251] H. Wang, Y. Wu, J. Zhang, G. Li, H. Huang, X. Zhang, Q. Jiang, En-hancement of the electrical properties of MXene Ti_3C_2 nanosheets by post-treatments of alkalization and calcination, Mater. Lett. 160 (2015) 537–540.

[252] E.S. Muckley, M. Naguib, I.N. Ivanov, Multi-modal, ultrasensitive, wide-range humidity sensing with Ti_3C_2 film, Nanoscale 10 (2018) 21689–21695.

[253] E.S. Muckley, M. Naguib, H.-W. Wang, L. Vlcek, N.C. Osti, R.L. Sacci, X. Sang, R. R. Unocic, Y. Xie, M. Tyagi, et al., Multimodality of structural, electrical, and gravimetric responses of intercalated MXenes to water, ACS Nano 11 (2017) 11118–11126.

[254] J. Halim, S. Kota, M.R. Lukatskaya, M. Naguib, M.-Q. Zhao, E.J. Moon, J. Pitock, J. Nanda, S.J. May, Y. Gogotsi, et al., Synthesis and characterization of 2D molybdenum carbide (MXene), Adv. Funct. Mater. 26 (2016) 3118–3127.

[255] M. Lu, H. Li, W. Han, J. Chen, W. Shi, J. Wang, X.-M. Meng, J. Qi, H. Li, B. Zhang, et al., 2D titanium carbide (MXene) electrodes with lower-F surface for high performance lithium-ion batteries, J. Energy Chem. 31 (2019) 148–153.

[256] H. Kim, B. Anasori, Y. Gogotsi, H.N. Alshareef, Thermoelectric propertiesof two-dimensional molybdenum-based MXenes, Chem. Mater. 29 (2017) 6472–6479.

[257] J.L. Hart, K. Hantanasirisakul, A.C. Lang, B. Anasori, Y. Gogotsi, M.L. Taheri, Direct correlation of mxene surface chemistry and electronic properties, Microsc. Microanal. 24 (2018) 1606–1607.

[258] M. Kurtoglu, M. Naguib, Y. Gogotsi, M.W. Barsoum, First principles study of two-dimensional early transition metal carbides, MRS Commun. 2 (2012) 133–137.

[259] U. Yorulmaz, A. Ozden, N.K. Perkgoz, F. Ay, C. Sevik, Vibrational and mechanical properties of single layer MXene structures: a first-principles investigation, Nanotechnology 27 (2016), 335702. Art. no.

[260] S. Stankovich, D.A. Dikin, G.H. Dommett, K.M. Kohlhaas, E.J. Zim-ney, E. A. Stach, R.D. Piner, S.T. Nguyen, R.S. Ruoff, Graphene-based composite materials, Nature 442 (2006) 282–286.

[261] V.N. Borysiuk, V.N. Mochalin, Y. Gogotsi, Bending rigidity of two-dimensional titanium carbide (MXene) nanoribbons: a molecular dynamics study, Comput. Mater. Sci. 143 (2018) 418–424.

[262] H. Tang, Q. Hu, M. Zheng, Y. Chi, X. Qin, H. Pang, Q. Xu, MXene–2D layered electrode materials for energy storage, Prog. Nat. Sci.: Mater. Int. 28 (2018) 133–147.

[263] K. Hantanasirisakul, Y. Gogotsi, Electronic and optical properties of 2D transition metal carbides and nitrides (MXenes), Adv. Mater. 30 (2018), 1804779. Art. no.

[264] Y. Zhang, L. Wang, N. Zhang, Z. Zhou, Adsorptive environmental applica-tions of MXene nanomaterials: a review, RSC Adv. 8 (2018) 19895–19905.

[265] X.-H. Zha, Q. Huang, J. He, H. He, J. Zhai, J.S. Francisco, S. Du, The thermal and electrical properties of the promising semiconductor MXene Hf_2CO_2, Sci. Rep. 6 (2016) 1–10.

[266] K. Luo, X.-H. Zha, Y. Zhou, Z. Guo, C.-T. Lin, Q. Huang, S. Zhou, R. Zhang, S. Du, First-principles study on the electrical and thermal properties of the semiconducting $Sc_3(CN)F_2$ MXene, RSC Adv. 8 (2018) 22452–22459.

[267] X.-H. Zha, J. Zhou, Y. Zhou, Q. Huang, J. He, J.S. Francisco, K. Luo, S. Du, Promising electron mobility and high thermal conductivity in Sc_2CT_2 (T=F, OH) MXenes, Nanoscale 8 (2016) 6110–6117.

[268] L. Chen, X. Shi, N. Yu, X. Zhang, X. Du, J. Lin, Measurement and analysis of thermal conductivity of Ti_3C_2Tx MXene films, Materials 11 (2018), 701. Art.no.

[269] S. Moskalenko, P. Khadzhi, I. Podlesny, E. Dumanov, M.A. Liberman, I. Zubac, Metastable bound states of the interacting two-dimensional mag- netoexcitons, Solid State Commun. 283 (2018) 14–21.

[270] Y. Yue, Fe_2C monolayer: an intrinsic ferromagnetic MXene, J. Magnet. Magnet. Mater. 434 (2017) 164–168.

[271] I. Shein, A. Ivanovskii, Graphene-like titanium carbides and nitrides $Ti_{n+1}C_n$,$Ti_{n+1}N_n$ (n=1,2 and 3) from deintercalated MAX phases: First-principles probing of their structural,electronic properties and relative stability, Comput. Mater. Sci. 65 (2012) 104–114.

[272] Q. Tang, Z. Zhou, P. Shen, Are MXenes promising anode materials for Li-ion batteries? Computational studies on electronic properties and Li storage capability of Ti_3C_2 and $Ti_3C_2X_2$ (X= F, OH) monolayer, J. Am. Chem. Soc. 134 (2012) 16909–16916.

[273] G. Gao, G. Ding, J. Li, K. Yao, M. Wu, M. Qian, Monolayer MXenes:promising half-metals and spin gapless semiconductors, Nanoscale 8 (2016) 8986–8994.

[274] Q. Meng, J. Ma, Y. Zhang, Z. Li, A. Hu, J.-J. Kai, J. Fan, Theoretical investigation of zirconium carbide MXenes as prospective high capacity anode materials for Na-ion batteries, J. Mater. Chem. 6 (2018) 13652–13660.

[275] H. Kumar, N.C. Frey, L. Dong, B. Anasori, Y. Gogotsi, V.B. Shenoy, Tun-able magnetism and transport properties in nitride MXenes, ACS Nano 11 (2017) 7648–7655.

[276] C. Zhang, B. Anasori, A. Seral-Ascaso, S.-H. Park, N. McEvoy, A. Shmeliov, G. S. Duesberg, J.N. Coleman, Y. Gogotsi, V. Nicolosi, Transparent, flexible, and conductive 2D titanium carbide (MXene) films with high volumetric capacitance, Adv. Mater. 29 (2017), 1702678. Art. no.

[277] G. Ying, S. Kota, A.D. Dillon, A.T. Fafarman, M.W. Barsoum, Conductive transparent V_2CT_x (MXene) films, FlatChem 8 (2018) 25–30.

[278] G. Berdiyorov, Optical properties of functionalized $Ti_3C_2T_2$ (T= F, O, OH) MXene: first-principles calculations, AIP Adv. 6 (2016), 055105. Art. no.

[279] M. Naguib, J. Come, B. Dyatkin, V. Presser, P.-L. Taberna, P. Simon, M. W. Barsoum, Y. Gogotsi, MXene: a promising transition metal carbide anode for lithium-ion batteries, Electrochem. Commun. 16 (2012) 61–64.

[280] D. Wang, Y. Gao, Y. Liu, D. Jin, Y. Gogotsi, X. Meng, F. Du, G. Chen, Y. Wei, First-principles calculations of Ti_2N and Ti_2NT_2 (T= O, F, OH) monolayers as potential anode materials for lithium-ion batteries and beyond, J. Phys. Chem. C 121 (2017) 13025–13034.

[281] M. Naguib, J. Halim, J. Lu, K.M. Cook, L. Hultman, Y. Gogotsi, M.W. Barsoum, New two-dimensional niobium and vanadium carbides as promising materials for Li-ion batteries, J. Am. Chem. Soc. 135 (2013) 15966–15969.

[282] M. Naguib, R.A. Adams, Y. Zhao, D. Zemlyanov, A. Varma, J. Nanda, V.G. Pol, Electrochemical performance of MXenes as K-ion battery anodes, Chem. Commun. 53 (2017) 6883–6886.

[283] S. Zhao, X. Meng, K. Zhu, F. Du, G. Chen, Y. Wei, Y. Gogotsi, Y. Gao, Li-ion uptake and increase in interlayer spacing of Nb_4C_3 MXene, Energy Storage Mater. 8 (2017) 42–48.

[284] Z. Yang, Y. Zheng, W. Li, J. Zhang, Investigation of two-dimensional Hf-based MXenes as the anode materials for Li/Na-ion batteries: a DFT study, J. Comput. Chem. 40 (2019) 1352–1359.

[285] Y. Dong, Z.-S. Wu, S. Zheng, X. Wang, J. Qin, S. Wang, X. Shi, X. Bao, Ti_3C_2 MXene-derived sodium/potassium titanate nanoribbons for high-performance sodium/potassium ion batteries with enhanced capacities, ACS Nano 11 (2017) 4792–4800.

[286] V. Shukla, N.K. Jena, S.R. Naqvi, W. Luo, R. Ahuja, Modelling high-performing batteries with Mxenes: the case of S-functionalized two-dimensional nitride Mxene electrode, Nano Energy 58 (2019) 877–885.

[287] Y. Ma, P. Qi, J. Ma, L. Wei, L. Zhao, J. Cheng, Y. Su, Y. Gu, Y. Lian, Y. Peng, et al., Wax-transferred hydrophobic CVD graphene enables water-resistant and dendrite-free lithium anode toward long cycle Li– air battery, Adv. Sci. 8 (2021), 2100488.

[288] M. Alhabeb, K. Maleski, T.S. Mathis, A. Sarycheva, C.B. Hatter, S. Uzun, A. Levitt, Y. Gogotsi, Selective etching of silicon from Ti_3SiC_2 (MAX) to obtain 2D titanium carbide (MXene), Angew. Chem. 130 (2018) 5542–5546.

[289] J. Filip, J. Tkac, Is graphene worth using in biofuel cells? Electrochim. Acta 136 (2014) 340–354.

[290] Y. Wang, Z.X. Huang, Y. Shi, J.I. Wong, M. Ding, H.Y. Yang, Designed hybrid nanostructure with catalytic effect: beyond the theoretical capacity of SnO_2 anode material for lithium ion batteries, Sci. Rep. 5 (2015) 1–8.

[291] J. Zhu, X. Zhang, H. Gao, Y. Shao, Y. Liu, Y. Zhu, J. Zhang, L. Li, VS_4anchored on Ti_3C_2 MXene as a high-performance cathode material for mag-nesium ion battery, J. Power Sources 518 (2022), 230731.

[292] N. Li, Y. Li, X. Zhu, C. Huang, J. Fan, Theoretical investigation of the intercalation mechanism of VS_2/MXene heterostructures as anode materialsfor metal-ion batteries, Appl. Surf. Sci. 543 (2021), 148772.

[293] Y. Zhang, Y. Wu, Y. Liu, J. Feng, Flexible and freestanding heterostructures based on COF-derived N-doped porous carbon and two-dimensional MXene for all-solid-state lithium-sulfur batteries, Chem. Eng. J. 428 (2022), 131040.

[294] C. Wei, Y. Wang, Y. Zhang, L. Tan, Y. Qian, Y. Tao, S. Xiong, J. Feng, Flexible and stable 3D lithium metal anodes based on self-standing MXene/COF frameworks for high-performance lithium-sulfur batteries, Nano Res. 14 (2021) 3576–3584.

[295] N. Ma, T. Wang, N. Li, Y. Li, J. Fan, New phases of MBenes M_2B (M= Sc,Ti, and V) as high-capacity electrode materials for rechargeable magnesium ion batteries, Appl. Surf. Sci. 571 (2022), 151275.

[296] X. Yuan, Z. Chen, B. Huang, Y. He, N. Zhou, Potential applications of MoS_2/M_2CS_2 (M= Ti, V) heterostructures as anode materials for metal-ion batteries, J. Phys. Chem. C 125 (2021) 10226–10234.

[297] X. He, R. Wang, H. Yin, Y. Zhang, W. Chen, S. Huang, 1T-MoS_2 monolayeras a promising anode material for (Li/Na/Mg)-ion batteries, Appl. Surf. Sci. 584 (2022), 152537.

[298] M.R. Kumar, S. Singh, Na adsorption on para boron-doped AGNR for sodium-ion batteries (sibs): a first principles analysis, J. Electron. Mater. 51 (2022) 2095–2106.

[299] C. Xiao, X. Tang, J. Peng, Y. Ding, Graphene-like BSi as a promising anode material for Li-and Mg-ion batteries: a first principle study, Appl. Surf. Sci. 563 (2021), 150278.

[300] Y.-B. Liang, K. Liu, Z. Liu, J. Wang, C.-S. Liu, Y. Liu, A First-Principles study of monolayer and heterostructure antimonene as potential anode materials for Magnesium-ion batteries, Appl. Surf. Sci. 577 (2022), 151880.

[301] A.A. Khan, I. Muhammad, R. Ahmad, I. Ahmad, Penta graphene: a superior anode material for Mg-ion batteries with high specific theoretical capacity, Ionics 27 (2021) 4819–4828.

[302] H. Dua, J. Deb, D. Paul, U. Sarkar, Twin-graphene as a promising AnodeMaterial for Na-ion rechargeable batteries, ACS Appl. Nano Mater. 4 (2021) 4912–4918.

[303] S. Xu, X. Fan, J. Liu, D.J. Singh, Q. Jiang, W. Zheng, Adsorption of Li-ion single-layer silicene for anodes of Li-ion batteries, Phys. Chem. Chem. Phys. 20 (2018) 8887–8896.

[304] J. Zhu, U. Schwingenschlogl, Silicene for Na-ion battery applications, 2D Mater. 3 (2016), 035012.

[305] Y. Teng, M. Mo, Y. Li, J. Xue, H. Zhao, Amorphous carbon-coated ZnO porous nanosheets: facile fabrication and application in lithium- and sodium-ion batteries, J. Alloys Compd. 744 (2018) 712–720.

[306] L. Peng, Y. Zhu, D. Chen, R.S. Ruoff, G. Yu, Two-dimensional materials for beyond-lithium-ion batteries, Adv. Energy Mater. 6 (2016), 1600025.

[307] J. Liu, X.-W. Liu, Two-dimensional nanoarchitectures for lithium storage, Adv. Mater. 24 (2012) 4097–4111.

[308] Z. Yin, H. Li, H. Li, L. Jiang, Y. Shi, Y. Sun, G. Lu, Q. Zhang, X. Chen, H. Zhang, Single-layer MoS_2 phototransistors, ACS Nano 6 (2012) 74–80.

[309] Z. Zeng, Z. Yin, X. Huang, H. Li, Q. He, G. Lu, F. Boey, H. Zhang, Single-layer semiconducting nanosheets: high-yield preparation and device fabrication, Angew. Chem. 123 (2011) 11289–11293.

[310] J.-G. Song, J. Park, W. Lee, T. Choi, H. Jung, C.W. Lee, S.-H. Hwang, J. M. Myoung, J.-H. Jung, S.-H. Kim, C.L. Matras, H. Kim, Layer-controlled, wafer-scale, and conformal synthesis of tungsten disulfide nanosheets using atomic layer deposition, ACS Nano 7 (2013) 11333–11340.

[311] S. Najmaei, Z. Liu, W. Zhou, X. Zou, G. Shi, S. Lei, B.I. Yakobson, J.-C. Idrobo, P. M. Ajayan, J. Lou, Vapour phase growth and grain boundary structure of molybdenum disulphide atomic layers, Nat. Mater. 12 (2013) 754–759.

[312] S.-J. An, Y.H. Kim, C. Lee, D.Y. Park, M.S. Jeong, Exfoliation of transitionmetal dichalcogenides by a high-power femtosecond laser, Sci. Rep. 8 (2018) 1–6.

[313] N. Kheirabadi, A. Shafiekhani, Graphene/Li-ion battery, J. Appl. Phys. 112 (2012), 124323.

[314] Ferre-Vilaplana, Storage of hydrogen adsorbed on alkali metal doped single-layer all-carbon materials, J. Phys. Chem. C 112 (2008) 3998–4004.

[315] C. Ataca, E. Akturk, S. Ciraci, H. Ustunel, High-capacity hydrogen storage by metallized graphene, Appl. Phys. Lett. 93 (2008), 043123.

[316] N.A. Kaskhedikar, J. Maier, Lithium storage in carbon nanostructures, Adv. Mater. 21 (2009) 2664–2680.

[317] K. Fan, Y. Ying, X. Li, X. Luo, H. Huang, Theoretical investigation of V_3C_2 MXene as prospective high-capacity anode material for metal-ion (Li, Na, K, and Ca) batteries, J. Phys. Chem. C 123 (2019) 18207–18214.

[318] K. Fan, Y. Ying, X. Luo, H. Huang, Monolayer PC5/PC6: promising anode materials for lithium-ion batteries, Phys. Chem. Chem. Phys. 22 (2020) 16665–16671.

[319] H. Gullapalli, K. Kalaga, S. Vinod, M.-T.F. Rodrigues, A. George, P.M. Ajayan, 2D material integrated macroporous electrodes for Li-ion batteries, RSC Adv. 7 (2017) 32737–32742.

[320] K.-S. Chen, I. Balla, N.S. Luu, M.C. Hersam, Emerging opportunities for two-dimensional materials in lithium-ion batteries, ACS Energy Lett. 2 (2017) 2026–2034.

[321] Z. Li, H. Wang, Z. Sun, J. Su, Z. Wang, L. Wang, Self-activated continuous pulverization film: an insight into the mechanism of the extraordinary long-life cyclability of hexagonal $H_{4.5}Mo_{5.25}O_{18}{\cdot}(H_2O)_{1.36}$ microrods, J. Mater. Chem. 4 (2016) 303–313.

[322] V.N. Popov, P. Lambin, Theoretical Raman fingerprints of α-, β-, and γ-graphyne, Phys. Rev. B 88 (2013), 075427.

[323] R. Baughman, H. Eckhardt, M. Kertesz, Structure-property predictions for new planar forms of carbon: layered phases containing sp^2 and sp atoms, J. Chem. Phys. 87 (1987) 6687–6699.

[324] Q. Song, B. Wang, K. Deng, X. Feng, M. Wagner, J.D. Gale, K. Mullen, L. Zhi, Graphenylene, a unique two-dimensional carbon network with nondelocalized cyclohexatriene units, J. Mater. Chem. C 1 (2013) 38–41.

[325] J. Zhou, X. Gao, R. Liu, Z. Xie, J. Yang, S. Zhang, G. Zhang, H. Liu, Y. Li, J. Zhang, et al., Synthesis of graphdiyne nanowalls using acetylenic coupling reaction, J. Am. Chem. Soc. 137 (2015) 7596–7599.

[326] M. Long, L. Tang, D. Wang, Y. Li, Z. Shuai, Electronic structure and carrier mobility in graphdiyne sheet and nanoribbons: theoretical predictions, ACS Nano 5 (2011) 2593–2600.

[327] Y. Jiao, A. Du, M. Hankel, Z. Zhu, V. Rudolph, S.C. Smith, Graphdiyne: a versatile nanomaterial for electronics and hydrogen purification, Chem. Commun. 47 (2011) 11843–11845.

[328] G. Brunetto, P. Autreto, L. Machado, B. Santos, R.P. Dos Santos, D.S. Galvao, Nonzero gap two-dimensional carbon allotrope from porous graphene, J. Phys. Chem. C 116 (2012) 12810–12813.

[329] B.R. Sharma, A. Manjanath, A.K. Singh, pentahexoctite, A new two-dimensional allotrope of carbon, Sci. Rep. 4 (2014) 1–6.

[330] B. Mandal, S. Sarkar, A. Pramanik, P. Sarkar, Doped defective graphene nanoribbons: a new class of materials with novel spin filtering properties, RSC Adv. 4 (2014) 49946–49952.

[331] J. Lahiri, Y. Lin, P. Bozkurt, I.I. Oleynik, M. Batzill, An extended defect ingraphene as a metallic wire, Nat. Nanotechnol. 5 (2010) 326–329.

[332] J. Ma, D. Alfè, A. Michaelides, E. Wang, The water-benzene interaction:Insight from electronic structure theories, J. Chem. Phys. 130 (2009), 154303.
[333] X. Fan, J. Li, G. Chen, New carbon allotropes with metallic conducting properties: a first-principles prediction, RSC Adv. 7 (2017) 17417–17426.
[334] S. Thomas, C.H. Lee, S. Jana, B. Jun, S.U. Lee, Phographene as a high-performance anode material with high specific capacity and fast Li diffusion: from structural, electronic, and mechanical properties to LIB applications, J. Phys. Chem. C 123 (2019) 21345–21352.
[335] X.-J. Ye, C.-S. Liu, W. Zhong, Z. Zeng, Y.-W. Du, Metalized T graphene: a reversible hydrogen storage material at room temperature, J. Appl. Phys. 116 (2014), 114304.
[336] Y. Liu, G. Wang, Q. Huang, L. Guo, X. Chen, Structural and electronicproperties of T graphene: a two-dimensional carbon allotrope with tetrarings, Phys. Rev. Lett. 108 (2012), 225505.
[337] S. Kawai, S. Saito, S. Osumi, S. Yamaguchi, A.S. Foster, P. Spijker, E. Meyer, Atomically controlled substitutional boron-doping of graphene nanoribbons, Nat. Commun. 6 (2015) 1–6.
[338] C. Zhang, J. Tan, Y. Pan, X. Cai, X. Zou, H.-M. Cheng, B. Liu, Mass production of 2D materials by intermediate-assisted grinding exfoliation, Natl. Sci. Rev. 7 (2020) 324–332.
[339] H. Liu, H. Dong, Y. Ji, L. Wang, T. Hou, Y. Li, The adsorption, diffusion and capacity of lithium on novel boron-doped graphene nanoribbon: a density functional theory study, Appl. Surf. Sci. 466 (2019) 737–745.